UNIVERSITÄT LEIPZIG

Institut für Experimentelle Physik II
Institute for Experimental Physics II

Report 2001

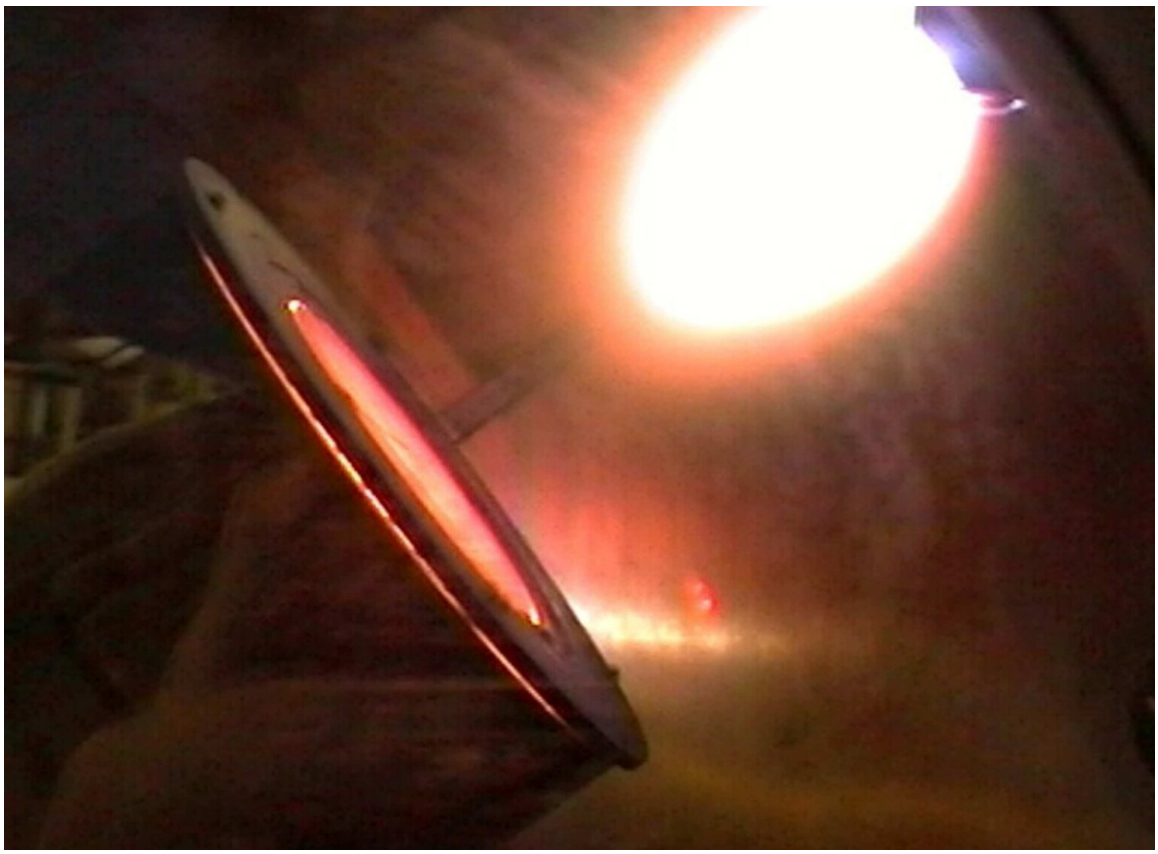

ISBN 3-934178-17-0

Printed in Germany by
MERKUR Druck und Kopierzentrum GmbH, Leipzig

Front cover
Plasma plume during pulsed laser deposition, used for large area, double sided epitaxy of oxide superconductors, ferroelectrics and semiconductors.

Back cover
Schematic sketch of a cubic liquid-crystalline phase. This so-called bicontinuous phase is composed of a minimum surface forming lipid bilayer that is interlaced by water channels.

Institut für Experimentelle Physik II
Fakultät für
Physik und Geowissenschaften
Universität Leipzig

Institute for Experimental Physics II
Faculty of Physics and Geosciences
Universität Leipzig

Report 2001

Address

Linnéstraße 5
D-04103 Leipzig
Germany

Phone: +49 341 9732 680
Fax: +49 341 9732 699
WWW: http://www.uni-leipzig.de/~exph2/

Contents

PREFACE

The Institute for Experimental Physics II of Universität Leipzig welcomes you to read its activity report 2001*. In the following some statistics about the structure of the institute, the people involved, and the teaching activities are summarized. The core of the report is built by the scientific activity reports – arranged according to the groups making up the institute: solid-state optics and acoustics, semiconductor physics, nuclear solid-state physics, physics of dielectric solids, superconductivity and magnetism.

After the remodeling of the main physics building, operations have moved back from their temporary quarters and are now fully reestablished at Linnéstraße. The year 2001 has seen the arrival of a new faculty member, Marius Grundmann, on the chair for semiconductor physics. He had previously worked at Technische Universität Berlin, mostly on nanostructure based optoelectronic devices.

Scientifically the year was quite successful. Among the highlights, are the magnetism and superconductivity of carbon-based compounds, the optical mass balance, the fabrication of a variety of high quality oxide thin films, the investigation of ferroelectric (perovskite) nanocrystals and the first ion tomography of cartilage cells. We invite you to look for further details in the report.

Major new pieces of equipment could be installed in 2001 - a new 750 MHz NMR magnet and a confocal laser scanning microscope. We could successfully continue to support our activities by acquiring external funding, among them projects within a BMBF "Wachstumskern" (growth nucleus), headed by the Leipzig startup company Solarion GmbH, projects within BMBF "Leitprojekte" (leading projects), and other major projects supported by the Deutsche Forschungsgemeinschaft (German Science Foundation) and the European Space Agency (ESA). Further support comes from the European Community (EU), the Deutsche Akademische Austauschdienst

* The nuclear solid-state physics group (NFP) reports for the years 2000 and 2001 following its report on the period from 1997-1999.

(DAAD), the German-Israeli Foundation (GIF), the Sächsisches Ministerium für Wissenschaft und Kunst (SMWK), the BMBF within WTZ-projects, and a number of small and medium size companies. At this point we like to thank all funding bodies for their support. We also appreciate the support of the university, e.g., in the form of startup grants, and the continuous support of the local government, although the 30% general budget cut has caused many problems.

We enjoy the many cooperations with colleagues worldwide. A document to the fact that also our colleagues enjoy this, is the respectable nomination of Dieter Michel as Honorary Professor of the State University of St. Petersburg.

The large number of publications, invited talks and conference presentations document our outreach into the scientific community. The new year, 2002, has already begun - it is pronounced "Year of the Geosciences". As in previous years we organize and participate in manifold activities to also reach out into the general public, from high school interns to public displays and Sunday lectures.

We hope you enjoy reading our report which is (in color) also available for on-line browsing at http://www.uni-leipzig.de/~exph2/report_2001.pdf .

Leipzig, February 2002

Marius Grundmann
Director

1 Structure and Staff of the Institute

1.1 Office of the Director

Prof. Dr. Wolfgang Grill (director)
Prof. Dr. Pablo Esquinazi (vice director)

since 1/2002
Prof. Dr. Marius Grundmann (director)
Prof. Dr. Dieter Michel (vice director)

1.2 Groups of the Institute

1.2.1 FKO

Festkörperoptik und -akustik
Solid-state optics and acoustics

Prof. Dr. Wolfgang Grill

Secretary
Mrs Wilhelmine Pfeiffer

Technical staff
Phys.-Lab. Adelheid Geyer
PTA Hans-Joachim vom Hofe
Dipl.-Phys. Friedrich Jilek
Dipl.-Ing. (FH) Ulrike Teschner

Academic staff
Dr. Stefan Knauth (presently Siemens AG, Leipzig)
Dr. Zbigniew Kojro
Dr. Volker Riede
Dr. Mathias Schubert
Priv.-Doz. Dr. Reinhold Wannemacher

Ph.D. candidates
Nurdin Ashkenov, M.Sc.
Carsten Bundesmann (Staatsexamen Physik)
Dipl.-Phys. Tino Hofmann
Dipl.-Phys. Alexander Kasic
Wilfred Ngwa, M.Sc.
Evgeny Twerdowski, M.Sc.
Bashkim Ziberi, M.Sc.

Students
Beri Mbenkum
Thomas Rudolph

1.2.2 HLP

Halbleiterphysik
Semiconductor Physics

Prof. Dr. Marius Grundmann

Secretary
Mrs. Wilhelmine Pfeiffer

Technical staff
Dipl.-Phys. Gabriele Benndorf
Ing. Gisela Biehne
Dipl.Ing. Holger Hochmuth
Dipl.-Phys. Jörg Lenzner
Ing. Dieter Natusch
PTA Gabriele Ramm
PTA Roswitha Riedel

Academic staff
Dr. Michael Lorenz
Priv.-Doz. Dr. Rainer Pickenhain
Priv.-Doz. Dr. Bernd Rheinländer
Dr. Heidemarie Schmidt

Ph.D. candidates
Dipl.-Phys. Karsten Goede
Susanne Hardt (Staatsexamen Physik)
Dipl.-Phys. Alexander Weber

Students
Jens Bauer
Daniel Fritsch
Dietmar Kitzig
Rüdiger Schmidt
Holger von Wenkstern

1.2.3 NFP

Nukleare Festkörperphysik
Nuclear solid state physics

Prof. Dr. Tilman Butz

Technical staff
Dipl.-Ing. Bernd Krause
PTA Raimund Wipper
Dipl.-Ing. Lothar Wulke

Academic staff
Dr. Dietmar Lehmann
Dr. Tilo Reinert (since december 2001)
Priv. Doz. Dr. Wolfgang Tröger
Dr. Jürgen Vogt

Ph.D. candidates
Dipl.-Phys. Frank Heinrich
Dipl.-Phys. Johannes Heitmann (until may 2000)
Dipl.-Phys. Steffen Jankuhn
Dipl.-Phys. Tilo Reinert (until november 2001)
Dipl.-Phys. Daniel Spemann

Students
Frank Menzel (since october 2001)
Michael Schwertner (since march 2001)
Lars Thomas (since november 2000)

1.2.4 PDF

Physik dielektrischer Festkörper
Physics of dielectric solids

Prof. Dr. Dieter Michel

Secretary
Mrs. Ursula Seibt

Technical staff
Dr. Winfried Böhlmann
Dipl.-Ing. J. Hoentsch
Dipl.-Phys. Gert Klotzsche

Academic staff
apl. Prof. Dr. Rolf Böttcher (Hochschuldozent)
Prof. Dr. Georg Völkel
Dr. habil. Horst Braeter
PD Dr. Andreas Pöppl
Dr. André Pampel

Physical-technical assistent
Mrs. Ursula Heinich

Ph. D. candidates
Emre Erdem
Özlen Erdem
Marlen Gutjahr
Samir Mulla Osman
Jörg Roland
Abdoullaye Taye

Students
Kyuseok Cho

1.2.5 SUM

Supraleitung und Magnetismus
Superconductivity and magnetism

Prof. Dr. Pablo D. Esquinazi

Technical saff
Klaus Grünwald
Annette Setzer
Monika Steinhardt

Academic staff
Dr. Kyoo-hyun Han
Dr. Roland Höhne
Dr. Hong Hoa Nguyen
Dr. H. C. Semmelhack
Dr. Michael Ziese

Ph.D. candidates
Heiko Kempa
Falk Mrowka
Roberto Ocaña

Students
Heiko Reckentin

1.3 Guests

Dr. Sergej Lebed (NFP)
Institute of Applied Physics, Sumy, Ukraine
20 weeks

Dr. Serguey Lebedev (SUM)
Institute for Nuclear Research, Russian Academy of Sciences, Russia
7.9.2001-25.11.2001

Prof. Dr. Igor L. Maksimov (SUM)
Department of Theoretical Physics, Nizhny Novgorod University, Russia
8.10.2001-23.12.2001

Dr. Malgorzata Lekka (NFP)
Institute of Nuclear Physics, Krakow, Poland
8 weeks

Dr. Janusz Lekki (NFP)
Institute of Nuclear Physics, Krakow, Poland
10 weeks

Prof. Dr. Yakov Kopelevich (SUM)
Instituto de Fisica, Universidade Estadual de Campinas, Brasil
22.11.2001-4.12.2001

Dr. Evgueni M. Kaidashev (HLP)
Mechanics and Applied Mathematics Research Institute, Rostov-on Don University, Rostov-on Don, Russia
01.09.2001 – 30.11.2001

Prof. Dr. Liu, Weiqiao (NFP)
Petroleum Institute, Fushun, China
5 months
ü
Dr. Marta Marszalek (NFP)
Institute of Nuclear Physics, Krakow, Poland
8 weeks

Prof. Dr. Jan Österreicher (NFP)
Purkyne Military Medical Academy, Hradec Kralove, Czech Republic
since july 2001

Dipl.-Phys. Wojciech Polak (NFP)
Institute of Nuclear Physics, Krakow, Poland)
1 week

Robson Ricardo da Silva (SUM)
Instituto de Fisica, Universidade Estadual de Campinas, Brasil
16.11.2001-5.2.2002

Dr. Jan Šik (HLP)
Institute of Condensed Matter Physics
Masaryk University Brno, Czech Republik
01.01.2001 – 31.03.2001

Dr. Z. Stachura (NFP)
Institute of Nuclear Physics, Krakow, Poland
1 week

Prof. Dr. Sun, Guida (NFP)
Beijing Institute of Petrochemical Engineering, Beijing, China
5 months

2 Teaching

Experimental Physics I (International Physics Studies Program)
Prof. Dr. W. Grill

Exercises to EPI (International Physics Studies Program)
S. Mellion, Evgeny Twerdowski

Experimental Physics II (International Physics Studies Program)
Prof. Dr. W. Grill, Dr. M. Schubert

Experimental Physics III (International Physics Studies Program)
P. Esquinazi

Exercises to EPII and EPIII (International Physics Studies Program)
Dr. M. Schubert

Applied Optics
M. Schubert, PD Dr. R. Wannemacher

Applied Optics I
PD Dr. R. Wannemacher

Advanced Laboratory Course
Dr. V. Riede (head)
Dr. M. Lorenz, Dr. J. Vogt

Semiconductor Physics I+II (Dipl.)
M. Grundmann

Semiconductor Physics I (International Physics Studies Program)
M. Grundmann

Nanotechnology (International Physics Studies Program)
M. Grundmann

Laboratory course in Semiconductor Physics I+II
M. Grundmann, M. Lorenz, R. Pickenhain, B. Rheinländer,
H. Schmidt, R. Schwabe, G. Benndorf, J. Lenzner, G. Biehne

Seminar on Optoelectronic Materials and Devices
M. Grundmann

Microcavities
B. Rheinländer

Seminar Experimental Physics IV
R. Pickenhain

Theoretical Problems in Semiconductor Physics I
R. Pickenhain/H. Schmidt

C for Physicists
R. Pickenhain

Semiconductor Optics
B. Rheinländer

Microresonators in Semiconductor Optoelectronics
B. Rheinländer

Experimental Physics for Chemistry Teachership Candidates
B. Rheinländer

Solid State Physics
P. Esquinazi

Superconductivity I and II
P. Esquinazi

Thin Film Technology of Magnetic and Superconducting Materials I+II
M. Ziese, P. Esquinazi

Laboratory course in Superconductivity
M. Ziese

Exercises Condensed Matter Physics
M. Ziese

Introductory Physics Laboratory
R. Höhne

Laboratory course for Bachelor Students in the group SUM
R. Höhne, Dr. H. C. Semmelhack

Lecture: Experimental Physics: Solid State Physics
R. Böttcher

Lecture: Introduction to solid-state EPR
R. Böttcher

Laboratory course in EPR
R. Böttcher

Exercises to Experimental Physics IV
H. Braeter

Exercises to Experimental Physics III
H. Braeter

Physics for Chemists
D. Michel

Magnetic Resonance and Relaxation
D. Michel

Experimental Physics III
D. Michel

Laboratory course for physics students
A.Pampel

Experimental Physics I (International Physics Studies Program)
A. Pöppl

Ferroelectrics and Ferroelastics as High-Tech Materials
G. Völkel

Laboratory course: physics for veterinary medicine students
M. Gutjahr

Lecture: „Struktur der Materie III (Kernphysik)“
T. Butz

Tutorial: „Experimentalphysik I“
D. Lehmann

Course: „Fachkundekurs Strahlenschutz“
D. Lehmann

Tutorial: „Struktur der Materie III (Kernphysik)“
D. Spemann

Lab Course „Blaue Kupferproteine“ in biophysics
T. Reinert, F. Heinrich

Seminar: „Nukleare Festkörperphysik“
T. Butz

Excursion “Forschungsreaktor München, MPI für Plasmaphysik, MPI für Quantenoptik”
W. Tröger

Lecture: „Fouriertransformation für Fußgänger“
T. Butz

Tutorial: „Experimentalphysik II“
D. Lehmann

Course: „Fachkundekurs Strahlenschutz“
D. Lehmann

Lab Course „Blaue Kupferproteine“ in biophysics
T. Reinert, F. Heinrich

Seminar: „Nukleare Festkörperphysik“
T. Butz

Tutorial: „Astrophysik“
J. Vogt

Lab course: „Fortgeschrittenenpraktikum“
J. Vogt

Lecture: „Struktur der Materie III (Kernphysik)“
T. Butz

Tutorial: „Experimentalphysik III“
D. Lehmann

Course: „Fachkundekurs Strahlenschutz“
D. Lehmann

Tutorial: „Struktur der Materie III (Kernphysik)“
D. Spemann

Lecture and Tutorial: “Structure of Matter III (Particle Physics)“
W. Tröger

Seminar: „Nukleare Festkörperphysik“
T. Butz

Excursion „Hahn-Meitner-Institut, Forschungsreaktor BER II, Ionenstrahllabor ISL“
W. Tröger

Tutorial: „Astrophysik“
J. Vogt

Lab course: „Fortgeschrittenenpraktikum“
J. Vogt

Lecture: „Hochenergie-Ionenmikroskopie I“
J. Vogt

Lecture and Tutorial: “Structure of Matter IV”
T. Butz

Seminar: “Nukleare Festkörperphysik”
T. Butz

Tutorial: „Experimentalphysik IV“
D. Lehmann

Course: „Fachkundekurs Strahlenschutz“
D. Lehmann

Lecture: „Nukleare Biophysik“
W. Tröger

Lab Course „Blaue Kupferproteine“ in biophysics
T. Reinert, F. Heinrich

Tutorial: „Galaxien und Kosmologie“
J. Vogt

Lecture: „Hochenergie-Ionenmikroskopie II“
J. Vogt

Lecture: “Nuclear and Particle Physics”
T. Butz

Lecture: “Fourier Transform for Pedestrians”
T. Butz

Seminar: “Nukleare Festkörperphysik”
T. Butz

Tutorial: „Experimentalphysik III“
D. Lehmann

Course: „Fachkundekurs Strahlenschutz“
D. Lehmann

Tutorial: “Nuclear and Particle Physics”
T. Reinert

Tutorial: „Struktur der Materie III (Kern- und Teilchenphysik)“
D. Spemann

Lecture and Tutorial: “Experimentalphysik I” for chemistry students
W. Tröger

Lecture: “Struktur der Materie III (Kern- und Teilchenphysik)”
W. Tröger

Excursion „Forschungsreaktor Rossendorf“
W. Tröger

Lecture: „Hochenergie-Ionenmikroskopie I“
J. Vogt

3 Participation in Committees

T. Butz
Member of the committees
“Erforschung kondensierter Materie” (BMBF)
“Forschung mit nuklearen Sonden und Ionenstrahlen” (BMBF)
„International Symposium on Nuclear Quadrupole Interactions“
Member of the International Advisory Board
of the „Hyperfine Interactions“ conference
Vorsitzender des wissenschaftlichen Beirates des
Instituts für Oberflächenmodifizierung e.V., Leipzig
Vertrauensdozent der Studienstiftung des deutschen Volkes

P. Esquinazi
Dean of Studies of the Faculty for Physics, Meteorology and Geophysics Studies

M. Grundmann
Member of Program Committee for SPIE/ISPA-Photonics and Applications, Nov. 2001, Singapore
Vertrauensdozent der Studienstiftung des deutschen Volkes

M. Schubert
Member of extended executive committee of "Arbeitskreis Ellipsometrie" at the Bundesanstalt für Materialprüfung und -forschung (BAM), Berlin

4 Reviewing and Refereeing Duties

T. Butz
Reviewer: BMBF, Deutsche Forschungsgemeinschaft, Studienstiftung des deutschen Volkes, National Science Foundation (USA), Washington State University (USA)
Referee: Chemische Technik, European J. Biochemistry, Hyperfine Interactions, Inorg. Chemistry, J. of Physics (Condensed Matter), J. Phys. Chem., Phys. Rev. B, Phys. Rev. Lett., Nucl. Instr. Meth. Phys. Res. B, Z. Naturforsch. A

R. Böttcher
Referee: J. Phys. C, J. Magnet. Res., Langmuir, Colloid & Polymer Science

P. Esquinazi
Project Reviewer: Deutsche Forschungsgemeinschaft, National Science Foundation (USA), German-Israeli Foundation
Referee: Phys. Rev. Lett., Phys. Rev. B, Europhys. Letters, phys. stat. sol. (b), J. Low Temp. Phys.

M. Grundmann
Project Reviewer: Deutsche Forschungsgemeinschaft, Alexander von Humboldt-Stiftung
Referee: Appl. Phys. Lett, Phys. Rev. B, Phys. Rev. Lett., Electr. Lett., Physica E

R. Höhne
Referee: phys. stat. sol. (b)

M. Lorenz
Project Reviewer: Fonds zur Förderung der wissenschaftlichen Forschung in Österreich

D. Michel
Referee: Phys. Rev., Phys. Rev. Letters, J. Phys. C, Z. Naturf., Physica stat. sol., Colloid & Polymer Science, J. Solid State Chemistry, Chem. Phys. Letters, Solid State Nuclear Magnetic Resonance

A. Pöppl
Referee: J. Am. Chem. Soc., J. Magn. Reson., Phys. Chem. Chem. Phys.

T. Reinert
Referee: Nucl. Instr. Meth. Phys. Res. B

M. Schubert
Referee: Appl. Phys. Lett., J. Appl. Phys., phys. stat. sol. (a), Appl. Opt., J. Opt. Soc. Am. A, Meas. Sci. Technol.

D. Spemann
Referee: Nucl. Instr. Meth. Phys. Res. B

W. Tröger
Referee: Hyperfine Interactions, J. of Physics (Condensed Matter), Mikrochim. Acta, Z. Naturforsch. A

J. Vogt
Referee: Mikrochim. Acta

G. Völkel
Referee: phys. stat. sol., J. Magn. Reson.

R. Wannemacher
Referee: Optics Communications, Colloids and Surfaces, Computer Physics Communications, Journal of Luminescence, The Journal of Physical Chemistry, Applied Physics B

M. Ziese
Project Reviewer: National Science Foundation (USA)
Referee: Phys. Rev. Lett., Phys. Rev. B, Eur. J. Phys. B, phys. stat. sol. (b), J. Magn. Magn. Mater., J. Low Temp. Phys.

5 FKO — SCIENTIC ACTIVITIES

5.1 Phase-Sensitive Acoustic Microscopy

Mode selective transmission microscopy of a functionally graded Al-Sn alloy sample
Sample 5.8 mm thick, recorded at 2 Mhz in water, images 10 mm wide

Longitudinal polarization

Measured phase

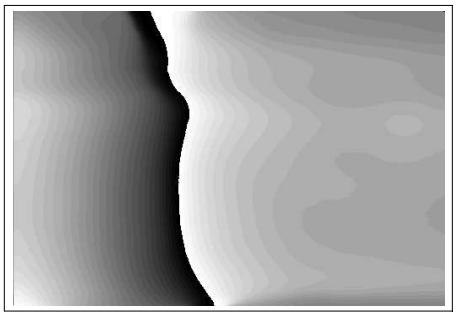

Sn Al

Measured amplitude

Sn Al

Transversal polarization

Measured phase

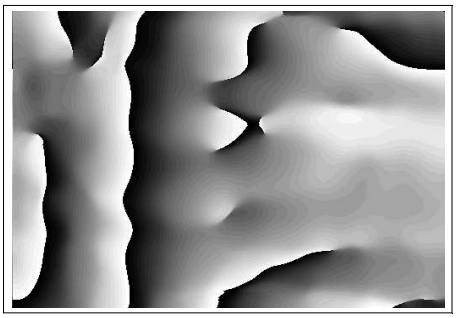

Sn Al

Measured amplitude

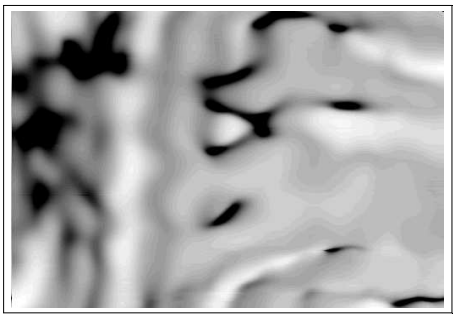

Sn Al

Calculated sound velocity distribution in the sample

Longitudinal polarization

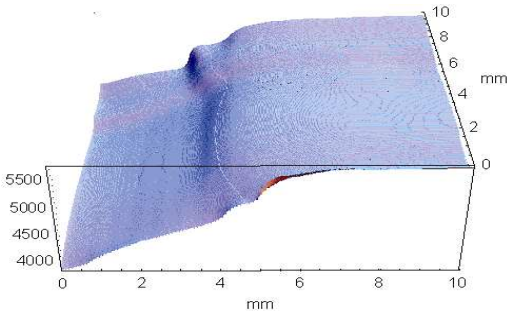

Transversal polarization

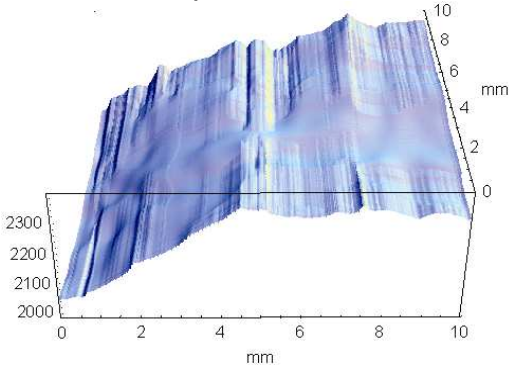

5.2 Ultrasound and Light Correlation spectroscopy

Z. Kojro

Scanning acoustic Doppler microscopy and scanning acoustic correlation microscopy

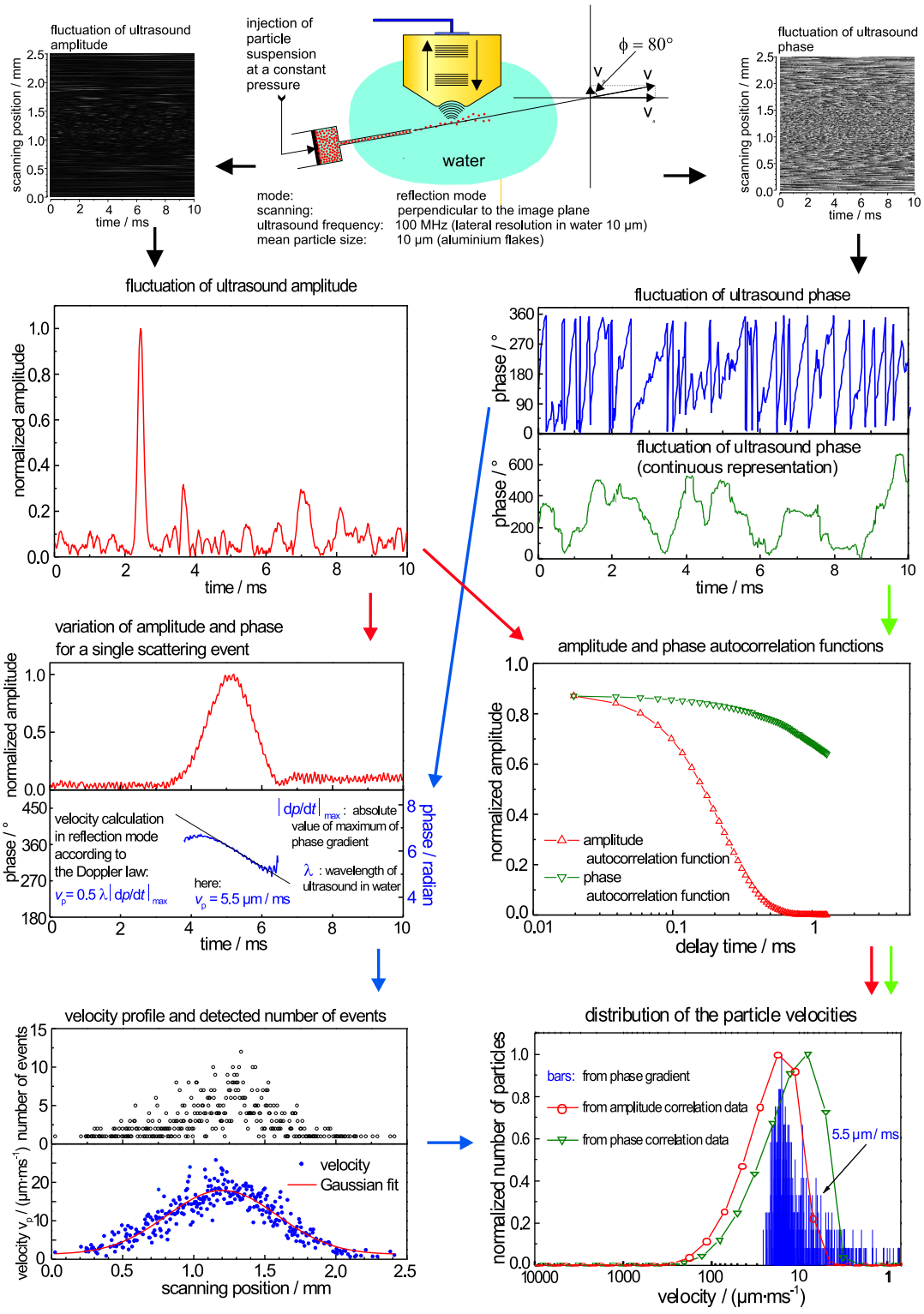

5.3 Development of Ultrasound Sensors and Transducers

Apodization of piezoceramic transducers by thermal treatment

J. Ndop, E. Twerdowski, and W. Grill
Universität Leipzig, Institut für Experimentelle Physik II, Linnéstraße 5, D-04103 Leipzig, Germany

Emission of acoustic radiation from apodized transducers

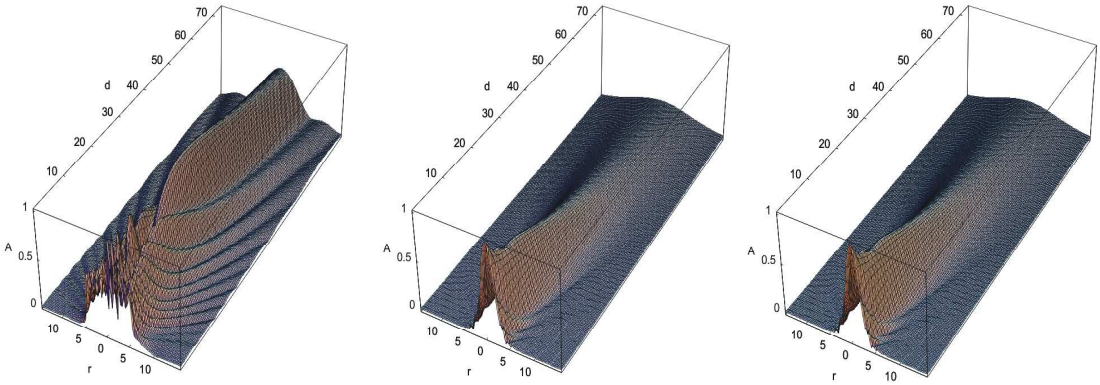

Calculated field distribution for a uniformly excited transducer disc (rectangular apodization)

Calculated field distribution for a transducer disc with Gaussian apodization

Measured field distribtion for the apodized transducer characterized below

r: radial direction; d: axial direction; A: amplitude; the center of the transducer with 10 mm diameter is positioned at r = 0, d = 0

Experimental setup for apodization of transducers

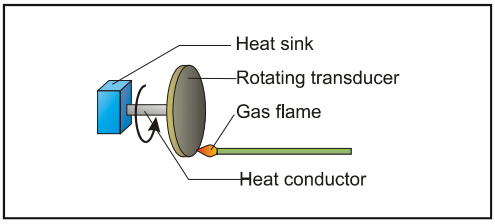

Detection scheme by PSAM

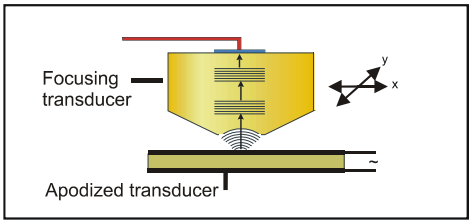

Characterization of an apodized transducer by SAM with vector contrast

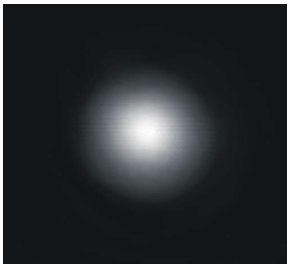

Amplitude

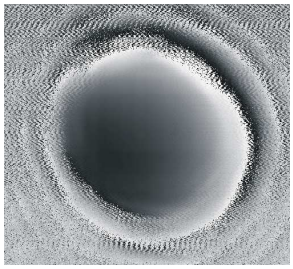

Phase

Images of the emission at the surface of a planar transducer observed at 2 Mhz in water

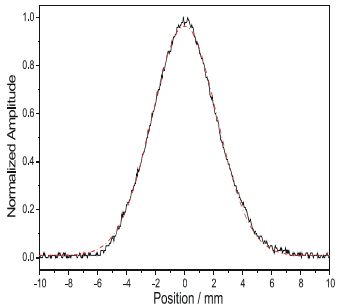

Line scan (horizontal, centered) and adjusted Gaussian profile (red)

Result:

A Gaussian apodization can be achieved by simple heat treatment of transducers leading to partial depolarization of the piezoceramic material (PZT). Such an apodization minimizes variations of the amplitude in the near field of the transducer.

5.4 Ultrasonic Diagnostic for In-Situ monitoring of Zeolite Synthesis

W. Grill, M. Schmachtl, B. Ziberi

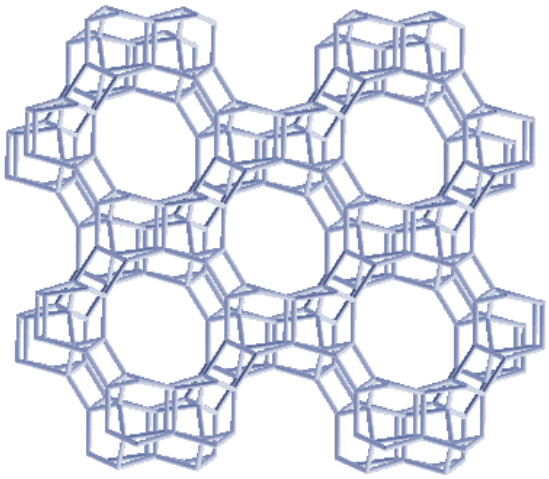

Fig. 1 Microporous structure of a zeolite crystal

Situation:

Zeolites are inorganic crystals with an open microscopic structure. They are used for a wide range of applications including:

- Ion exchanger in detergents,
- Cracking catalyst in petrochemistry,
- Drying agent for removal of moisture,
- Environmental clean up processes,
- Selective molecular sieves.

Zeolite crystals are grown via a hydrothermal synthesis from aqueous solutions. This synthesis process however is still a “black box”. Appropriate diagnostic tools to monitor the nucleation and crystal growth are needed.

Monitoring scheme:

Ultrasound is observed in transmission with the aid of transducers. For small reaction vessels they can be mounted at the outside of the container. For large vessels inserted sensors are employed. During the synthesis process significant variations are observed for the detected phase and amplitude corresponding to:

- The gel formation process,
- The onset of crystallization,
- The termination of crystallization.

The monitoring scheme is non-destructive and does not interfere with chemical reactions.

The method is currently applied for:
- Control of zeolite production facilities.
- Basic scientific research,

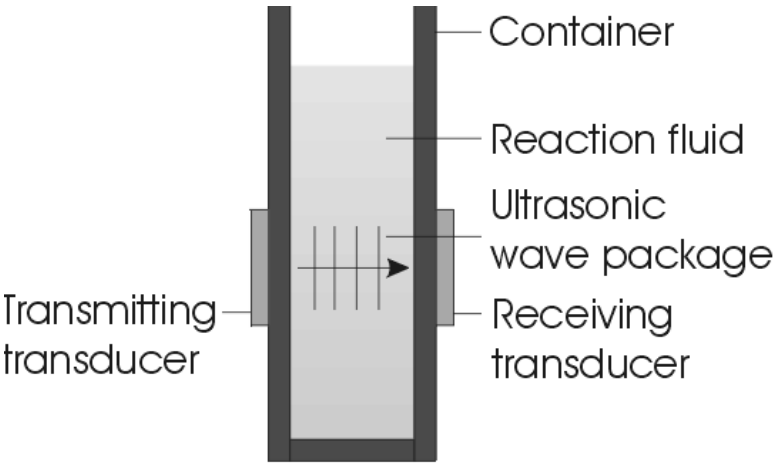

Fig. 2 Ultrasonic sensor for chemical reactions and crystallization

Fig. 3 Miniaturized vessel for 1 ml reaction fluid with ultrasonic transducers at the center of the glass container

Results:

Monitoring of the (normalized) amplitude and the velocity of ultrasound reveals distinct variations. Initial features are caused by heating and gel formation. Variations observed at later times correlate to the crystallization process. This is demonstrated by x-ray diffraction analysis for samples collected during processing.

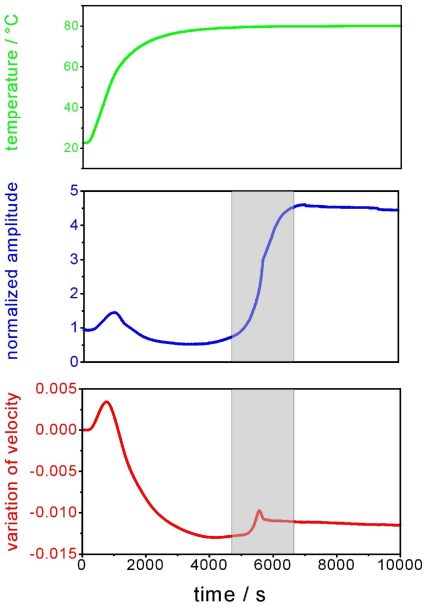

Fig. 4 Result of ultrasonic monitoring:
The gray region indicates the time range of the crystallization process.

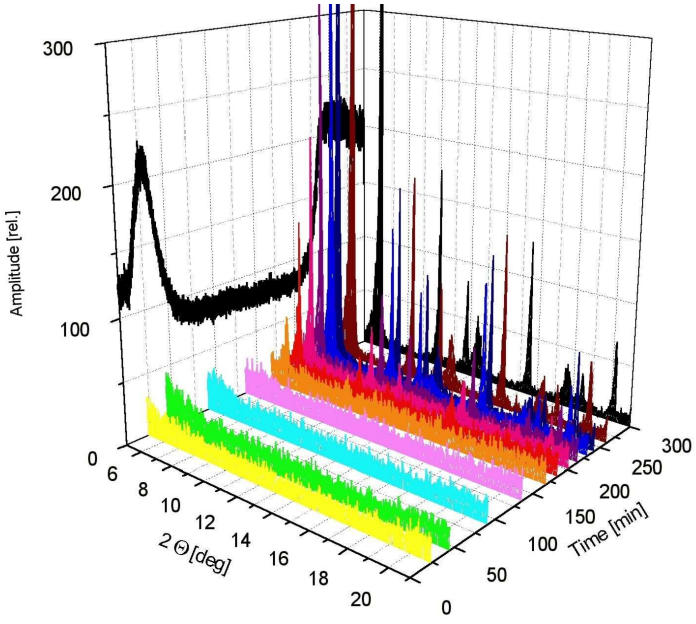

Fig. 5 Demonstration of the correlation between observed variations of the amplitude of the ultrasonic signal and x-ray diffraction analysis of samples collected at different reaction times. The variation of the amplitude for times up to 75 minutes relates to heating and gel formation. The final variation represents zeolite crystallization.

This work has been performed in cooperation with Astrium GmbH, DASA, TRICAT GmbH, and Universität Erlangen under support of ESA, ESTEC and DLR.

5.5 Confocal Light Microscopy

A new home-built confocal laser scanning microscope was constructed, which is designed to allow new contrast mechanisms. In addition, a commercial confocal Raman microsope and spectrometer was modified to allow diffraction-limited spatial resolution in Raman spectroscopy.

Microscope Lens: 100x/0.95NA
Samples: multi-layered GaN samples on sapphire substrates
Example: diffraction-limited scans with 200 nm resolution

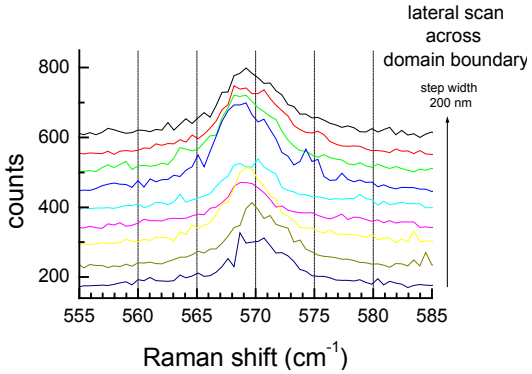

Fig. 1 Lateral scan across domain boundary

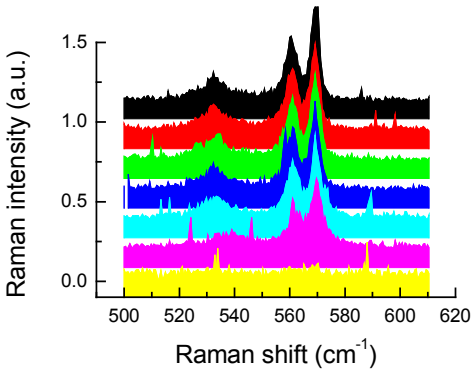

Fig. 2 Depth scan of Raman scattered light (sample B)

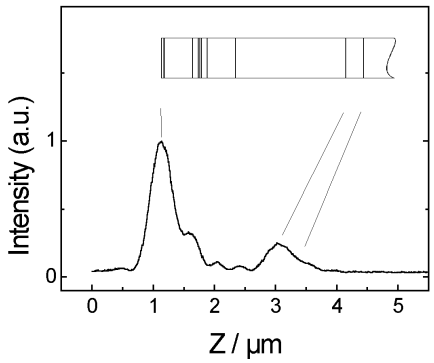

Fig. 3 Depth scan of reflected light (sample A)

Funding
Development of a Miniaturized Advanced Diagnostic Technology Demonstrator, European Space Agency

5.6 Nanooptics

PD Dr. R. Wannemacher

5.6.1 Plasmon Spectroscopy

Plasmon-Supported Transmission of Light through Small Holes in Conductive Screens

- Transmission of light through small holes in infinitely thin ideally conducting screens is proportional to r^6 (r=radius of the hole)
- Light transmission through small holes in a thin film of a real metal is strongly influenced by the excitation of surface plasmon polaritons
- transmission through the hole increases with increasing wavelength in certain wavelength ranges

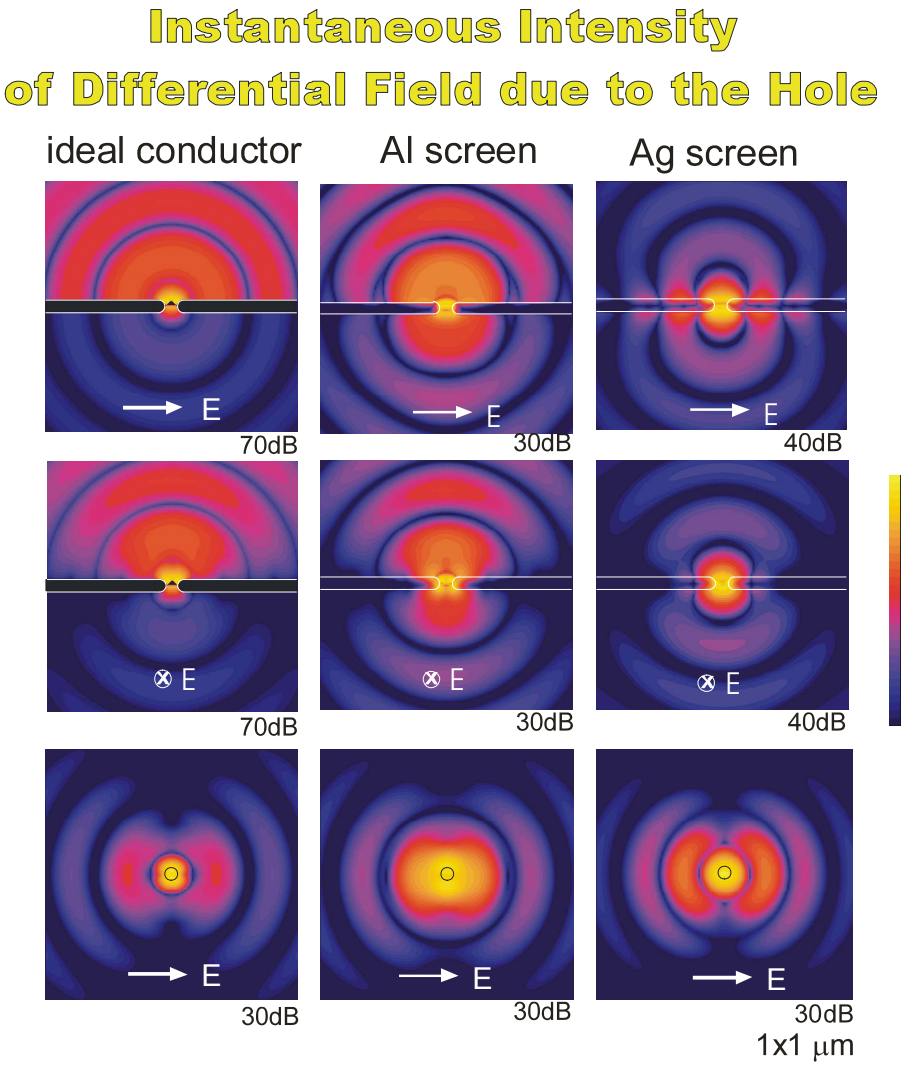

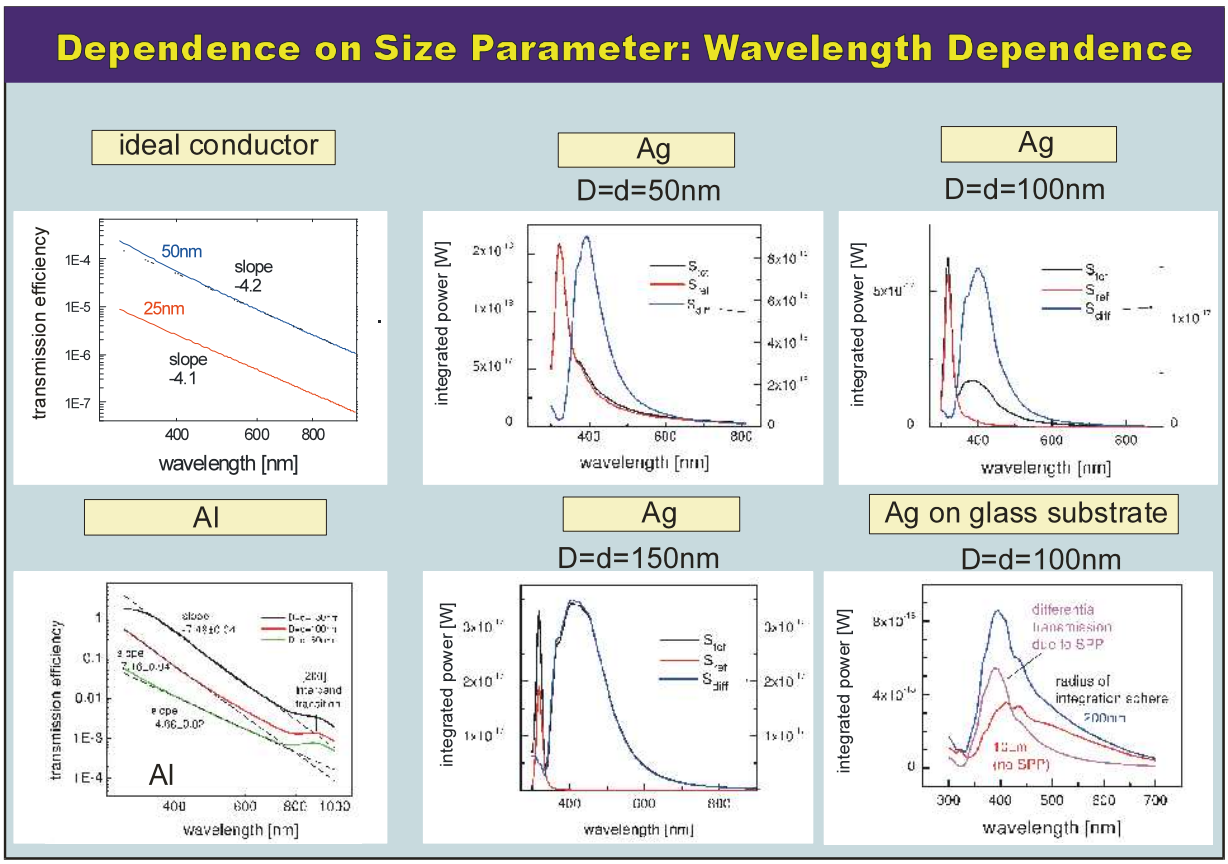

MMP calculation of transmission spectra of small holes in metallic thin films

R. Wannemacher, Opt. Commun. **195**, 107-118 (2001)

5.6.2 Failure of Local Mie Theory: Optical Properties of Colloidal Aggregates

- The optical spectra of colloidal aggregated metallic nanoparticles have been calculated in local approximation, i.e. with a local dielectric function of the metal.
- We have shown, that, when the incident light is polarized parallel to the dimer axis, a surface plasmon polariton (SPP) is excited, which is strongly localized to the contact point of the dimer.
- This SPP dominates the optical properties of the dimer and is related with extremely high electric field in the contact region
- It causes very slow convergence in aggregate Mie theory, such that very high multipolar orders are required to describe the existence of the SPP, in spite of the small size (≅nm) of the particles.
- This result is unphysical, because the finite compressibility of the electron gas and the related excitation of longitudinal bulk plasmons near the contact point strongly damps the highly localized SPP.
- A nonlocal dielectric function *must* therefore be used.
- Convergence is significantly improved in nonlocal aggregate Mie theory. Still, relatively high multipolar orders are required in order to describe correctly the remnants of the highly localized SPP. A calculation of the optical spectra of aggregated metal particles in the approximation of local dipole-dipole interactions is therefore not appropriate.

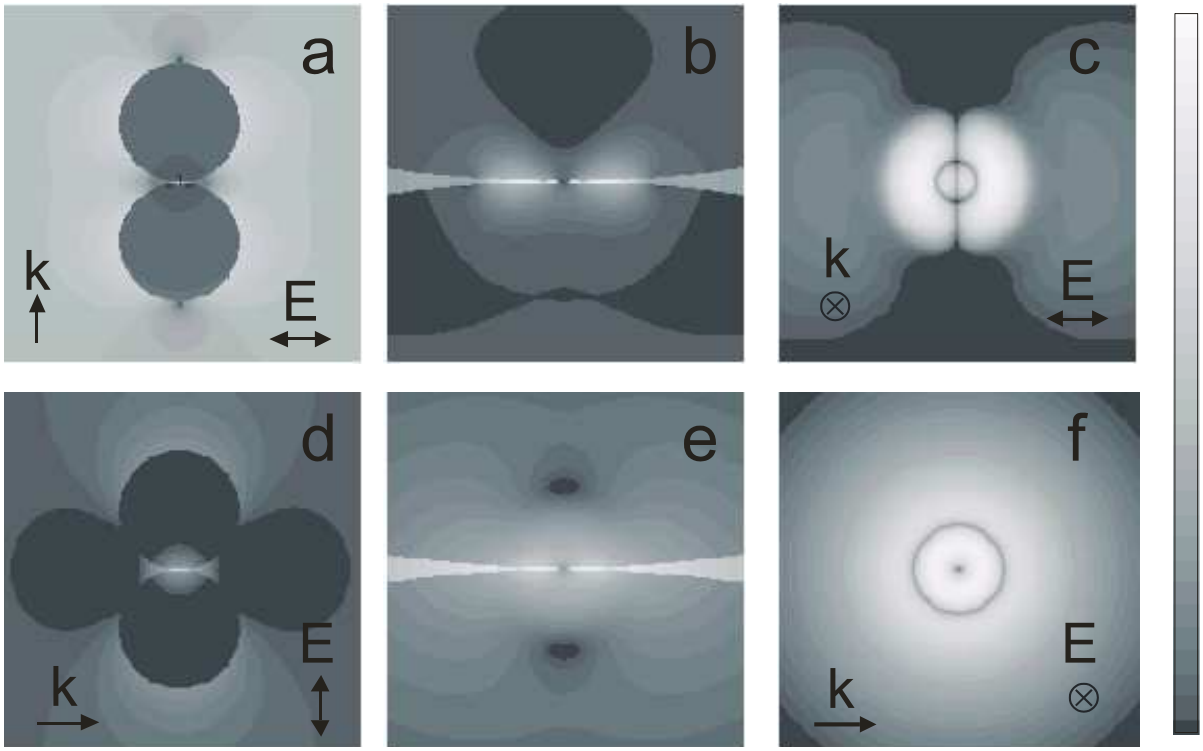

Fig. 1 Highly localized surface plasmon polariton near the contact point of a metallic nanodimer (Local MMP calculation).

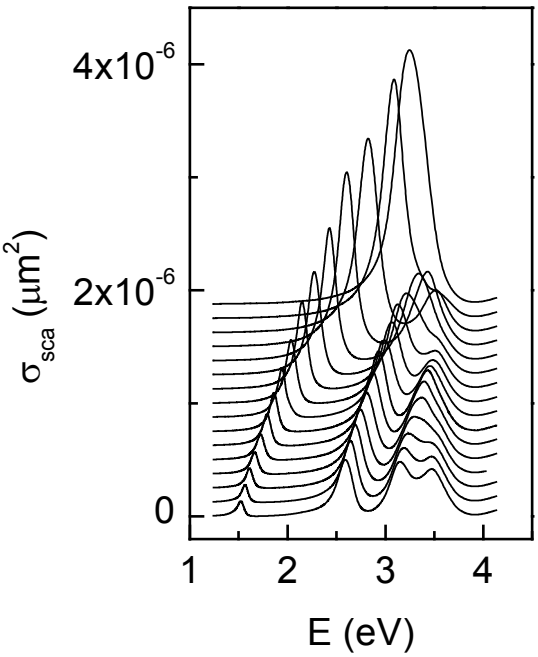

Fig. 2 Extremely slow convergence of the optical spectra of aggregated metal particles within local Mie theory: Scattering cross sections for a contacting dimer of spherical silver particles of radius a = 5 nm, excited by a plane wave polarized parallel to the dimer axis. The values shown were calculated by local aggregate Mie theory with a cut-off multipole order of 1 (top spectrum) and 2 to 30 in steps of 2 (following spectra from top to bottom). For clarity the spectra are shifted by a constant amount.

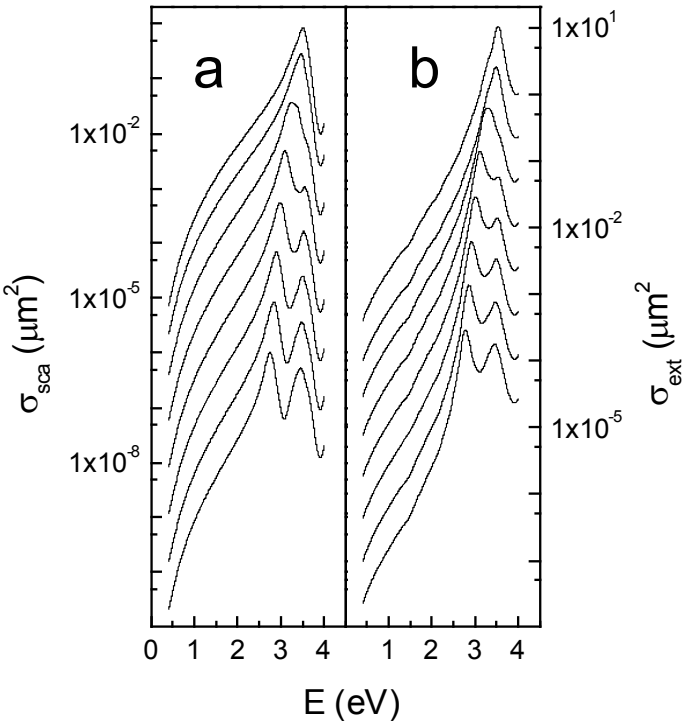

Fig. 3 Converged optical scattering and extinction spectra of a dimer of metallic nanoparticles as a function of the interparticle distance calculation by nonlocal aggregate Mie theory (Cut-off multipole order 20).

A. Pack, M. Hietschold, R. Wannemacher, Opt. Commun. **194**, 277-287 (2001)

5.6.3 Laser Microstructuring and Scanning Microscopy of Plasmapolymer/Silver Composite Layers

- Laser irradiation causes thermally induced coalescence of metallic nanoparticles in silver/plasmapolymer composite thin films.
- The coalescence changes the transmission spectra of the thin films.
- This can be used to produce unusual diffractive microoptical elements.

Optical properties of a Fresnel lens written in a silver/plasmapolymer composite thin film in different wavelength regions. The double focus, typical for a Fresnel lens is clearly visible. A 'dark focus' exists in the long wavelength range.

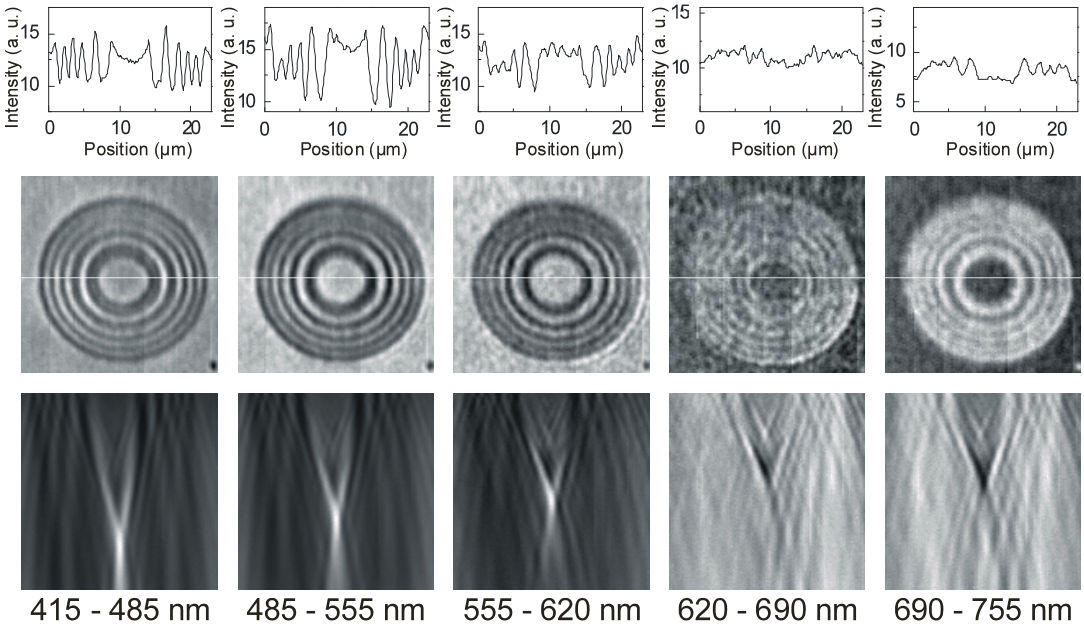

Generation of the structures by laser scanning microscopy. Detection by white-light scanning microscopy.

Funding
Project 'Spectroscopy of Plasmons', supported by Deutsche Forschungsgemeinschaft

J. Martin, A. Kiesow, A. Heilmann, R. Wannemacher, Appl. Opt. **40**, 5726-5730 (2001)

5.6.4 Interaction of Semiconductor Nanodots with Microcavities

Photons confined in hollow microspheres

Incorporation of CdSe quantum dots into a thin (<1 μm) surface shell of polymer microspheres ($R \cong 2$–4 μm) is achieved. The room-temperature emission spectra of single, hollow microcavities show several, spectrally well-separated cavity modes in the red-orange spectral range which have been assigned to high-Q whispering gallery modes (WGM) with radial quantum number n=1 and high angular quantum number l. An enhancement of the cavity finesse Q by a factor of about 10 with respect to CdSe-doped bulk polymer microspheres is found.

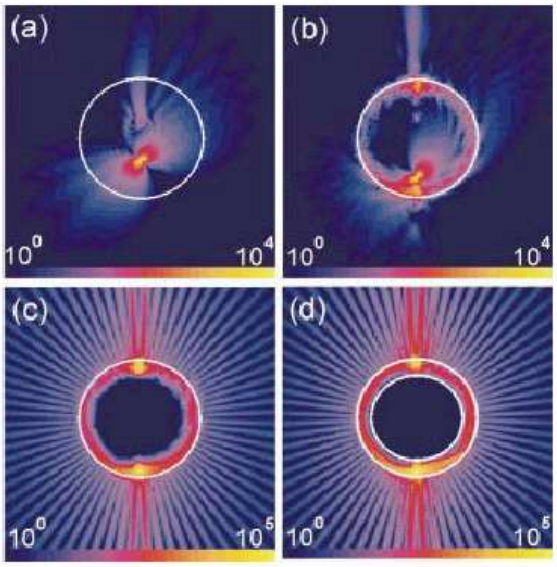

FIG. 1. (Color) Calculated electromagnetic field distribution in and outside a spherical microcavity containing a single emitting dipole at distance r from the center of the sphere. The dipole is in resonance with a cavity mode (TM^1_{36}) of (a)–(c) a bulk PMMA sphere of radius $R=2.77$ μm and index of refraction $n=1.5$, resonance wavelength 619.22 nm, $r=1.0$ μm (a), 1.8 μm (b), and 2.5 μm (c), and (d) for a hollow PMMA sphere (same cavity mode TM^1_{36}, resonance wavelength 618.88 nm) with same outer radius of $R_{ou}=2.77$ μm, an inner radius $R_i=2.108$ μm, $r=2.5$ μm, and same index of refraction. In all images the dipole is oscillating under 45° to the radial direction. Plotted is the time-averaged Pointing vector $|\langle S\rangle|$ on arb. logarithmic scale.

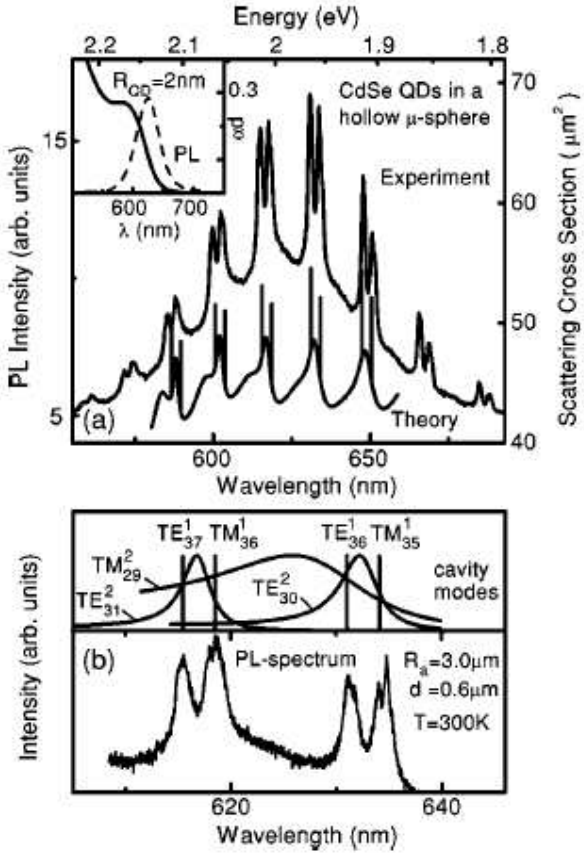

M. V. Artemyev, U. Woggon, R. Wannemacher
Appl. Phys. Lett. **78**, 1032 (2001)

FIG. 3. (a) Room-temperature emission spectrum of a single, hollow sphere of $R_{ou}=3\pm0.25$ μm outer radius and $d=0.6\pm0.1$ μm shell thickness excited by an Ar-ion laser. For comparison the calculated cross section of light scattering is shown for a hollow PMMA sphere (refractive index of $n=1.5$) of outer and inner radii $R_{ou}=2.781$ μm and $R_i=2.267$ μm. The inset shows the room temperature absorption (solid line) and luminescence spectra (dashed line) of CdSe quantum dots of 4 nm in diameter before embedding. (b) Room temperature photoluminescence spectrum obtained with higher instrumental resolution in the spectral range around 630 nm showing the dominant excitation of the $n=1$ cavity modes. To assign the cavity modes to TE/TM, l and n, the cavity modes are calculated and plotted in the upper part (normalized to same intensity).

Light Trapped in a Photonic Dot

Microspheres Act as a Cavity for Quantum Dot Emission. Optical microcavities that confine the propagation of light in all three dimensions (3D) are fascinating research objects to study 3D-confined photon states, low-threshold microlasers, or cavity quantum electrodynamics of quantum dots in 3D microcavities. A challenge is the combination of complete electronic confinement with photon confinement, e.g., by linking a single quantum dot to a single photonic dot. Here we report on the interplay of 3D-confined cavity modes of single microspheres (the photonic dot states) with photons emitted from quantized electronic levels of single semiconductor nanocrystals (the quantum dot states). We show how cavity modes of high cavity finesse are switched by single, blinking quantum dots. A concept for a quantum-dot microlaser operating at room temperature in the visible spectral range is demonstrated. We observe an enhancement in the spontaneous emission rate; i.e., the Purcell effect is found for quantum dots inside a photonic dot.

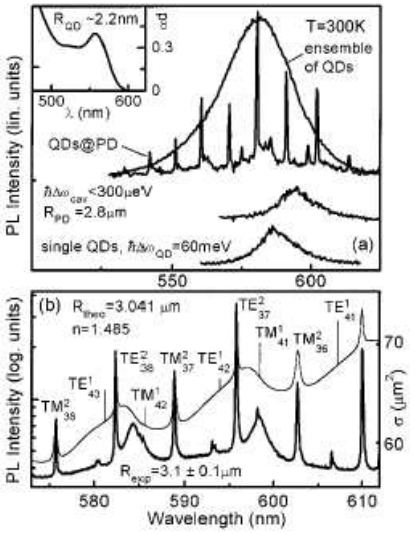

Figure 2. (a) Room-temperature emission spectra of quantum dots before and after attaching them to a single photonic dot. Plotted are the spectra for an ensemble of QDs, single QDs, and an ensemble of QDs incorporated in a thin surface shell of a PD. Inset: Absorption spectrum of the QD ensemble. The QD emission is excited nonresonantly by a focused Ar-ion laser ($\lambda = 488$ nm, $I_{pump} = 50$ W/cm^2) and detected by use of a microscope objective with a numerical aperture of 0.95, an imaging spectrometer and a CCD camera ($\sim$0.4 μm spatial resolution, $\sim$0.08 nm spectral resolution) for a single PD selected by a pinhole. (b) Emission spectrum of a $R_{PD} = 3.1$ μm PD taken with a factor of 4 higher spectral resolution for the spectral range around 595 nm (thick line). For the experimental cavity, Q values of $\sim$7500 have been determined. For comparison, the calculated scattering cross section σ characterizing the cavity eigenmodes is shown (thin line). The most pronounced PD eigenstates are labeled by their quantum numbers TE/TM, l and n. Within the detected spectral window the quantum numbers vary between $l = 32$ and $l = 42$ with $n = 1, 2$ for the sharp modes while modes with $n \geq 3$ form the weak background.

Purcell effect: modification of spontaneous emission rate

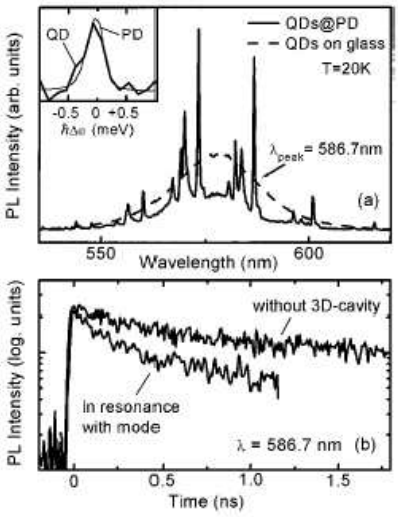

Figure 6. (a) Low-temperature emission spectra of a high-Q QDs@PD-structure and a reference ensemble of CdSe QDs on glass prepared under identical experimental conditions. Inset: Spectral line widths at $T = 20$ K measured in a separate experiment with highest spectral resolution for a representative single CdSe QD and a representative PD mode. (b) Dynamics of radiative emission measured at $T = 20$ K at 586.7 nm after excitation by a 120 fs pulse at 445 nm (frequency-doubled Ti:Sa laser). The emission is detected spatially and spectrally and is temporally resolved using a microscope objective (spatial resolution 0.5 μm), an imaging spectrometer (spectral resolution 0.1 nm), and a Streak camera (time resolution 20 ps). For the CdSe QDs on glass a monoexponential decay is found with a radiative lifetime of 1.1 ns, for QDs on PD a decrease in decay time is observed, resulting in fast initial decay with 220 ps.

M.V. Artemyev, U. Woggon,
R. Wannemacher, H. Jaschinski,
W. Langbein, Nanolett. 1, 309 (2001)

5.6.5 Laser Cleaning and Laser Nanostructuring

Field Enhancements in the vicinity of Polystyrene Spheres on a Silicon Substrate (MMP calculation)

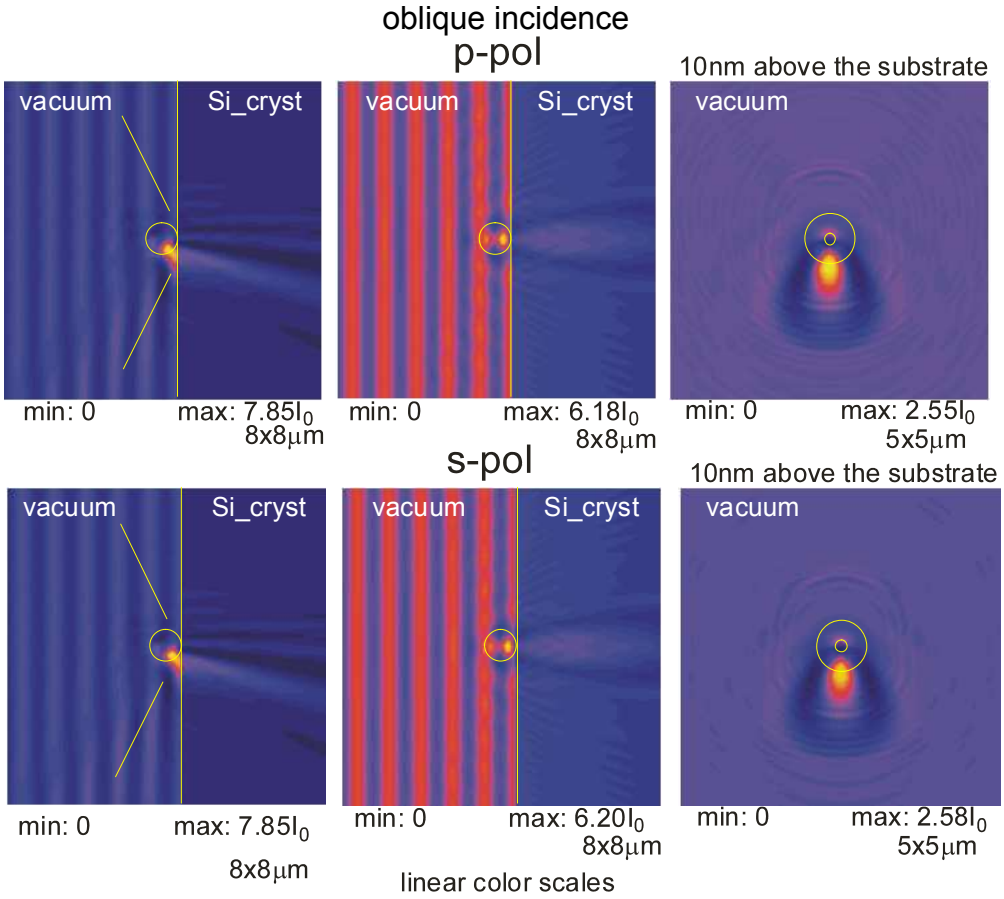

Silicon wafers for the production of integrated electronic circuits may be cleaned by irradiation with picosecond and femtosecond lasers.

Laser irradiation of dust particles produces strong intensity enhancements in the near field of the dust Particles, which, in turn can lead to laser ablation of the particle.

Field enhancements can be employed for laser nanostructuring of substrate surfaces

5.7 Optical spectroscopy of $CuInX_2$–ZnX (X = Se, S) mixed crystals and III-V mixed crystals

V. Riede

5.7.1 Characterization of laser deposited $Zn_{2(1-x)}Cu_xIn_xSe_2$ ($0 \leq x \leq 1$) thin films: Raman scattering and band gap properties

Samples: Layers on Infrasil and GaP substrates using PLD (pulsed laser deposition) method with KrF excimer laser
(*Co-operation with Semiconductor Physics Group, University Leipzig)*
(*Co-operation with Institut für Mineralogie, Kristallographie und Materialwissenschaft, University Leipzig)*

Stoichiometry: Determined with:
- Energy dispersive X-ray analysis (EDX)
  (*Co-operation with Semiconductor Physics Group, University Leipzig)*
- Rutherford backscattering (RBS) and particle induced X-ray emission(PIXE)
  (*Co-operation with Division of Nuclear Solid State Physics, University Leipzig)*
- Microprobe

(*Co-operation with Institut für Mineralogie, Kristallographie und Materialwissenschaft, University Leipzig)*

Raman scattering: Argon ion laser (514,5 and 457.9 nm)

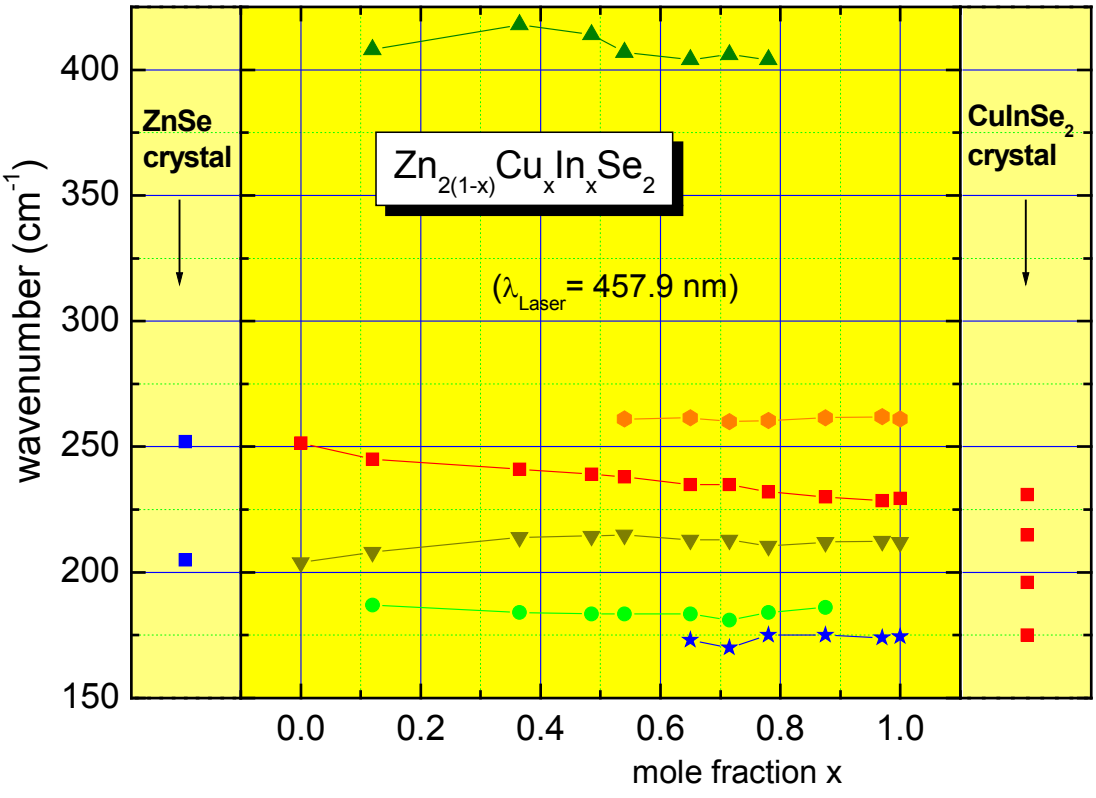

Fig.: Compositional dependence of lattice vibration modes

Results:

- End member modes in agreement with values of bulk samples
- Total symmetric A1 mode (175 cm^{-1}) disappears for $x \leq 0.65$:
- **Phase transition** from chalcopyrite to disordered zincblende structure at x=0.65
- Mode at 260 cm^{-1} is related to Cu-Se vibration
- Mode at 184 cm-1 exists only in mixed layers with a maximum of intensity at x=0.5

5.7.2 Transmission and reflectivity in the UV-VIS-NIR wavelength range

(from 200 to 2500 nm)

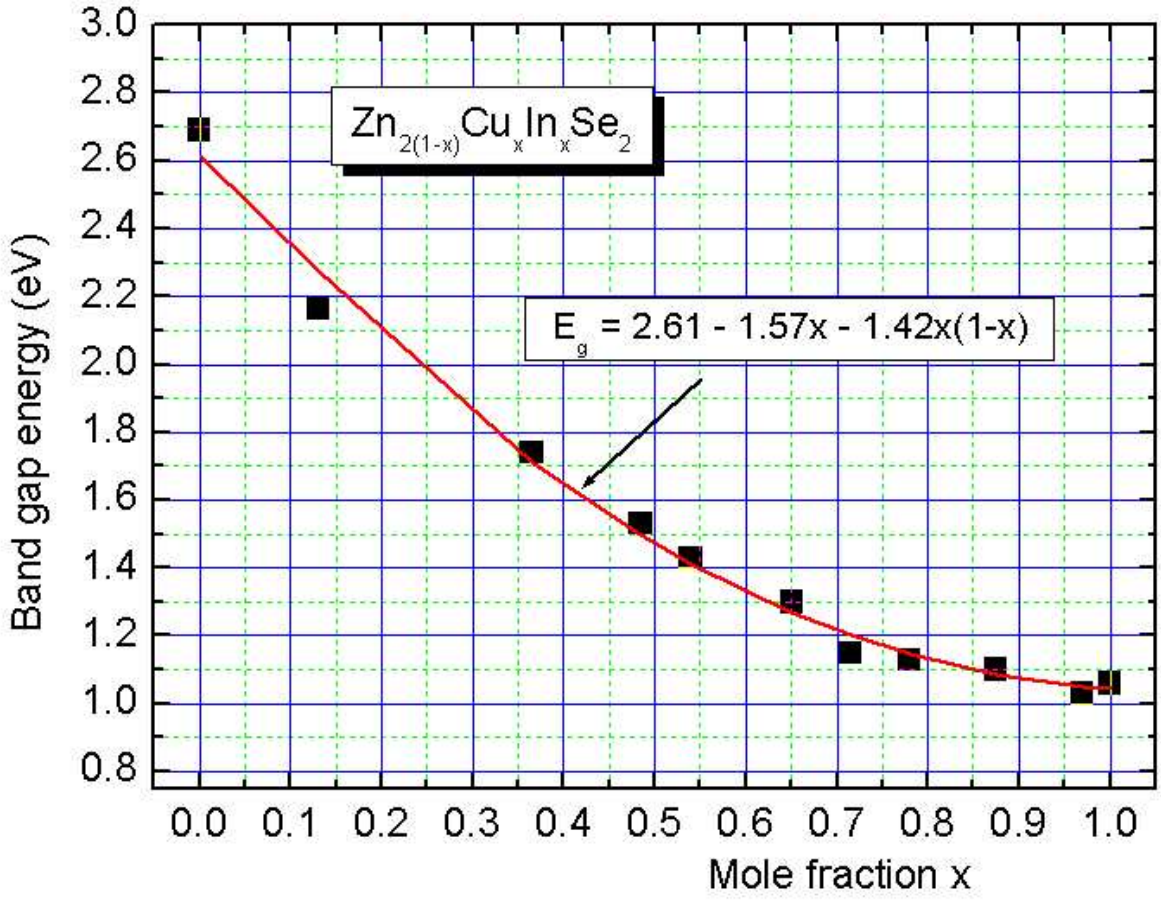

Fig.: Compositional dependence of energy gap

Results:

- Parabolic dependence of the band gap energy on the mole fraction
- No discontinuity at the phase transition

5.8 Analysis of group-III nitride device heterostructures

A. Kasic, M. Schubert

Infrared Spectroscopic Ellipsometry (IRSE, λ= 2 … 33μm) is used for measurement of free-carrier and crystal-structure properties of complex semiconductor heterostructures for device applications. Its excellence is demonstrated here by the IRSE data, best-fit spectra, and high-resolution TEM images shown below for a laser diode (LD) structure (Uni Bremen, Prof. Dr. Hommel) designed for blue-light emission. Concentration and mobility of *n*- and *p*-type free carriers, *n*-*p*-junction location, thickness, alloy composition, film strain, and crystal quality of device constituents are available upon the IRSE data analysis.

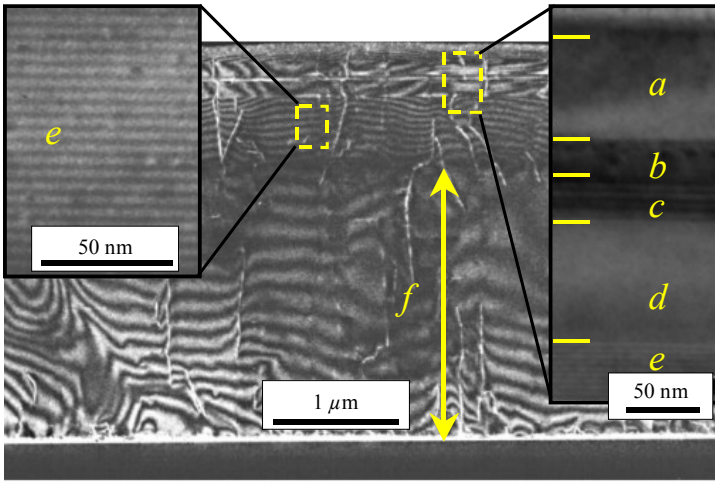

(TEM: Dr. G. Wagner, IOM Leipzig e.V.)

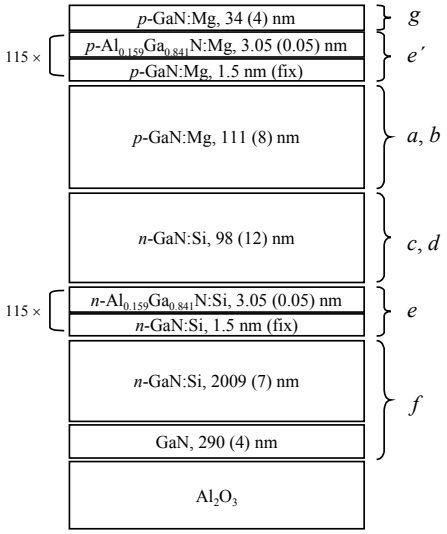

Above: TEM dark field images from parts of the LD structure [e: lower AlGaN/GaN SL; d & a: GaN waveguide; b: AlGaN *e*-blocking; c: InGaN/GaN SL; f: *n*-GaN base). The *p*-*n*-junction is located between *b*-*c*. Below: Experimental (circles) and best-fit (solid lines) IRSE Ψ and Δ spectra of the LD structure. Vertical arrows mark phonon modes of individual layers. Right: IRSE data analysis layer model with best-fit thickness results. Table: TEM and IRSE values for the *p*- (d_p = d_g+$d_{e'}$+d_a+d_b) and *n*-type (d_n = d_e+d_f) doped regions, the $Al_xGa_{1-x}N$/GaN SL period $d_{e/115}$, and the Al fraction *x* in the SL barriers. Free-carrier concentration *N* and mobility μ in the *n*- and *p*-type region as obtained from the IRSE data analysis.

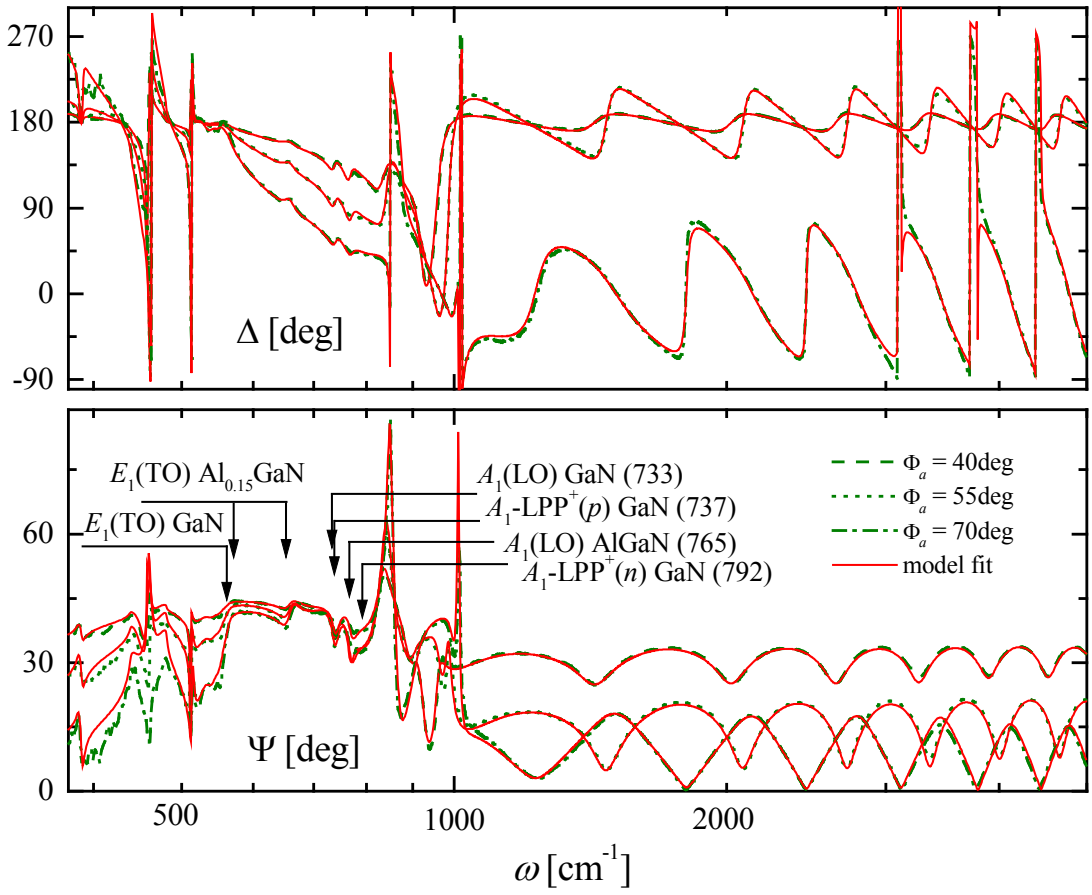

	IRSE	TEM
d_p [nm]	668 (±18)	665 (±7)
d_n [nm]	2920 (±17)	2879 (±29)
$d_{e/115}$ [nm]	4.55 (±0.05)	4.54 (±0.05)
x	0.159 (±0.002)	n.A.
N_e [cm^{-3}] $\times 10^{18}$	2.2 (±0.1)	n.A.
μ_e [cm^2/(Vs)]	184 (±5)	n.A.
N_h [cm^{-3}] $\times 10^{17}$	3.9 (±0.2)	n.A.
μ_h [cm^2/(Vs)]	22 (±4)	n.A.

n.A.: Not available from TEM.

Research supported by DFG Rh 28/3-2 in Schwerpunktprogramm SPP 1032 "Gruppe III-Nitride und ihre Heterostrukturen"

M. Schubert *et al.*, phys. stat. sol.(a) **228**, 437; SPIE Vol. **4449**, 8; Mat. Sci. & Eng. B **82**, 178.
A. Kasic *et al.*, Appl. Phys. Lett. **78**, 1526; J. Appl. Phys. **87**, 3720.

5.9 Critical point energies and phonon modes in GaInNAs, GaNP, and BGaAs semiconductor compounds

G. Leibiger, V. Gottschalch, M. Schubert, M. Grundmann

The quest for novel semiconductor compound materials suited for applications in novel opto-electronic device structures have directed investigations to the influence of N and B in Ga(In)As and GaP. Possible applications are long-wavelength laser diodes and solar cell materials. Crucial for understanding of material properties are optical investigations of direct band-to-band transitions energies, and phonon mode frequencies. Ga(In)NAs, GaNP and BGaAs layers were grown by metal-organic vapour-phase epitaxy, and studied by Spectroscopic Ellipsometry for photon energies from 0.035 to 8.9eV, in collaboration with the Center for Microelectronic and Optical Materials Research, University Lincoln, U.S.A. Second derivatives of the pseudodielectric function in the MIR-VIS-UV-DUV are shown in Figs. 1 and 2 for $GaN_{0.017}As_{0.983}$/ GaAs and $B_{0.016}Ga_{0.984}As$/GaAs, as example, compared to GaAs as reference, respectively.

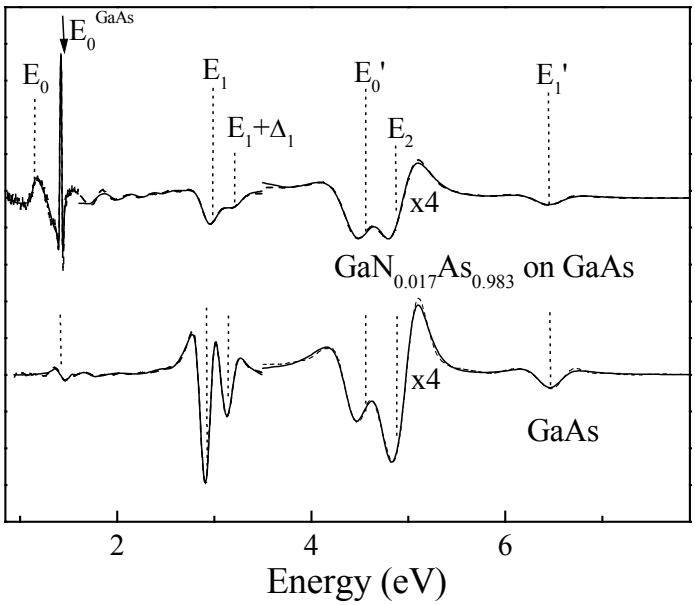

Fig. 1 Second derivative of the pseudodielectric function of a $GaN_{0.017}As_{0.983}$/ GaAs and a GaAs reference sample. Dashed and solid lines depict experimental and best-fit model spectra, respectively. The high-energy part of the spectrum (3.5 – 8eV) has been multiplied by a factor of 4. The spectrum of the $GaN_{0.017}As_{0.983}$/GaAs sample has been shifted for better comparison.

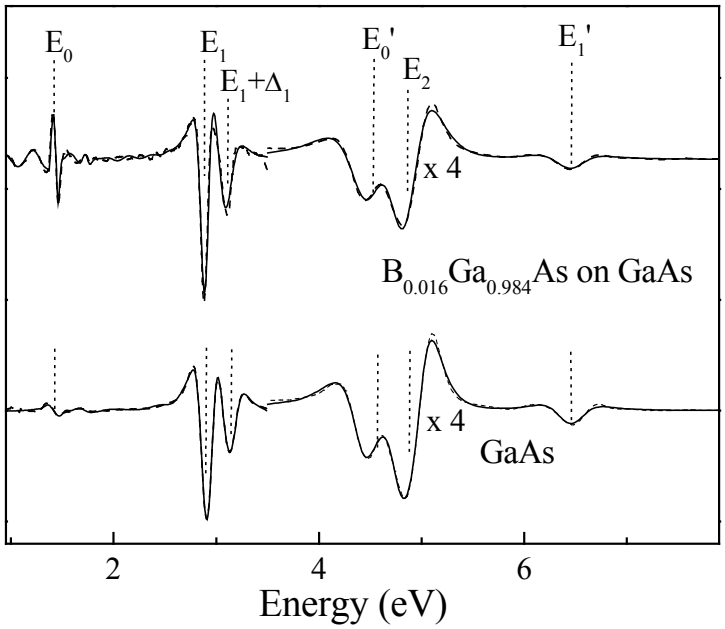

Fig. 2 Second derivative of the pseudodielectric function of a $B_{0.016}Ga_{0.984}As$/GaAs and a GaAs reference sample. Dashed and solid lines depict experimental and best-fit model spectra, respectively. The high-energy part of the spectrum (3.5 – 8eV) has been multiplied by a factor of 4. The spectrum of $B_{0.016}Ga_{0.984}As$/GaAs sample has been shifted for better comparison.

Vertical dotted lines indicate energies of direct band-to-band transitions. Whereas the fundamental band gap is strongly redshifted in GaAsN, almost no shift is seen in BGaAs, reflecting the different nature of the chemical bonds in the two alloys. The high electron negativity of nitrogen combined with a large lattice mismatch causes a strong short-range perturbation potential, which gives rise to strong localization effects. In contrast, the B-As bonding is almost homopolar. Thus the perturbation potential of boron is weaker causing only a small change of the bandstructure.

Research supported by DFG Rh 28/3-2, Go 129/4-1, NSF-DMI 9901510

G. Leibiger, V. Gottschalch, A. Kasic, M. Schubert, Appl. Phys. Lett. **79**, 3407.
G. Leibiger, V. Gottschalch, M. Schubert, J. Appl. Phys. **90**, 5951.
G. Leibiger, V. Gottschalch, G. Benndorf, R. Schwabe, M. Schubert, phys. stat. sol.(a) **228**, 279.
G. Leibiger, V. Gottschalch, M. Schubert, phys. stat. sol.(a) **228**, 259.
J. Sik, M. Schubert, G. Leibiger, V. Gottschalch, J. Appl. Phys. **89**, 294.
G. Leibiger, V. Gottschalch, B. Rheinländer, J. Sik, M. Schubert, J. Appl. Phys. **89**, 4927.

5.10 Far-infrared Magneto-Optic Generalized Ellipsometry: A new optical inert-mass scale for free charge carriers in matter

T. Hofmann, M. Schubert, M. Grundmann

A repeatedly recurring quest is the accurate measurement of the inert-mass of free charge carriers in matter as a function of frequency and momentum, in all materials' divisions. Atoms – the constituents of matter – contain electrons, some of which are free to move within correlated systems, when literally countless atoms compose to liquid or solid state materials. In semiconductors, free electrons – captured from their host sites – clear positive charges, which support "free-hole" transport just as for electrons. Attracted by electric fields free charge carriers drift, upon acceleration, with their peculiar mobility between regions of different potentials, being dressed with an effective mass according to the law of inertia. Coulomb attraction forces staggering allegiance of the free charge carriers to electromagnetic radiation, with inert-mass and mobility depending on frequency and momentum. No distinction can be made from optical absorption and reflection measurement alone between their density (N), inert mass (m), and mobility (μ), nor can the sign of the charge q be read.

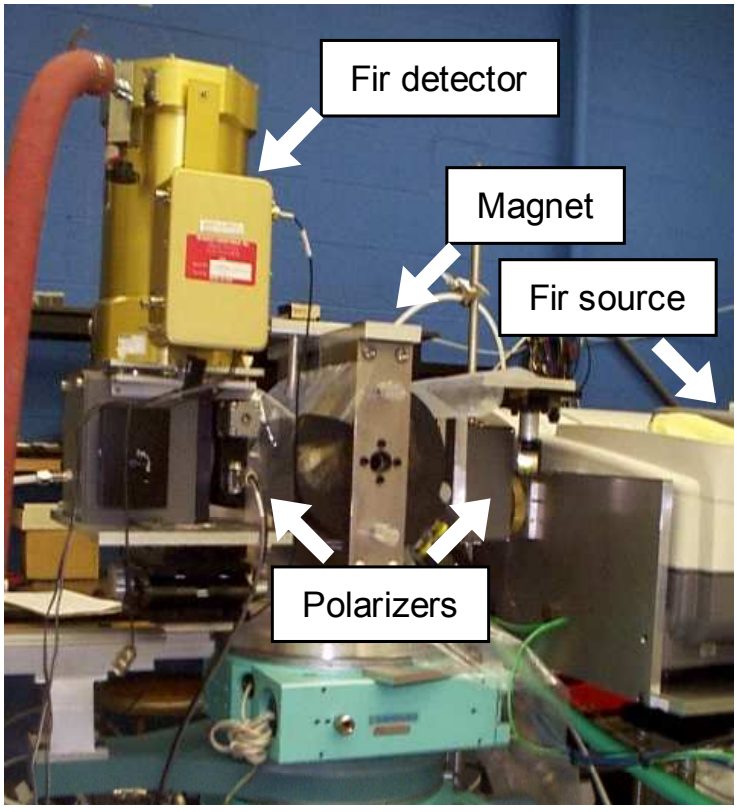

Fig.1. The first FIR-Magneto-Optic Ellipsometer (FIR-MO-GE), equipped with a He-cooled bolometer detector.

In a magnetic field, the carriers are diverted by the Lorentz force, an axial vector, which is sensitive to the sign of q, and which cause birefringence proportional to their inert-mass. The dielectric response at optical wavelengths is than a complex tensor, predicted by the Drude theory. Its first complete measurement at infrared

wavelengths was performed in collaboration with the Center for Microelectronic and Optical Materials Research at the University of Nebraska-Lincoln, U.S.A. The FIR-MO-GE setup is shown in Fig.1. We have recently developed a new global approach to anisotropic materials – Generalized Ellipsometry – for measurement of materials' complex dielectric function tensor elements, and fir-MO-GE spectra for *n*-type GaAs are shown in Fig. 2. The best-fit (solid lines) revealed the minus sign for the carrier type, the free charger carrier concentration *N*, their room-temperature mobility μ and effective (inert) mass *m* in excellent agreement with results from traditional experiments such as Shubnikov-de-Haas effect measurements, and with uncertainty limits of less than 1% only. FIR-IR-MO-GE is thereby demonstrated as optical "inert"-mass scale for semiconductor compound materials.

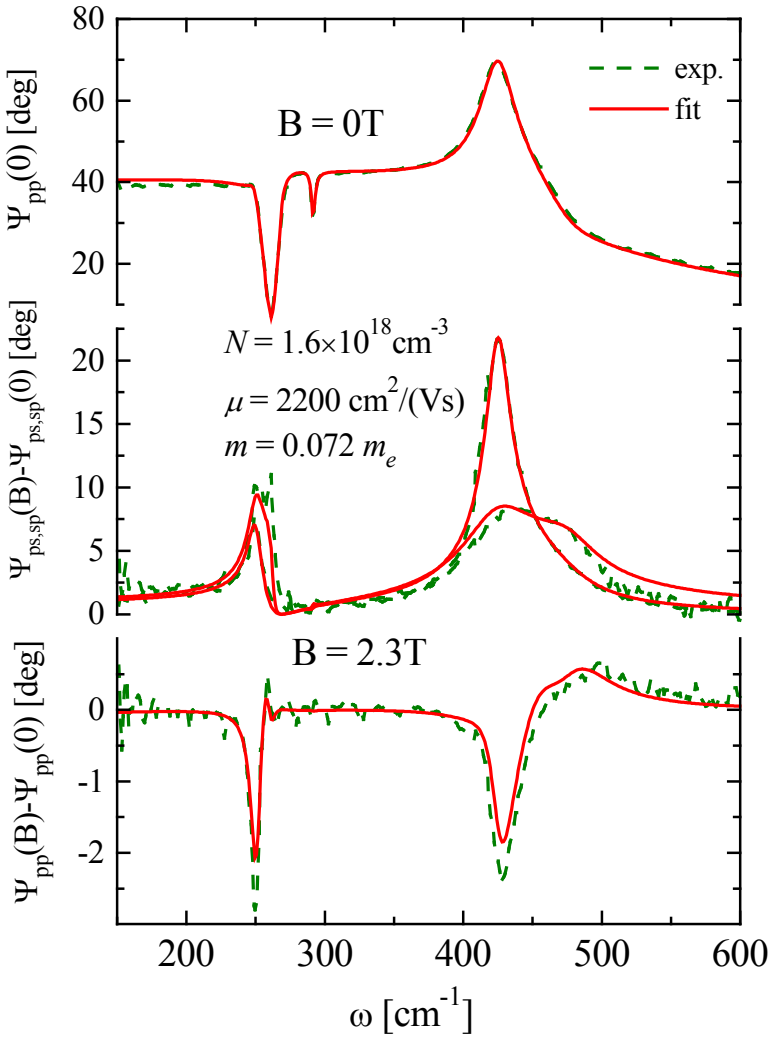

Fig. 2. Fir-MO-GE spectra for *n*-type GaAs.

Research supported by NSF-DMI 9901510

5.11 Infrared dielectric anisotropy and phonon modes of wurtzite ZnMgO semiconductor compounds

C. Bundesmann, N. Ashkenov, Beri N. Mbenkum, V. Riede, M. Schubert, M. Lorenz, M. Grundmann

The ionic crystal ZnO possesses many attracting properties for applications in vision and display devices because it can host sufficient free carriers but maintain high transparency at visible wavelengths. ZnO films may eventually replace indium tin oxide as transparent electrode materials, a challenging idea because resources of indium are currently becoming depleted worldwide. New research interest is now focused on the wide-band gap properties of ZnO-related compounds, such as ZnMgO, for possible use in semiconductor heterostructures, paving the road to ever-shorter wavelength emitter and detector designs. Fundamental properties of this novel alloy include phonon modes, free-carrier properties, and dielectric anisotropy at long wavelengths, which we have explored by Infrared Spectroscopic Ellipsometry, Hall effect, and Raman scattering measurements.

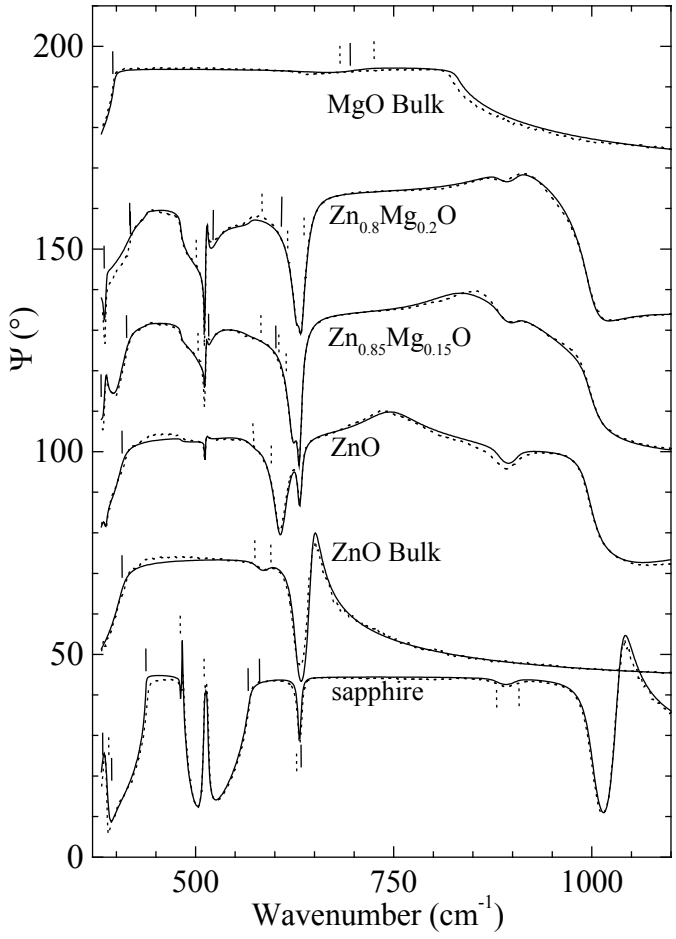

Fig. 1: Ellipsometric Ψ-Spectra of ZnO, MgO, sapphire, and ZnMgO thin films on c-plane sapphire. The dotted curves are the measured spectra; the solid curves are the best-fit model calculations. Vertical lines indicate the transverse (dotted lines) and longitudinal (solid lines) optical phonon mode frequencies.

The ZnMgO thin films were grown on c-plane sapphire by pulsed laser deposition (PLD).

Figure 1 depicts spectra of the ellipsometric parameter Ψ of sapphire, ZnO, MgO, and ZnMgO thin films. The composition dependences of the phonon modes are sketched in Figure 2. Future research will cover the influence of Al and Ga in ZnO and related compounds for design of semiconductor heterostructure constituents.

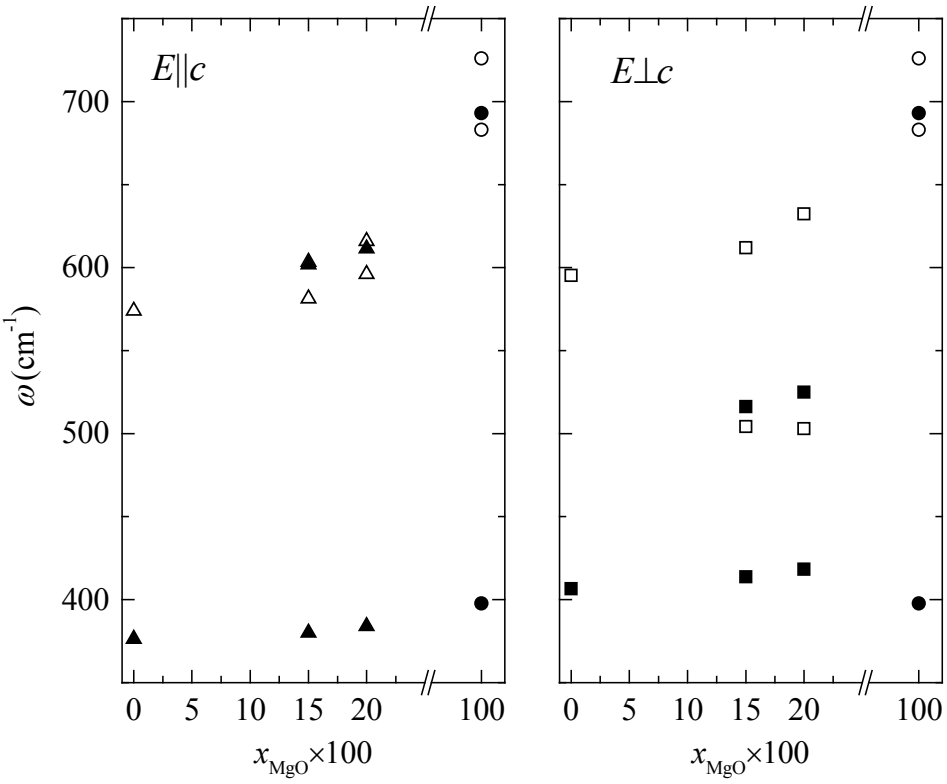

Fig. 2: Optical phonon modes of $Zn_{1-x}Mg_xO$ compounds for light polarized parallel (left panel) and perpendicular (right panel) to the *c*-axis. Solid and open symbols indicate transverse and longitudinal optical modes, respectively.

5.12 Optical properties of helically sculptured dielectric films

E. Schubert, H. Neumann, M. Schubert

A new class of designed matter is about to emerge upon sculpturing solid-state materials in thin film form. Such techniques involve physical deposition techniques in three-dimensional growth regimes, where, depending on growth parameters and appropriate substrate rotation, “zig-zag” pattern, “S”-shapes or helices can be deposited. Design dimensions can be well within the nanometer region, providing interesting grounds for new applications such as micro-filters, micro-antenna arrays, micro-springboards, or “frozen” liquid crystals for chiral optical filters. Crucial for design is the choice of the right dimensions, because electrical and optical properties will depend on confinement effects, such as form birefringence.

Fig. 1 High-resolution TEM image of a sculptured thin film consisting of TiO_2 helices, deposited on silicon. (Cross-section and samples are provided with kind support from Prof. Dr. Ian Hodgkinson and Matthew Arnold, Otago University, New Zealand).

Due to the complexity of such films, optical characterization is a challenge. A new global approach – Generalized Ellipsometry – was developed in our research group, for characterization of arbitrarily anisotropic materials in stratified media. This approach was extended to helical dielectric materials, and its first application is shown below in terms of measured and modelled data. The structure studied here was deposited on a rotating silicon substrate to achieve a “liquid-crystal-like” sculptured solid-state film. The high-resolution TEM cross-section reveals excellent coherency of the design structure, which was provided by Professor Dr. Ian Hodgkinson from the University of Otago, New Zealand. The ellipsometry data

provided the same geometry information, in addition to the inherent anisotropic optical constants, and shall become a general tool for exact measurement of sculptured thin film optical properties.

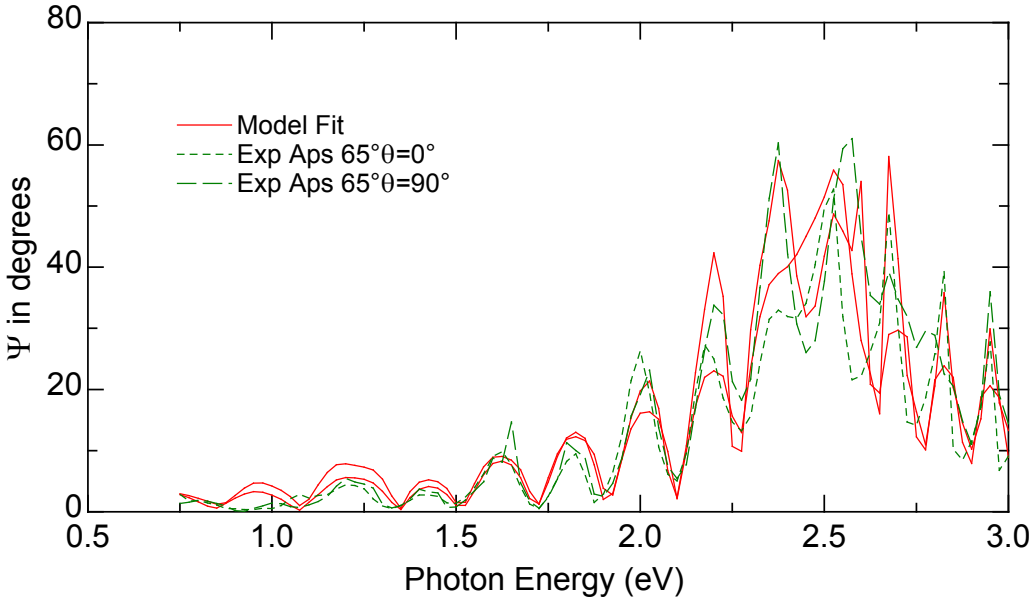

Fig. 2 Generalized Ellipsometry spectra Aps = ArcTan{r_{ps}/r_{pp}} from the sample to the left at 65° angle of incidence, and for two different sample in-plane azimuths θ. Best-fit (solid lines) model calculations of the experimental data (broken lines) provide non-destructive insight into geometry parameters such as the number of vertical rotations, and handedness of the helices, besides the anisotropic optical constants. The structure was designed with the chiral Bragg band to appear near $\hbar\omega \sim$ 2.5eV.

Research supported by SMWK-HWP3 and NSF-DMI 9901510

M. Schubert, C. M. Herzinger, phys. stat. sol.(a) **188**, 1563.

5.13 Funding

Microwave Heating Equipment
ESTEC-Studie, Dornier GmbH/DaimlerChrysler Aerospace Friedrichshafen
Prof. Dr. W.Grill

Development and Test of a Technology Demonstrator
Astrium GmbH/ Space European Space Agency Friedrichshafen
Prof. Dr. W.Grill

Development of a Miniaturized Advanced Diagnostic Technology Demonstrator „DIAMOND“ – Technology Study Phase 2“
ESTEC/DASA/Astrium GmbH(früher Dornier GmbH) Friedrichshafen
Prof. Dr. W.Grill

Functionally Graded Materials
in Schwerpunktprogramm „Gradientenwerkstoffe“
Deutsche Forschungsgemeinschaft GR 566/6-5
Prof. Dr. W.Grill

Spectroscopy of Plasmons
Deutsche Forschungsgemeinschaft Bo 935/15-1
Prof. Dr. von Borczyskowski, Prof. Dr. W.Grill (cooperative project)

Research and Development Contract SCHOTT Glas Mainz
Prof. Dr. W.Grill

Research and Development Contract Heidelberger Druckmaschinen AG
Prof. Dr. W.Grill

Verallgemeinerte Infrarot-Ellipsometrie von Kristallstruktur- und Ladungsträger-Effekten in komplexen Heterostrukturen von Gruppe-III Ntriden
Generalized Infrared-Ellipsometry of crystal-structure and free-carrier effects in complex group-III nitride heterostructures
Dr. M. Schubert, Dr. B. Rheinländer
Deutsche Forschungsgemeinschaft, Rh 28/3-2

Untersuchung elektronischer und gitterdynamischer Eigenschaften des Mischsystems $Zn_{2(1-x)}Cu_xIn_xS2$ (ZCIS)
Dr. Volker Riede
Deutsche Forschungsgemeinschaft Ri 756/2

Infrared ellipsometry capabilities for charaterization of III-V nitrides and ordered III-V semiconductors
M. Schubert
Subcontract in SBIR phase 2 grant of National Science Foundation (NSF), DMI9901510

5.14 External cooperations

Universities and Research Institutes
University of Erlangen (Zeolites)
University of Wroclaw, Poland (Ultrasound)
University of the Witwatersrand, Johannesburg, South Africa (Theory of Ultrasound)
University of Konstanz (Laser Cleaning, Total Internal Reflection Microscopy)
University of Dortmund (Nanooptics)
Fraunhofer Institute for Mechanics of Materials, Halle (Thin Films)
Research Center Rossendorf (Focussed Ion Beam Modification of Materials)
University of Lincoln, Nebraska, USA (Ellipsometry)
University of Linköping, Sweden (Ellipsometry)
University of Otago, New Zealand (Ellipsometry, sculptured thin films)
University of Bremen (III-Nitrides)
University of Stuttgart (III-Nitrides)
University of Paderborn (III-Nitrides)
University of Magdeburg (III-Nitrides)
University of München (III-Nitrides)
IOM Leipzig, e.V. (Ellipsometry, sculptured thin films)

Companies (Technology Transfer)
Access, Aachen (Ultrasound Monitoring of Solidification Processes)
Acoustix, Leipzig (Ultrasound Technology)
Tricat, Bitterfeld (Ultrasound Monitoring of Zeolite Crystal Growth)
Astrium GmbH, München (Ultrasound Technology)
Heidelberger Druckmaschinen, Heidelberg (Ultrasound Sensors)
Schott Glas GmbH, Mainz (Ultrasound Sensors)
Solarion GmbH, Leipzig (Solar Cells)
Honeywell GmbH, Glinde (Ultrasound Monitoring)
Joanneum Forschungsgesellschaft mbH, Austria (Ellipsometry)

5.15 Publications

5.15.1 Journals

J. Martin, A. Kiesow, A. Heilmann, R. Wannemacher
Laser Microstructuring and Scanning Microscopy of Plasmapolymer/Silver Composite Layers
Appl. Opt. **40**, 5726-5730 (2001)

M. V. Artemeyev, U. Woggon, R. Wannemacher
Photons confined in hollow microspheres
Appl.Phys. Lett. **78**, 1032-1034 (2001)

R. Wannemacher
Plasmon-Supported Transmission of Light through Nanometric Holes in Conductive Screens
Opt. Commun. **195**, 107-118 (2001)

J. Martin, L. Bischoff, R. Wannemacher
Microscopy of Ion-Beam Generated Fluorescent Color Center Patterns in LiF
Opt. Commun. **188**, 119-128 (2001)

M.V. Artemyev, U. Woggon, R. Wannemacher, H. Jaschinski, W. Langbein
Light trapped in a photonic dot: microspheres act as cavity for quantum dot emission
Nanolett. **1**, 309-314 (2001)

A. Pack, M. Hietschold, R. Wannemacher
Failure of Local Mie Theory: Optical Properties of Colloidal Aggregates
Opt. Commun. **194**, 277-287 (2001)

Phonon modes of $GaP_{1-y}N_y$ measured by mid-infrared spectroscopic ellipsometry
G. Leibiger, V. Gottschalch, A. Kasic, M. Schubert
Appl. Phys. Lett. **79**, 3407 - 3409 (2001)

Optical functions, phonon properties, and composition of InGaAsN single layers derived from far - and near -infrared spectroscopic ellipsometry
G. Leibiger, V. Gottschalch, M. Schubert
J. Appl. Phys. **90**, 5951 - 5958 (2001)

Ellipsometry on anisotropic materials: Bragg conditions and phonons in dielectric helical thin films
M. Schubert, C. M. Herzinger
phys. stat. sol.(a) **188**, 1563 - 1575 (2001)

Optical constants, critical points, free carrier effects, and phonon modes of GaAsN single layers and GaAsN/InAs/GaAs superlattices
G. Leibiger, V. Gottschalch, B. Rheinländer, A. Kasic, M. Schubert, J. Sik
IEEE (Proceedings, 27th Conference on Compound Semiconductors, Monterey, 2000)

Optical properties of AlxIn1-xN thin films determined by spectroscopic ellipsometry
A. Kasic, M. Schubert, B. Rheinländer, J. Off, F. Scholz, C. M. Herzinger
IEEE (Proceedings, 27th Conference on Compound Semiconductors, Monterey, 2000)

Phonon modes and critical points of GaNP
G. Leibiger, V. Gottschalch, G. Benndorf, R. Schwabe, M. Schubert
phys. stat. sol.(a) **228**, 279 - 282 (2001)

Phonon modes of InGaAsN measured by far infrared spectroscopic ellipsometry
G. Leibiger, V. Gottschalch, M. Schubert
phys. stat. sol.(a) **228**, 259 - 262 (2001)

Infrared Ellipsometry- a novel tool for characterization of group-III-Nitride Heterostructrues for electronic and optoelectronic device applications
M. Schubert, A. Kasic, S. Einfeldt, D. Hommel, U. Köhler, J. D. As, B. Kuhn, J. Off, F. Scholz, and J. A. Woollam
phys. stat. sol.(a) **228**, 437 - 440 (2001)

Spectroscopic Ellipsometry from 2 micro-m to 50 micro-m for nondestructive characterization of free-carrier and crystal-structure properties of III-V semiconductor device heterostructures
M. Schubert, A. Kasic, S. Einfeldt, D. Hommel, U. Köhler, J. D. As, B. Kuhn, J. Off, F. Scholz, J. A. Woollam, and C. M. Herzinger
SPIE Vol. **4449,** 8 (2001).

Infrared dielectric function and phonon modes of highly disordered $(Al_xGa_{1-x})_{0.52}In_{0.48}P$
T. Hofmann, G. Leibiger, I. Pietzonka, V. Gottschalch, M. Schubert
Phys. Rev. B **64**, 155206 1-11 (2001)

Disorder-activated infrared modes and surface depletion layer in highly Si-doped hexagonal GaN
A. Kasic, M. Schubert, B. Kuhn, F. Scholz, S. Einfeldt, D. Hommel
J. Appl. Phys. **87**, 3720 - 3734 (2001)

Infrared Ellipsometry characterization of porous silicon Bragg reflectors
S. Zangooie, M. Schubert, C. Trimble, D. W. Thompson, J. A. Woollam
Appl. Opt. **88**, 906 - 912 (2001)

Optical properties of amorphous and crystalline tantalum oxide thin films measured by IR-VIS-VUV (0.03eV-8.5eV) spectroscopic ellipsometry
E. Franke, M. Schubert, C.L. Trimble, J.A. Woollam
Thin Solid Films **388**, 283 - 289 (2001)

Band-gap energies, optical constants, phonons and free carrier properties in GaNAs/InAs/GaAs superlattice heterostructures measured by spectroscopic ellipsometry
J. Sik, M. Schubert, G. Leibiger, V. Gottschalch
J. Appl. Phys. **89**, 294 - 305 (2001)

Anisotropic dielectric function spectra from single crystal $CuInSe_2$ with orientation domains
A. Kreuter, K. Otte, G. Lippold, G. Wagner, A. Schindler, M. Schubert
Appl. Phys. Lett. **78**, 195 - 197 (2001)

IR-VUV Dielectric Function of $Al_{1-x}In_xN$ determined by spectroscopic ellipsometry
A. Kasic, M. Schubert, B. Rheinländer, J. Off, F. Scholz, C. M. Herzinger
Mat. Res. Soc. Symp. **639**, G6.13 (2001)

Optical Constants, Critical Points, and Phonon Modes of GaAsN Single Layers
G. Leibiger, V. Gottschalch, A. Kasic, B. Rheinländer, J. Sik, M. Schubert
Mat. Res. Soc. Symp. **639**, G6.35 (2001)

Strain and composition dependence of the E1(TO) mode in hexagonal $Al_xIn_{1-x}N$ thin films
A. Kasic, M. Schubert, J. Off, F. Scholz
Appl. Phys. Lett. **78**, 1526 - 1528 (2001)

Model dielectric function spectra of GaAsN for far-infrared and near-infrared to ultra violet wavelengths
G. Leibiger, V. Gottschalch, B. Rheinländer, J. Sik, M. Schubert
J. Appl. Phys. **89**, 4927 - 4938 (2001)

Infrared optical properties of aged porous GaAs
S. Zangooie, T. E. Tiwald, M. Schubert, J. A. Woollam
J. Mat. Res. **16**, 1241 - 1244 (2001)

Infrared response of multiple component free-carrier plasma in heavily doped p-type GaAs
S. Zangooie, M. Schubert, D. W. Thompson, J. A. Woollam
Appl. Phys. Lett. **78**, 937 - 939 (2001)

Phonons and free carriers in strained hexagonal GaN/AlGaN superlattices measured by Infrared ellipsometry and Raman spectroscopy
M. Schubert, A. Kasic, J. Sik, S. Einfeldt, D. Hommel, V. Haerle, J. Off, F. Scholz
Mat. Sci. & Eng. B **82**, 178 - 181 (2001)

Effective carrier mass and mobility versus carrier concentration in p- and n-type GaN determined by infrared ellipsometry and Hall resistivity measurements
A. Kasic, M. Schubert, B. Rheinländer, V. Riede, S. Einfeldt, D. Hommel, B. Kuhn, J. Off, F. Scholz
Mat. Sci. & Eng. B **82**, 74 - 76 (2001)

5.15.2 in press

Z. Kojro, J. Jahny, T. J. Kim, M. Schmachtl, and W. Grill
Scanning acoustic Doppler microscopy and scanning acoustic correlation microscopy
Ultrasonics

Optical phonon modes and interband transitions in cubic AlGaN
A. Kasic, M. Schubert, T. Frey, U. Köhler, D. J. As, C. M. Herzinger
Phys. Rev. B

Evolution of the optical properties of III-V Nitride alloys: Band-to-Band transitions in GaPN
G. Leibiger, M. Schubert, V. Gottschalch, G. Benndorf, R. Schwabe
Phys. Rev.

Infrared spectroscopic ellipsometry - a new tool for characterization of semiconductor heterostructures
A. Kasic, M. Schubert, S. Einfeldt, D. Hommel
Vibrational spectroscopy **179**, XXX - XXX (2002)

Effective carrier mass and phonon mode behavior in n-type hexagonal InN
A. Kasic, M. Schubert, Y. Saito, Y. Nanishi, G. Wagner
Phys. Rev. B XX XXXXXX-XXXXXX (2002)

Interband transitions in [001]-(GaP)1(InP)m superlattices
M. Schubert, H. Schmidt, J. Šik, T. Hofmann, V. Gottschalch, W. Grill, G. Böhm, G. Wagner
Mat. Sci. & Eng. B XX, XXX – XXX (2002)

All-Solid-State Electrochromic Multilayer Systems For Surface Heat Radiation Control
E. Franke, H. Neumann, M. Schubert, C. L. Trimble, J. A. Woollam
Surf. Coat. & Techn. XX, XXX (2002)

5.15.3 Invited talks

Ellipsometry on anisotropic materials- treatment of surface and interface layers
M. Schubert
256. Heraeus Seminar, Optical Spectrocopy at Interfaces (OSI), Bad Honnef, May 2001

5.15.4 Conference Contributions

(T: talk, P: poster)

Infrared ellipsometry
M. Schubert, A. Kasic
1. Int.Conference on Advanced Vibrational Spectroscopy, Turku, Finnland, August 2001 (P)

All-solid state electrochromic multiplayer systems for surface heat radiation control
E. Franke, M. Schubert, C. L. Trimble, J. A. Woollam
Spring European MRS-Meeting, Strasbourg, France, June 2001 (P)

Composition determination of InGaAsN using X-ray diffraction and far-infrared ellipsometry
G. Leibiger, V. Gottschalch, M. Schubert
4. Int. Conf. on Nitride Semiconductor Research, Denver, U.S.A., July 2001 (P)

Optical properties of GaNP
G. Leibiger, V. Gottschalch, G. Benndorf, R. Schwabe, M. Schubert
4. Int. Conf. on Nitride Semiconductor Research, Denver, U.S.A., July 2001 (P)

Generalized Infrared Ellipsometry- A novel tool for characterization of group -III-Nitride Heterostructrues
for electronic and optoelectronic device applications (P)
M. Schubert, A. Kasic, S. Einfeldt, D. Hommel, J. Off, F. Schloz, B. Kuhn, D. J. As, J. A. Woollam
4. Int. Conf. on Nitride Semiconductor Research, Denver, U.S.A., July 2001 (P)

Ellipsometrische Untersuchungen von Gitterschwingungen und Bandlückenenergien kubischer $Al_xGa_{1-x}N$-Filme
A. Kasic, M. Schubert, D. J. As
German Physical Society Spring Meeting, Hamburg, March 2001(P)

Characterization of III-Nitride optoelectronic-device heterostructures using infrared ellipsometry
A. Kasic, M. Schubert, S. Einfeldt, D. Hommel, J. Off, F. Scholz
Spring European MRS-Meeting, Strasbourg, France, June 2001 (P)

Optische Konstanten, Phononen-Eigenschaften und Zusammensetzung von InGaAsN Einzelschichten
G. Leibiger, M. Schubert, V. Gottschalch
German Physical Society Spring Meeting, Hamburg, March 2001 (P)

Untersuchung der Phononeneigenschaften von hochgradig ungeordnetem $(Al_xGa_{1-x})_{0.52}In_{0.48}P$ (0 .. x .. 1) mittels Ferninfrarot Spektralellipsometrie und Ramanspektroskopie
T. Hofmann, M. Schubert, G. Leibiger, V. Gottschalch
German Physical Society Spring Meeting, Hamburg, March 2001 (P)

Spectroscopic Ellipsometry from 2 mm to 50 mm for nondestructive characterization of free-carrier and crystal-structure properties of III-V semiconductor device heterostructures
M. Schubert, A. Kasic, S. Einfeldt, D. Hommel, J. Off, F. Schloz, B. Kuhn, D. J. As, J. A. Woollam, C. M. Herzinger
46. Annual SPIE Meeting, San Diego, U.S.A., August 2001 (T)

Interband transitions in (GaP)1/(InP)m monolayer superlattice structures grown on (001) InP
J. Sik, M. Schubert, T. Hofmann, H. Schmidt, G. Böhm, V. Gottschalch
Spring European MRS-Meeting, Strasbourg, France, June 2001 (T)

Verallgemeinerte Infrarot-Ellipsometrie - eine neue Charakterisierungsmethode für Halbleiter-Heterostrukturen
A. Kasic, M. Schubert
German Physical Society Spring Meeting, Hamburg, March 2001 (T)

Interband transitions in $(GaP)_1/(InP)_m$ monolayer superlattice structures grown on (001) InP
J. Sik, M. Schubert, T. Hofmann, H. Schmidt, G. Böhm, V. Gottschalch
German Physical Society Spring Meeting, Hamburg, March 2001 (T)

U. Woggon, M.V. Artemyev, B. Moller, W. Langbein, R. Wannemacher
Photons confined in 3D microcavities doped with quantum dots
MRS Fall Meeting, Symposium K: Microphotonics - Materials, Physics, and Applications
Boston, 26.-30.November 2001

U. Woggon, M.V. Artemyev, H. Jaschinski, A. Pack, R. Wannemacher
Photons Confined in 3D Microcavities Doped with Quantum Dots
Quantum Electronics and Laser Conference (QELS)
Baltimore, 5.-11. Mai 2001

5.16 Graduations

5.16.1 PhD

Stefan Knauth
Elektronenstrahlangeregter ballistischer Transport in metallischen Einkristallen

Michael Schmachtl
Meßverfahren zur Bestimmung der Wachstumsgeschwindigkeit bei gerichteter Erstarrung von metallen mit geführten Schallwellen

5.16.2 M.Sc.

Nurdin Ashkenov
Optical phonons in wurtzite InGaN, 30. September 2001

Yahia Elkuni
Nondestructive testing of metal rods

Bashkim Ziberi
Ultrasound Monitoring of the Synthesis of Zeolites in Real Time

5.16.3 B.Sc.

Beri N. Mbenkum
Optical phonon modes in zinc oxide, 25. September 2001

5.17 Awards

Special Prize of the Peter Jungen Holding
in the framework of the Innovation Prize of the City of Leipzig,
for the most successful business venture developed from University research
(Acoustix GmbH, Prof. Dr. W. Grill)

6 HLP — SCIENTIC ACTIVITIES

6.1 Inter-sublevel Transitions in Quantum Dots

K. Goede, A. Weber, M. Grundmann

We have studied the mid-infrared absorption properties of *quantum dots* consisting of InAs in a GaAs matrix [1]. Due to their size in the nm range, the electronic structure of these "artificial atoms" consists of narrow and well-defined energy levels for both electrons and holes instead of the usual band structure of semiconductors. The main focus [2,3] in quantum-dot research during the past years has been on interband transitions, i.e., transitions where electrons and holes recombine. Optoelectronic devices in the near-infrared range which utilize these transitions include lasers and radiation detectors. Because of their specific advantages, quantum-dot based optoelectronic devices can be expected to replace many standard quantum-well based devices within the near future [4].

However, also transitions which involve only one kind of charge carrier in the dots are possible, as for instance electrons can be excited or relax between different electronic sublevels. Understanding these intersublevel transitions in detail is both crucial for properly designing near-infrared devices as for developing new devices in the mid-infrared range (50 meV to 1 eV). *Radiative*, i. e., photonic, intersublevel spectra have been published [4] together with evidence that the radiation is already emitted in the laser mode. Yet, until now one cornerstone was missing: Direct, spectrally resolved observation of intersublevel transitions by utilizing *nonradiative*, i. e., phononic, relaxation of the electrons as signal.

We could observe such spectra by combining Fourier transform spectroscopy with Calorimetric Absorption Spectroscopy (CAS) at low temperatures (T = 4.25 K). With this novel technique FT-CAS, an interferogram of the sample heating by phonons is recorded and converted into a spectrum. These phonons are created by the relaxation of charge carriers previously excited due to absorption of mid-infrared radiation in the sample (see Fig. 1). Due to the thermal sample-detector contact, the sample heating also causes a temperature change of the resistance sensor which serves as measurement signal.

The quantum dots are charged with electrons because of the n-doping of the surrounding material. With increasing reverse bias applied to the diode structure of the sample, however, the dots are stepwise emptied. Capacitance-voltage measurements allow for an ascription of certain charging situations to bias voltage values. According FT-CAS spectra of the relative absorptance change as compared to 0 V bias are shown in Fig. 2. As the bias increases, the absorptance increases, shows a distinct peak for -4 V at 83 meV (FWHM 20 meV) and decreases again for higher bias. This behavior corresponds to the initial emptying of the *final* (excited quantum dot) state of the intersublevel transition making this transition possible, while later also the *initial* (ground) state of the transition is emptied which means that there remain no charge carriers in the dots which could be excited.
The bias-dependent *spectral* changes are due to few-paricle effects (electron-electron interaction) in both the electronic quantum dot ground state and the excited state. At -4V, there are two electons in a quantum dot. At -5V, however,

only one electron remains. This results in a lowered ground state energy for this electron and, accordingly, in a blueshift of the intersublevel transition energy, as is observed.

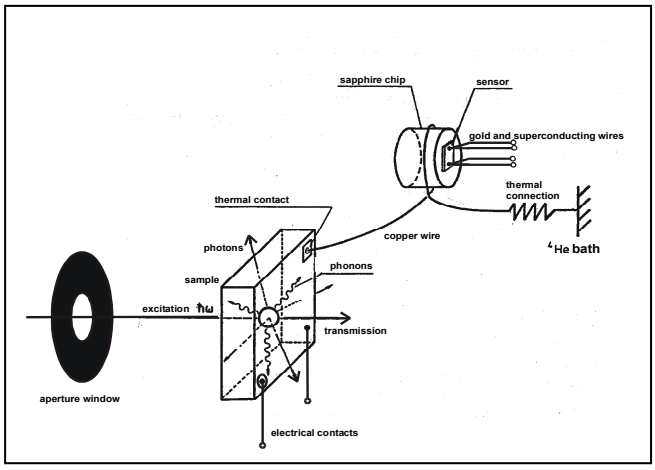

Fig. 1: Measurement scheme of Fourier transform Calorimetric Absorption Spectroscopy (FT-CAS). Incident radiation on the sample excites electrons which relax via photon or phonon emission. The phononic relaxation is detected by thermally contacting the sample to a separate, heat-sensitive detector.

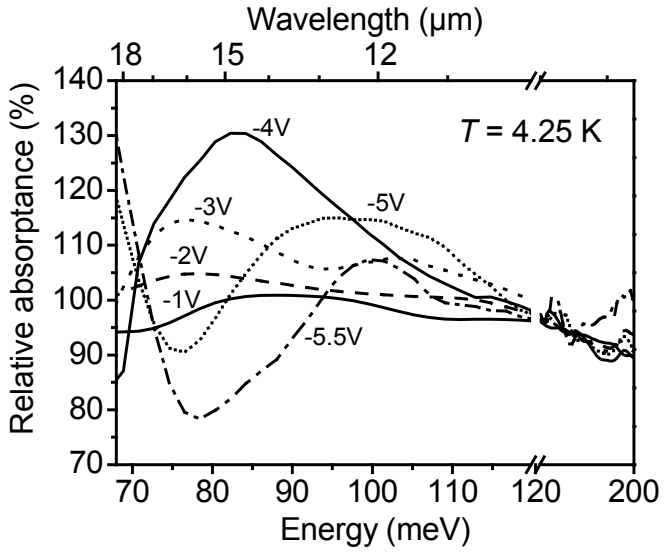

Fig. 2: FT-CAS measurements for different reverse bias voltages. Each curve has been divided by the curve for 0 V, thus showing only the relative change in the absorption caused by creating a certain quantum-dot charging situation.

[1] K. Goede, A. Weber, F. Guffarth, C. M. A. Kapteyn, F. Heinrichsdorff, R. Heitz, D. Bimberg, and M. Grundmann, Phys. Rev. B 64, 245317 (2001)
[2] D. Bimberg, M. Grundmann, and N. N. Ledentsov, Quantum Dot Heterostructures (Wiley, Chichester, 1999) and references therein
[3] M. Grundmann, Physica E 5, 167 (2000) and references therein
[4] M. Grundmann, A. Weber, K. Goede, V. M. Ustinov, A. E. Zhukov, N. N. Ledentsov, P. S. Kop'ev, and Zh. I. Alferov, Appl. Phys. Lett. 77, 4 (2000)

6.2 Bandstructure Theory Using Empirical Pseudopotentials

The bandstructure of binary and ternary semiconductor materials with potential applications, i.e., to substitution layer/host material systems /1,2/ and group-III-nitrides /3/, has been theoretically analyzed and calculated by means of the with experimental data well associable empirical pseudopotential (EPP) method.

6.2.1 Isovalent monolayers

H. Schmidt

By photoluminescence, absorption, and reflection measurements it has been experimentally shown that the optical properties of a semiconductor host material can be drastically modified by embedding two-dimensional isovalent substitution layers. Such substitution layer/host material systems with efficient excitonic transitions are expected to play a crucial role for next generation optical devices. We have calculated the bandstructure of the InP/GaP, GaP/InP, InAs/GaAs, and GaN/GaAs system by means of the EPP method and have discussed the dependence of the optical properties of the host material on the chemical and structural effects associated with the embedded two-dimensional isovalent substitution layer. Fundamental optical transitions are most efficient if charge carriers in the highest valence band state (VBM) and the lowest conduction band state (CBM) are localized around the ultrathin substitution layer. It has been theoretically shown that only for the InAs/GaAs system charge carriers in VBM and CBM are localized around the InAs substitution layer (Tab.1).

$\bar{\bar{\rho}}_{int}$(InP/GaP)	$GaP_{1,s}/GaP_{14,us}$	$InP_{1,s}/GaP_{14,us}$	$InP_{1,us}/GaP_{14,us}$
CBM	0.147	0.139	0.134
VBM	0.543	0.549	0.134
$\bar{\bar{\rho}}_{int}$(GaP/InP)	$InP_{1,s}/InP_{14,us}$	$GaP_{1,s}/InP_{14,us}$	$GaP_{1,us}/InP_{14,us}$
CBM	0.114	0.159	0.141
VBM	0.031	0.037	0.170
$\bar{\bar{\rho}}_{int}$(InAs/GaAs)	$GaAs_{1,s}/GaAs_{14,us}$	$InAs_{1,s}/GaAs_{14,us}$	$InAs_{1,us}/GaAs_{14,u}$
CBM	0.211	0.200	0.129
VBM	0.483	0.397	0.063
$\bar{\bar{\rho}}_{int}$(GaN/GaAs)	$GaAs_{1,s}/GaAs_{14,us}$	$GaN_{1,s}/GaAs_{14,us}$	$GaN_{1,us}/GaAs_{14,u}$
CB1	0.407	0.747	0.665
CBM	0.754	0.555	0.470
VBM	0.104	0.008	0.011

Tab.1 Double macroscopically averaged density distribution of charge carriers in the VBM and CBM around the substitution layer of the InP/GaP /1/, GaP/InP /2/, InAs/GaAs /1/, and GaN/GaAs /1/ system. Charge carriers are localized or delocalized around the substitution layer for $\bar{\bar{\rho}}_{int}$ >0.13 or $\bar{\bar{\rho}}_{int}$ <0.13, respectively.

By comparing the calculated electronic properties of the GaN/GaAs system with those of the InP/GaP, GaP/InP, and InAs/GaAs material system, we have found that GaN/GaAs which can be regarded as an ordered GaAsN alloy has anomalous electronic properties, e.g., not only *one* but the *two* lowest GaN/GaAs-conduction bands behave like eigenstates of the GaN substitution layer (Fig.1).

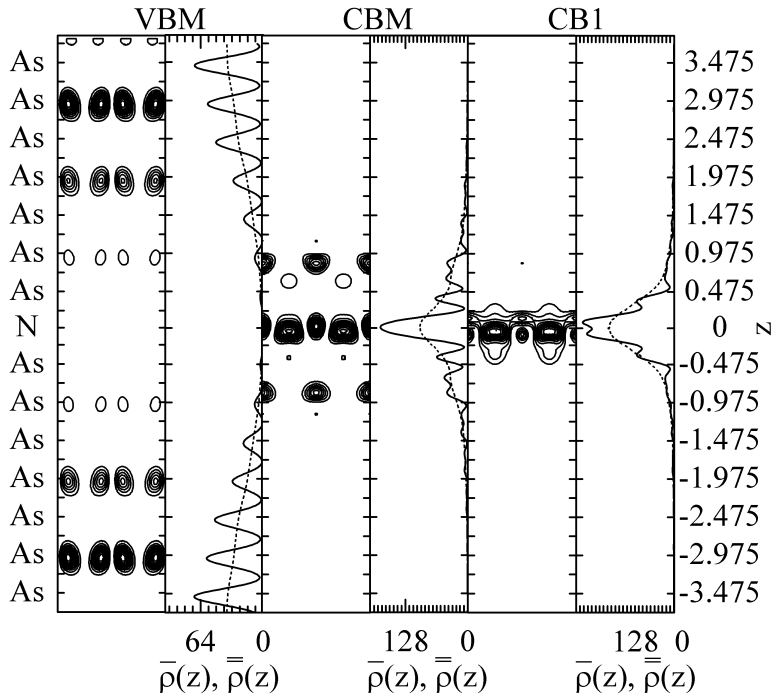

Fig.1. Γ-point probability function of charge density in the VBM (left panel), CBM (middle panel), and second lowest conduction band (CB1, right panel) in units of *e* per unit cell of the GaN/GaAs structure. The panels left columns depict the contour plot of $\rho(z)$ of two unit cells in the (110) plane. The right columns present the integral electronic charge density $\bar{\rho}(r)$ (solid line), spatially averaged over the x and y direction, i.e., over the (110) plane, and the macroscopical averaged charge density $\bar{\bar{\rho}}(r)$ (scattered line).

We have investigated the origin of the two lowest conduction band states in the GaN/GaAs system in detail and have found some similarities with respect to the origin of the *two* lowest (defect) levels which appear in the bandgap of the anomalous GaAsN alloy material in the conduction band region. For the two lowest conduction bands in the GaN/GaAs system we have demonstrated that the localization and the shift into the GaAs-bandgap is caused by the structural and chemical effect associated with the embedded N atomic layer /1/, respectively.
N atoms are also the anionic constituents of group III-nitrides which have been demonstrated to be very promising for high power and high speed electronic applications. In order to improve the performance level of device simulations, the determination of material parameters, e.g., transition energies and effective masses, becomes a major issue.

/1/ H. Schmidt, R. Pickenhain, G. Böhm
Chemical and structural effects of two-dimensional isovalent substitutions in A(III)-B(V) semiconductors
Phys. Rev. B 65 (2002) 0453231-04532312.

/2/ M. Schubert, H. Schmidt, J. Šik, T. Hofmann, V. Gottschalch, W. Grill, G. Böhm, G. Wagner
Interband transitions in [001]-$(GaP)_1(InP)_m$ superlattices
Mater. Sci. Eng. B 00 (2001) XXXX1-XXXX4, in press.

6.2.2 Wurtzite-type nitrides

H. Schmidt, D. Fritsch

We have determined the EPP parameters of the ionic potentials for *wurtzite-type* GaN, InN, and AlN on the basis of a simple empty core model by fitting experimental low-temperature transition energies of nine *zincblende-type* binary materials (Ga,In,Al/As,P,N). The obtained ionic potentials are identical for common ion types and have been used in our EPP *wurtzite-type* bandstructure calculations as well /3/. For the screening of the ionic potentials we have taken the model dielectric function $\varepsilon(q)$ derived from Levine and Louie /A/ where anisotropic screening, e.g. in wurtzite materials, can easily be incorporated.

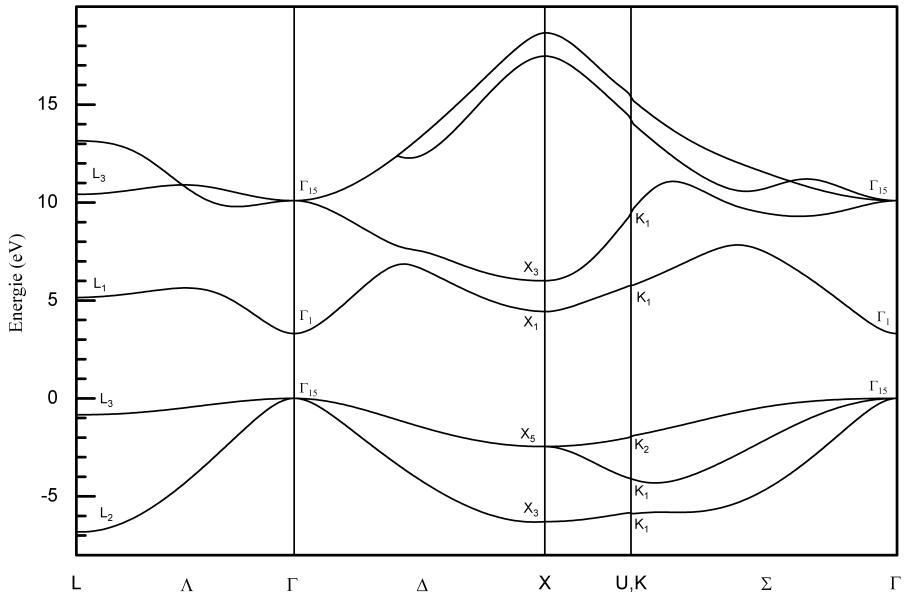

Fig.2. Energy dispersion of β-GaN along special lines in the zincblende Brillouin zone.

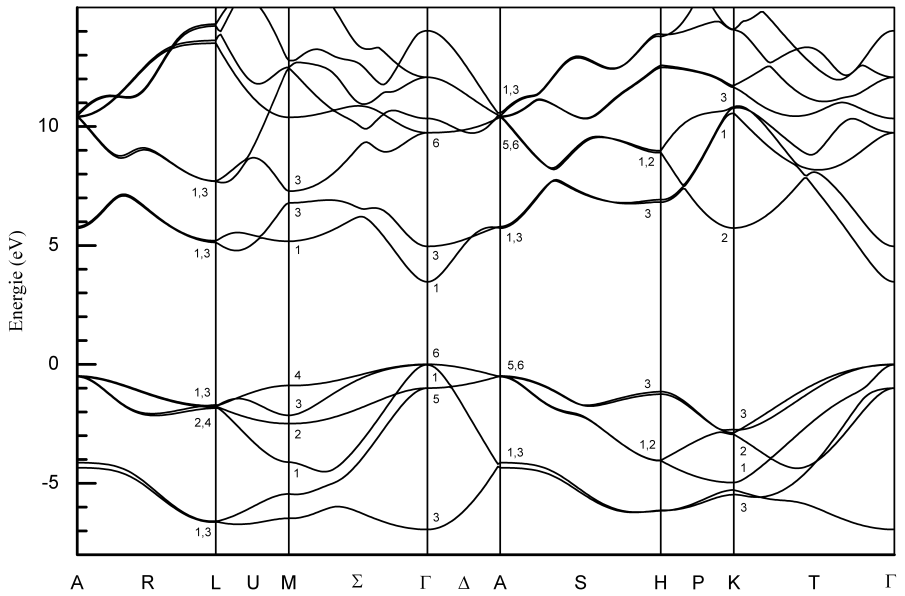

Fig.3. Energy dispersion of α-GaN along special lines in the wurtzite Brillouin zone.

As a result, we have dealt in detail with the anisotropy of important band structure parameters of wurtzite GaN, InN, and AlN. The determined Luttinger-like parameters A_i, i=1..7, are crucial to the design of wide-gap nitride-based semiconductor devices. By calculating the parameter A_7 which describes the nonparabolicity of valence bands of wurtzite-type nitrides in the (kx,ky)-plane and is generally assumed to be zero we were able to point out that especially for InN and GaN A_7 is non-negligible.
The bandstructures calculated on the basis of the fitted pseudopotential parameters (Figs. 2. and 3.) and the effective masses derived from the bandstructures demonstrate the structural transferability of our EPP parameters for the group-III-nitrides /1/.

Furthermore, we have demonstrated by means of EPP calculations with anisotropically and artificially isotropic screened ionic potentials that for wurtzite GaN and AlN the anisotropy of the static dielectric function is of little importance. For wurtzite InN we suggest that the anisotropy of the static dielectric function is substantial and that this anisotropy has to be taken into account for example by analyzing plasma reflection measurements.

Because the EPP method can be used for bandstructure calculations of both covalent and ionic semiconductors, the advantages of our program for fitting pseudopotential parameters and of the implemented anisotropic screening of the ionic pseudopotentials will be exploited for the determination of structural transferabel pseudopotentials for Zn, Mg, Cd, O, Te und S from experimentally determined transition energies and deformation potentials of MgO und CdO in rocksalt structure, of ZnO, MgS, and CdS in wurtzite structure and of ZnTe, MgTe, CdTe, and ZnS in wurtzite and zincblende structure. The Zn, Cd, Mg, and O potential parameters will then represent the basis for highly needed bandstructure calculations of the transparent conducting oxides (Zn,Cd,Mg)O.

/1/ D. Fritsch, H. Schmidt, M. Grundmann
Empirical pseudopotential (EPP) calculations of effective-mass parameters of wurtzite-type GaN, InN, and
AlN
DPG-Tagung Regensburg, März 2002, FV Halbleiterphysik, Themenkreis: (6) III-V-Halbleiter, Veröffentlichung in Vorbereitung
/A/ Z.H. Levine and S.G. Louie, Phys. Rev. B 25 (1982) 6310.

6.3 Photocurrent Spectroscopy of Nanostructures

H. Schmidt, H. von Wenkstern

InAs monolayers (1-1.7 ML) embedded in GaAs can effectively bind Frenkel-like excitons in the perpendicular direction and have efficient optical heavy hole (hh)-e- and light hole (lh)-e-transitions below the GaAs bandgap. Despite the fact that the theoretically predicted extension of the hh-, lh-, and e-wave function into the GaAs host material lets expect a sizeable Quantum Confined Stark Effect (QCSE) for 1 and 1.7 ML InAs, up to now possible electro-absorption effects in the InAs-ML/GaAs system have not yet been experimentally investigated. In order to study the QCSE in the InAs-ML/GaAs system, we have performed photocurrent (PC) measurements on Au/n-GaAs Schottky diodes containing single 1 or 1.7 ML InAs in the intrinsic GaAs

region at 4 K under a variation of the external bias voltage in the perpendicular direction /1,2/. The investigated layer samples were grown pseudomorphically by low pressure metal-organic vapor phase epitaxy (MOVPE) on $5 \cdot 10^{16}$-$1 \cdot 10^{18} cm^{-3}$ Te-doped (001) GaAs substrates misoriented 2° toward the (011) direction. Before growth, the substrates were cleaned from oxides by thermal heating. Trimethylgallium (TMGa), Trimethylindium (TMIn), and arsine were used as precursors for the epitaxial layers which are nominally undoped. Prior to the InAs-ML growth, a GaAs buffer layer of about 200 nm thickness was deposited. The 1-1.7 ML InAs were capped with a GaAs layer of about 40 nm thickness. In the following our samples containing 1 or 1.7 ML InAs are referred to as S1ML and S2ML, respectively.

Experimental Results Typical PC spectra measured on the S1ML sample at 4 K in the energy range from 1.4 to 1.6 eV under an increase of the applied forward bias from 0.15 V to 0.68 V are represented in Fig. 1.

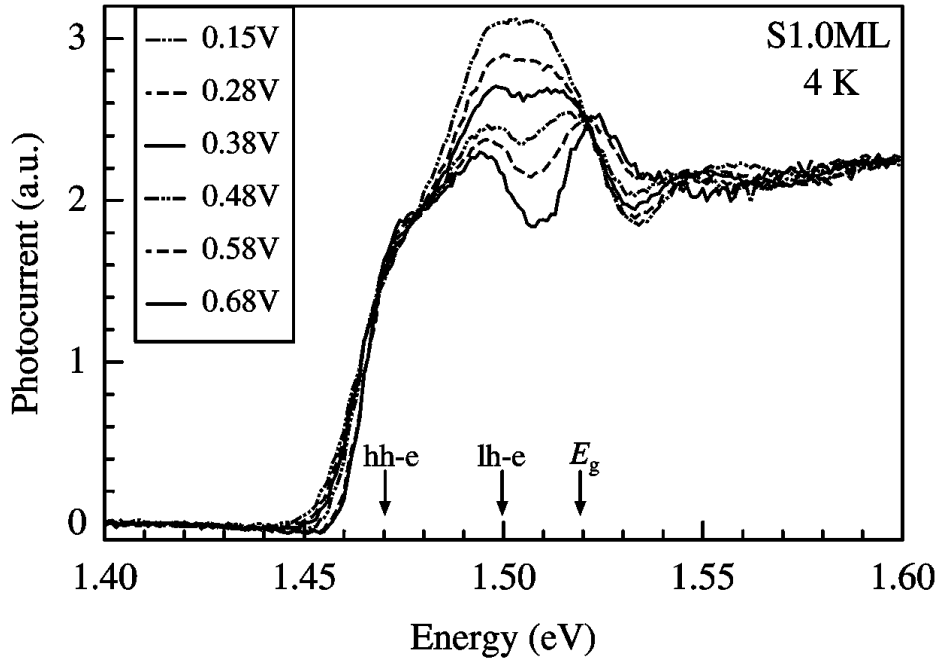

Fig.1. Photocurrent spectra of S1.0 ML measured under various biases at 4 K. The 0.68 V-spectrum clearly shows the hh-e- and lh-e-transitions measured in the zero-field case.

As expected the optical hh-e- and lh-e-transitions which are close to the fundamental bandgap of GaAs (E_G) contribute to the spectral PC feature below E_G . It should be noted that under a bias of 0.68 V the flat band case is nearly reached and that the 0.68 V-spectrum of S1ML clearly shows the hh-e- and lh-e-transition measured in the field case 50 and 20 meV below E_G, respectively. For reverse biases the spectra clearly exhibit damped Franz-Keldysh oscillations (FKO) above E_G and a spectral feature around E_G. The FKO and CV measurements yield the electric field strength as a function of the applied bias in the reverse bias case and the forward bias case, respectively. It should be noted that the spectral features around E_G, i.e., the bias dependent feature C-DAP and E_1 and the FKO of the GaAs host material E_2 and E_3 complicate the evaluation of the hh-e- and lh-e-transition for higher reverse biases.
In order to clarify the physical origin of the spectral feature around E_G, we first modelled the PC spectra of the reference sample which did not contain the ML InAs.
Afterwards, the information we gained from the reference sample was used to investigate the spectra of S1ML and S2ML. By way of example the modelling

procedure of the PC spectra of S2ML measured under +0.6 V and -2.0 V is illustrated in Fig. 2.

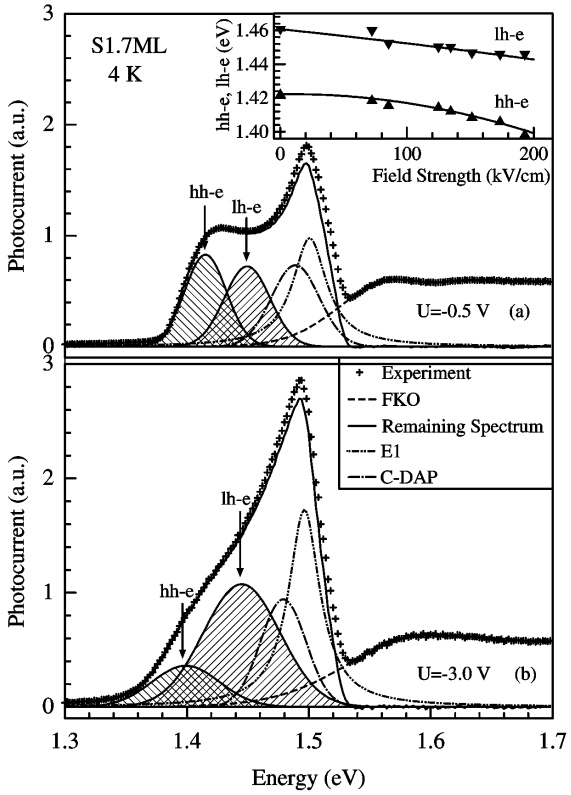

Fig.2. Photocurrent spectra of S1.7ML measured under -0.5 V (a) and -3.0 V (b) at 4 K. The remaining spectrum which is obtained by subtracting the FKO from experimental data has been modeled by superpositioning the hh-e-, lh-e-, E1, and C-DAP-peaks. The inset in part (a) represents the hh-e- and lh-e-transition energies as a function of the electric field strength.

The obtained Stark shift of the hh-e- and lh-e transition energies is represented in the inset of Fig. 2. For an electric field of 150 kV·cm^{-1} this Stark shift amounts to 17 and 12 meV for the hh-e- and lh-e-transition, respectively. From the $\Delta E(F)$-dependence we have determined the polarizability β of the hh-e-transition of 1.7 ML InAs which amounts to $(5\pm2)\times10^{-7}$ eVcm^2 /kV^2. This value lies in between the β-value of the InAs-Dot/GaAs system (3×10^{-7} eVcm^2 /kV^2 /A/) and the InGaAs-QW/GaAs system (39×10^{-7} eVcm^2 /kV^2 /B/). With increasing electric field strength the oscillator strength of the hh-e-transition decreases, whereas that of the lh-e-transition slightly increases.

/1/ H. v. Wenckstern, H. Schmidt, R. Pickenhain, V. Gottschalch
Quantum confined Stark effect (QCSE) und Franz-Keldysh-Oszillationen (FKO) für InAs-Monolagen in GaAs, DPG-Tagung Regensburg März 2001, FV Halbleiterphysik, Themenkreis: (11) Heterostrukturen

/2/ H. v. Wenckstern, H. Schmidt, R. Pickenhain, V. Gottschalch
Quantum confined Stark effect of Excitons localized at very thin InAs layers embedded in GaAs, accepted for publication in phys. stat. sol. (b) 00 (2002) (in Proceedings of OECS7, Montpellier 2001).

/A/ P.W. Fry et al., phys. stat. sol. (a) 178 ,269 (2000).

/B/ J. Barnes *et al.*, J. Appl. Phys. 79, 7775 (1996).

6.4 Semiconducting n-type $Zn_{1-x}(Ga, Al, Mg, Cd)_x$ oxide thin films by pulsed laser deposition

M. Lorenz, E. M. Kaidashev*, H. v. Wenckstern, D. Spemann, H. Hochmuth, G. Ramm, M. Grundmann
** on leave from Rostov-on-Don State University, Rostov-on-Don, Russia*

ZnO is a direct-band-gap semiconductor with an energy gap of about 3.3 eV and is considered as a future material for UV and blue light-emitting devices /1/. It has higher exciton binding energy (60 meV for ZnO versus 28 meV for GaN) and higher optical gain (300 cm^{-1}) than GaN (100 cm^{-1}) at room temperature /2/. There are two major challenges for the successful realization of ZnO-based current injection lasers and LEDs. The first one is the reduction of background carrier (free electron) concentration which is controlled by the oxygen nonstoichiometry in the ZnO films. The second important task is to achieve p-type conductivity in ZnO /2/.
Series of ZnO thin films either undoped or doped with Ga or Al or mixed with Mg or Cd were deposited by pulsed laser deposition (PLD) using a KrF excimer laser on C-plane sapphire (0001) substrates. The resulting PLD ZnO thin films were characterized by Hall measurement, and various optical techniques as UV-VIS and IR ellipsometry and transmission, and X-ray diffraction, and RHEED, and Rutherford backscattering RBS. Epitaxial PLD ZnO films with very flat surface were obtained as confirmed by streaky RHEED patterns at 30 keV. The band gap energy of ZnO:Mg thin films could be shifted from 3.3 up to 3.8 eV by adding up to 7 weight% MgO to the ZnO target. Although usually a stoichiometry transfer from sintered PLD bulk target to the thin film is observed as in case of Ga-doped ZnO, we found for the mixed systems an excess of Mg by a factor of 1.6 and a strong deficit of Cd (factor 0.11) by RBS. Table 1 summarizes electrical and structural data of the $Zn_{1-x}(Ga, Al, Mg, Cd)_xO$ thin films. Electrical DC-resistivity of the n-type conducting ZnO thin films can be chosen over 6 orders of magnitude by selecting the doping or mixing element and the oxygen partial pressure during PLD, thereby offering great potential for future applications. Work on p-type conducting oxide thin films by PLD is in preparation.

Table 1. Overview on optimized structural and typical electrical data of n-type conducting PLD thin films deposited from different targets.

PLD - target Stoichiometry	FWHM XRD ZnO(002) peak	resistance [Ω cm]	carrier conc. [cm^{-3}]	Hall mobility [cm^2/Vs]	band gap [eV]
ZnO	0.164°	1.2	7×10^{16}	77	3.3
$Zn_1Mg_{0.10}O_{1.10}$	0.189°	> 10			3.6
$Zn_1Cd_{0.02}O_{1.02}$	0.188°	9.5	2×10^{17}	4	3.3
$Zn_1Ga_{0.004}O_{1.006}$	0.189°	3×10^{-3}	2×10^{19}	66	3.3
$Zn_1Al_{0.008}O_{1.012}$	0.183°	9×10^{-4}	9×10^{19}	70	3.3

/1/ D. S. Ginley, C. Bright (eds.) “Transparent conducting oxides” MRS bulletin **25** No. 8 (2000), 15ff.
/2/ S. Choopun, R. D. Vispute, W. Noch, A. Balsamo, R. P. Sharma, T. Venkatesan, A. Iliadis, D. C. Look, “Oxygen pressure-tuned epitaxy and optoelectronic properties of laser-deposited ZnO films on sapphire” Appl. Phys. Lett. **75** (1999) 3947.

6.5 High-T_c superconducting $YBa_2Cu_3O_{7-\delta}$ thin films by PLD for microwave applications

M. Lorenz, H. Hochmuth, D. Natusch, G. Ramm, M. Grundmann

High-T_c superconducting (HTSC) $Y_1Ba_2Cu_3O_{7-\delta}$ (YBCO) thin films on low dielectric loss substrates as for example sapphire are suitable candidates for applications as passive microwave components for future communication systems. There is a huge number of activities in many countries to develop microwave devices using HTSC thin films, because in this field real market applications of HTSC subsystems seem to be possible in the nearest future. Devices like microwave stripline filters for satellite communication systems require high-quality HTSC thin films on both sides of large-area single crystal wafers. Therefore, to support the breakthrough of HTSC microwave devices to real market applications, highly reproducible and well established HTSC deposition techniques are necessary. Only a few processes worldwide as for example thermal coevaporation and pulsed laser deposition (PLD) /1/ up to now fulfill these quality requirements for large-area HTSC thin films.
In the framework of the German research program on "superconductors and ceramics for future communication technology", a highly reproducible PLD process for large-area 3-inch diameter and double-sided YBCO films on sapphire substrates for microwave applications is developed and continuously improved at University of Leipzig /1/. YBCO:Ag thin films and CeO_2 buffer layers are deposited by PLD, using a KrF excimer laser, on both sides of 3-inch diameter R-plane sapphire wafers of 430 µm thickness. Despite the simple deposition principle of PLD there is a huge number of difficult to handle influences which may affect the quality of the deposited films /1/.
The double-sided PLD YBCO thin films of size 3-inch diameter and 71 x 75 mm² (figure 1) are sent to the project partners BOSCH in Stuttgart and Cryoelectra in Wuppertal for optimization of high-performance microwave bandpass filters for satellite and mobile communication systems of the future /2/ (figure 2). Table 1 shows typical structural and microwave properties of the YBCO thin films deposited by our space qualified PLD process /1/.

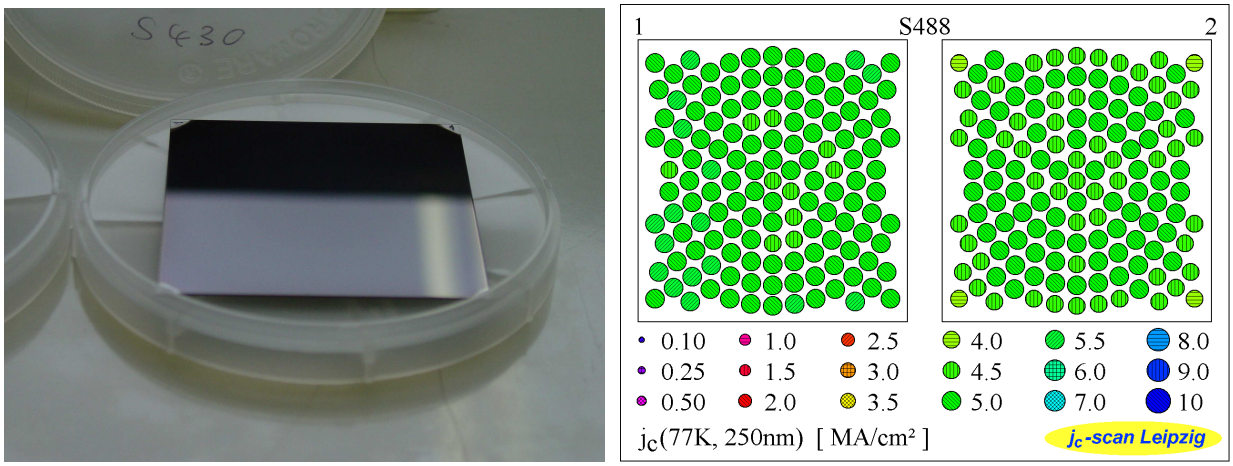

Figure 1. Large-area and double-sided PLD-YBCO:Ag thin films of size 71 x 75 mm² exhibiting mirrorlike optical (left) and electrical homogeneity (right). The scan of the critical current density is measured using self made system "j_c-scan Leipzig".

Table 1. Typical structural and electrical properties of large-area PLD-YBCO thin films on sapphire substrates suitable for microwave applications.

Property	Typical Value
YBCO-thickness d_{YBCO}	(230 ± 30) nm
c-axis lattice constant c	(11.659 ± 0.006) Å
a-axis lattice constant a	(3.829 ± 0.003) Å
orthorhombic splitting (b-a)/a	(1.52 ± 0.05) %
percentage of a-axis oriented grains	0 to 0.5 %
in-plane epitaxially oriented film area to total illuminated area in Raman spectroscopy	75 to 94 %
critical temperature T_c	87.5 to 90 K
critical current density j_c at 77 K and B=0	3.5 to 5.5 MA/cm^2
surface resistance R_s at 10 GHz and 77 K	500 to 600 μΩ
microwave surface magnetic field B_s at 8.5 GHz and 77 K for R_s + 20 %	8 to 10 mT
surface resistance R_s at 145 GHz and 77 K	40 to 60 mΩ

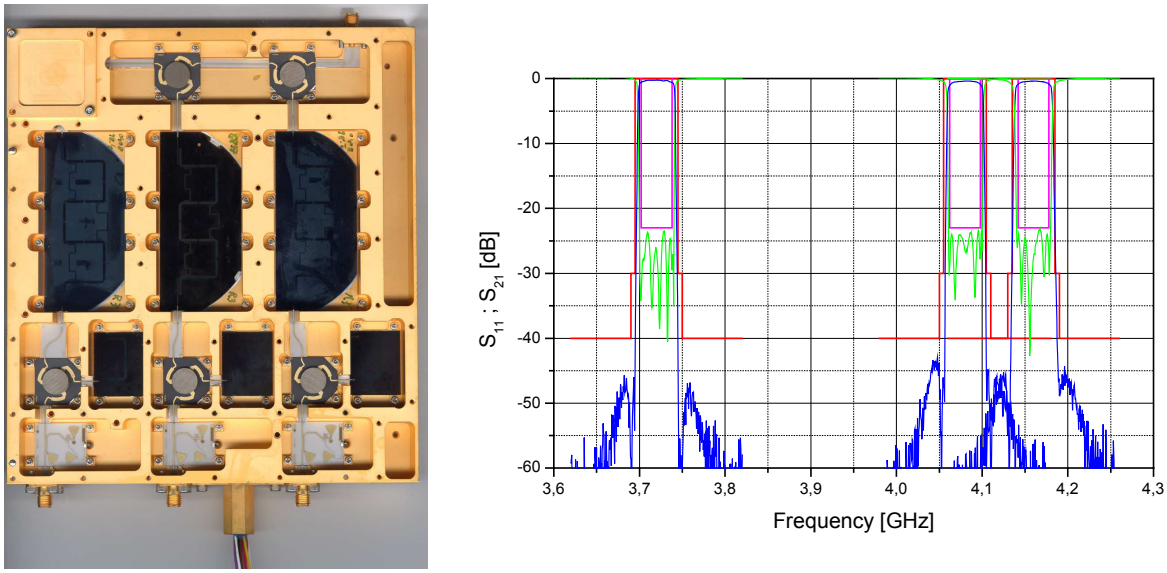

Figure 2. Integrated three channel input multiplexer for satellite communication demonstrator system with 8 pole quasielliptic HTSC YBCO filters (left) and its microwave transmission and reflection characteristics (right). (BOSCH Stuttgart /2/)

Supported by the BMBF and Robert BOSCH GmbH under Grants No. FKZ 13N7390 and 13N8158 within project network “Superconductors and new ceramics for the communication technique of the future”.

/1/ M. Lorenz, H. Hochmuth, D. Natusch, M. Kusunoki, V. L. Svetchnikov, V. Riede, I. Stanca, G. Kästner, D. Hesse, “High-quality Y-Ba-Cu-O Thin Films by PLD – Ready for Market Applications” IEEE Transact. Appl. Superconductivity 11, 3209 (2001).

/2/ M. Klauda, T. Kässer, B. Mayer, C. Neumann, F. Schnell, B. Aminov, A. Baumfalk, H. Chaloupka, S. Kolesov, H. Piel, N. Klein, S. Schornstein, M. Bareis „ Superconductors and Cryogenics for future communication systems” IEEE Transact. Microwave Theory a. Techniques 48 (2000) 1227.

6.6 Ferroelectric $Ba_xSr_{1-x}TiO_3$ thin films for electrically tuneable capacitors and microwave phase shifters

M. Lorenz, M. Schallner*, H. Hochmuth, D. Natusch, G. Ramm, M. Grundmann

* Marconi Communications GmbH, Backnang

Tuneability of permittivity and loss tangent and its temperature dependence are the basic parameters characterizing ferroelectrics for applications in electrically tuneable microwave devices like varactors or phase shifters /1/. To develop devices for applications in future microwave communication systems, $Ba_xSr_{1-x}TiO_3$ thin films on polycrystalline Al_2O_3 ceramic substrates have to be optimized using pulsed laser deposition (PLD). In the first attempts, the permittivity ε_r of $Ba_{0.6}Sr_{0.4}TiO_3$ thin films at 30 GHz could be adjusted between 90 and 1,400 by selection of proper substrate temperature and oxygen partial pressure during PLD. The corresponding loss tangent of the thin films was between 0.05 and 0.2 which is about one order of magnitude higher than reported for $Ba_{0.6}Sr_{0.4}TiO_3$ bulk material. Figure 1 shows the tuneability of ε_r (right), and the temperature dependence of ε_r (left) of a PLD $Ba_{0.6}Sr_{0.4}TiO_3$ thin film of about 0.5 µm thickness. The tuneability and temperature dependence have to be further optimized by the Barium stoichiometry and the PLD deposition conditions within the required working temperature range from –45°C up to 80°C for applicable devices. Mg-doping is reported to reduce loss tangent of ferroelectric materials /2/. The current project is scheduled up to June 2003.

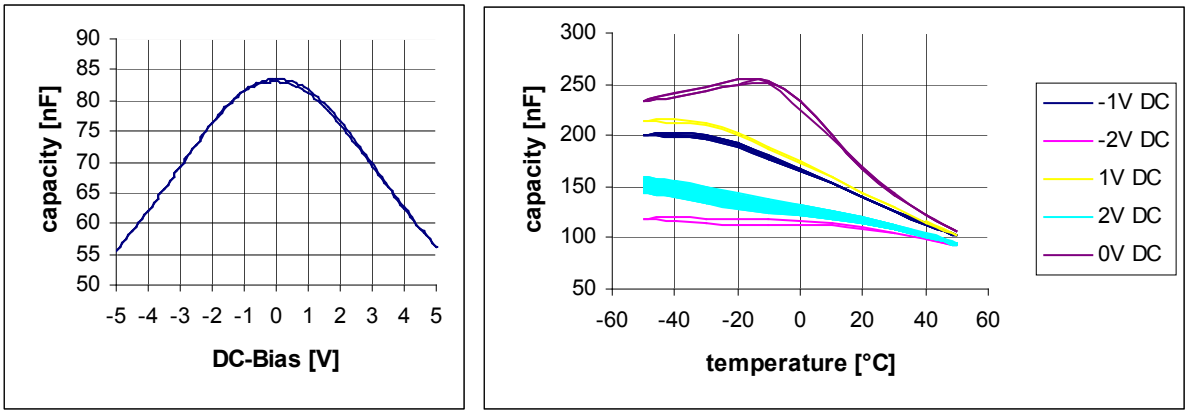

Figure 1. Capacity corresponding to ε_r of a planar Au / $Ba_{0.6}Sr_{0.4}TiO_3$ / Au PLD thin film structure No. G 987 in dependence on DC bias (left), and temperature for different DC-bias (right). Measurement by Marconi Communications GmbH.

Supported by the BMBF under Grant No. FKZ 13N8158 within project network “Superconductors and new ceramics for the communication technique of the future”

/1/ S. S. Gevorgian, E. L. Kollberg “Do we really need ferroelectrics in paraelectric physe only in electrically controlled microwave devices” IEEE Transactions on Microwave Theory and Techniques **49** (2001) 2117.

/2/ L. C. Sengupta, S. Sengupta „Breakthrough advances in low loss, tuneable dielectric materials“ Mat. Res. Innovat. **2** (1999) 278.

6.7 Pulsed laser deposition of $Zn_{2(1-x)}Cu_xIn_xS_2$ (ZCIS) thin films

G. Wagner*, A. Teichert*, K. Bente*, G. Ramm, H. Hochmuth, M. Lorenz
* Institute for Crystallography, Mineralogy und Materials Science, University Leipzig

Within a project network of groups from Institute for Crystallography, Mineralogy and Materials Science and Institute of Experimental Physics II basic research work was done on structural, optical and electrical properties of the $Zn_{2(1-x)}Cu_xIn_xS_2$ (ZCIS) mixed crystal system. The $Cu(In,Ga)(S,Se)_2$ material can be effectively used as solar cell absorber as thin film due to its very high optical absorption coefficient compared to silicon. By means of mixing with ZnS a further modification and optimisation of the absorber properties to achieve higher efficiency is expected.

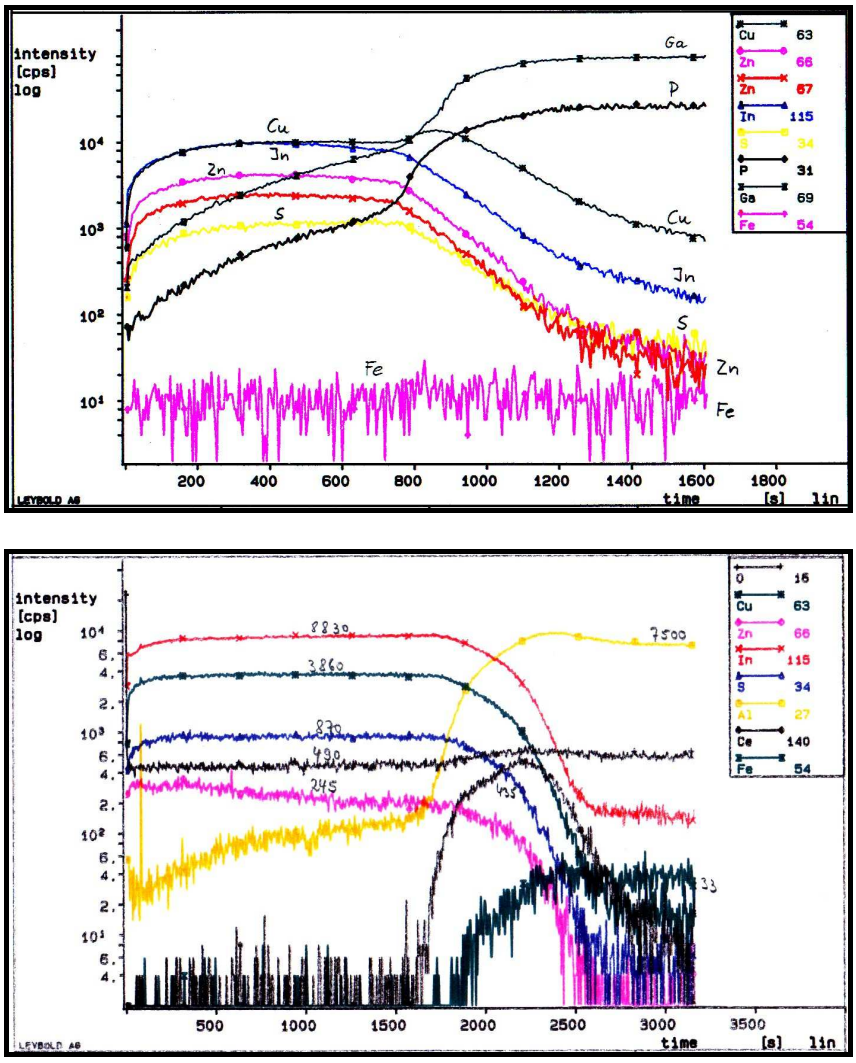

Figure 1. SNMS depth profiles of PLD ZnS-$CuInS_2$ thin films on GaP (001) (top, sample No. ZCIS 61) and r-plane sapphire with CeO_2 buffer layer (bottom, ZCIS 64) demonstrating suppressed interdiffusion in case of CeO_2/sapphire substrate.

Therefore, to investigate the basic properties and to be able to built demonstrator solar cells, the deposition of ZCIS thin films on GaP, CeO_2/sapphire, CaF_2 and Mo/glass substrates was the main task of this particular project. By means of the flexible pulsed laser deposition (PLD) together with secondary neutrals mass spectrometry (SNMS, figure 1) the optimisation of ZCIS thin films /1, 2, 3/ was successfully performed.

Kindly supported by the Deutsche Forschungsgemeinschaft under Grant No. LO 790/1-1 from July 2000 to June 2001.

/1/ G. Wagner, U. Lange, K. Bente, J. Lenzner, M. Lorenz, "Defect structure of monocrystalline (001)-oriented $Zn_{0.62}Cu_{0.19}In_{0.19}S$ films grown on GaP by pulsed laser deposition", J. Cryst. Growth **209** (2000) 68 – 74.

/2/ G. Wagner, U. Lange, J. Lenzner, M. Lorenz, K. Bente, "Structural properties of thin $Zn_{0.62}Cu_{0.19}In_{0.19}S$ alloy films grown on (111) Si substrates by pulsed laser deposition", Thin Solid Films **358** (2000) 80 - 85.

/3/ A. Teichert, Diplomarbeit "Stöchiometrie, Kristallstruktur und Gitterstörungen in PLD $(2ZnS)_{1-x}$ $(CuInS_2)_x$-Mischkristallschichten", Universität Leipzig, Fakultät für Chemie und Mineralogie 2001.

6.8 UV-VIS-Ellipsometry applied to ZnO and related compounds

R. Schmidt, B. Rheinländer, M. Schubert, M. Lorenz, M. Grundmann

Spectroscopic ellipsometry is a highly developed and often used nondestructive method in order to investigate the dielectric function and the optical constants of bulk and layered semiconductor materials. It is a powerful tool in the determination of the optical properties as well as the layer thicknesses in electronic and optoelectronic devices structures. Whereas the ellipsometry in the UV-VIS-NIR range yields informations on the electronic band structure and exciton features the infrared ellipsometry enables the investigation of phonon, free-carrier plasmon,and interface polariton effects.

The wurtzite crystal ZnO is an appropriate material for transparent conducting layers and for photon generation in the near ultraviolet spectral range as it is demonstrated in the literature by laser and LED operation. The fundamental band gap E_G has an energy near to 3.4 eV. The optical transitions starting from the threefold splitted valence band to the conduction band have different optical polarizations with respect to the optical axes (c-axis). The respective three free excitons have binding energies E_B of approximately 60 meV. The photon generation is dominated by the exciton transitions. A blueshift of all optical transitions for tuning the light emission can be obtained by adding of MgO to ZnO.

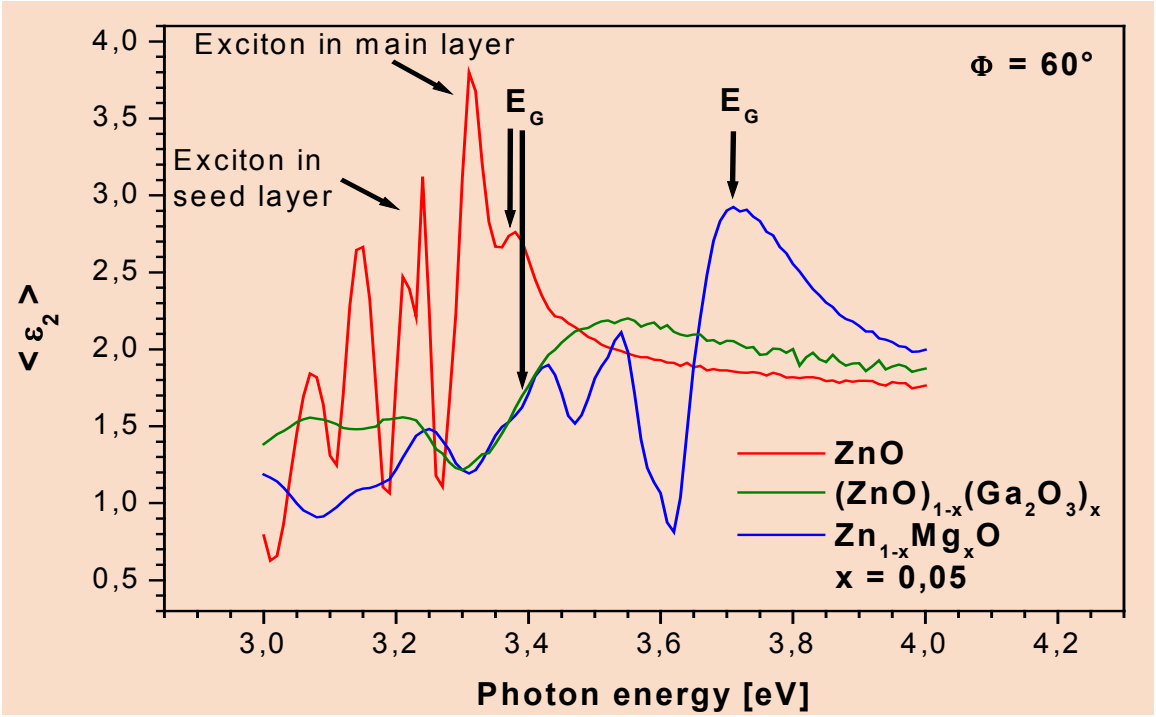

Fig. 1 Imaginary part of the pseudo-dielectric function for three materials: ZnO, Mg-doped ZnO and Ga_2O_3-doped ZnO.

In order to form p-n junctions highly doped n- and p-type material is needed. Whereas the n-type conductance can be easily achieved by nonstoechiometric oxygen excess or mixing with Ga_2O_3, the p-type conductance remains a serious problem. Using UV-VIS spectroscopic ellipsometry we have determined the optical transition energies, probabilities, and broadenings for the band-band transitions on the three E_0 critical points and the respective free excitons in ZnO, $Zn_{1-x}Mg_xO$, and $(ZnO)_{1-x}(Ga_2O_3)_x$. In the figure, the imaginary part of the pseudo-dielectric function of all materials named is shown. [The value x gives the target composition in Laser Plasma Deposition (PLD) applied for the growth of these samples.] In the spectral absorption range, this function reflects the spectrum of oscillator strength. For ZnO we have found for the lowest fundamental gap E_G = 3.377 eV and the binding energy E_B = 60.8 meV. In the case of $Zn_{1-x}Mg_xO$ the strong blushift of the fundamental band gap is easily seen. The analysis of the spectra has revealed the exciton binding energy E_B = 42 meV. For $(ZnO)_{1-x}(Ga_2O_3)_x$ the absence of a shift of the band gap is remarkable.

6.9 Funding

Untersuchung der Intersubniveau-Übergänge in selbstordnenden Quantenpunkten, Entwicklung neuartiger Infrarot-Detektoren und -Laser
Investigation of inter-sublevel transitions in self-ordered quantum dots, development of novel infrared detectors and lasers
Prof. M. Grundmann
Deutsche Forschungsgemeinschaft, Gr 1011/7-2

Herstellung und Optimierung von doppelseitigen PLD - RE 123 - Schichten
Fabrication and Optimization of double-sided PLD-RE 123-Layers
Dr. M. Lorenz
Unterauftrag B-3281 innerhalb BMBF-Leitprojekt FKZ 13N7390 der Robert BOSCH GmbH Stuttgart (until 06/2001)

PLD von neuartigen dielektrischen und HTSL-Dünnschichten für zukünftige Anwendungen im Richt- und Mobilfunk
PLD of novel dielectric and HTSL thin films for future applications in mobile communication
Dr. M. Lorenz
BMBF, FKZ 13N8158 (from 7/2001) (within BMBF-Leitprojekt)

Laser-Plasmaabscheidung von $Zn_{2(1-x)}Cu_xIn_xS_2$ – Dünnfilmen
Laser plasma deposition of $Zn_{2(1-x)}Cu_xIn_xS_2$ thin films
Dr. M. Lorenz
Deutsche Forschungsgemeinschaft, Lo 790/1-1 (until 6/2001)

Lichtemitter und Fotodetektoren auf der Basis von III-V-Halbleiter-Nanostrukturen
Light emitters and photodetectors on the basis of III-V semiconductor nanostructures
Priv.-Doz. Dr. B. Rheinländer
BMBF-Förderung ausgeführt durch das Internationale Büro der DLR
Bilaterale WTZ Deutschland-Slowakei:
Projekt SVK 01/001

Elektronische und optische Eigenschaften, in-situ-Ramanstreuung, in-situ-Ellipsometrie und Ionenstrahlanalytik von flexiblen Cu(In,Ga)-(Se,S)-Dünnfilm-Solarzellen
Electronic and optical properties, in-situ Raman scattering, in-situ ellipsometry amd ion-beam analysis of flexible Cu(In,Ga)-(Se,S) thin film solar cells
Prof. M. Grundmann (jointly with Dr. M. Schubert, Prof. T. Butz)
BMBF, 03WKI09 (from 8/2001) (within BMBF-Wachstumskern "INNOCIS")

Verallgemeinerte Infrarot-Ellipsometrie von Kristallstruktur- und Ladungsträger-Effekten in komplexen Heterostrukturen von Gruppe-III Ntriden
Generalized Infrared-Ellipsometry of crystal-structure and free-carrier effects in complex group-III nitride heterostructures
Dr. M. Schubert, Dr. B. Rheinländer
Deutsche Forschungsgemeinschaft, Rh 28/3-2

6.10 External cooperations

Academic

A.F. Ioffe-Institut, St. Petersburg
Prof. Zh.I. Alferov, Dr. V.M. Ustinov, Dr. G. Cirlin
Forschungszentrum Karlsruhe, Institut für Materialforschung III
Dr. H. Heidinger, Dr. J. Halbritter
Institute for Metal Physics of National Academy of Sciences of Ukraine, Kiev, Ukraine
Prof. Dr. V. M. Pan
Institut für Oberflächenmodifizierung e.V., Leipzig
Prof. B. Rauschenbach
Universität Leipzig, Fakultät für Biowissenschaften, Pharmazie und Psychologie
Prof. A. Beck-Sickinger
Max-Planck-Institut für Mikrostrukturphysik, Halle/Saale
Dr. O. Breitenstein, Dr. D. Hesse
St. Petersburg State Technical University
Prof. L. Vorob'jev, Dr. V. Shalygin
Slovak University of Technology, Bratislava, Slovak
Prof. J. Kováč, Dr. F. Uherek
Technische Universität Berlin
Prof. D. Bimberg, Prof. N.N. Ledentsov
Universidade de Aveiro, Portugal
Prof. N. Sobolev
Yamagata University, Department of Electrical Engineering, Yonezawa, Japan
Dr. M. Kusunoki
Paul Scherrer Institut, Villingen
Prof. H. Sigg
Université Paris-Sud
Prof. F. Julien

Industry

BOSCH-SatCom GmbH Backnang
Dr. T. Kässer
Cryoelectra GmbH Wuppertal und Bergische Universität Wuppertal
Prof. H. Piel
Marconi Communications GmbH Backnang
Dr. M. Schallner
Solarion GmbH, Leipzig
Dr. G. Lippold

6.11 Publications

6.11.1 Journals

Macroscopic and microstructural properties of CSi_xN_y thin films deposited by RF nitrogen-plasma-assisted pulsed laser deposition
T. Thärigen, M. Lorenz
Appl. Surf. Sci. 179, 156-160 (2001)

Electron Emission from arc-modified diamond like carbon films at low electric field
T. Thärigen, E. Hartmann, M. Lenk, A. Mende, K. Otte, M. Lorenz, K.-H. Hallmeier
Appl. Surf. Sci. 182, 142-149 (2001)

High-quality Y-Ba-Cu-O Thin Films by PLD – Ready for Market Applications
M. Lorenz, H. Hochmuth, D. Natusch, M. Kusunoki, V. L. Svetchnikov, V. Riede, I. Stanca, G. Kästner, D. Hesse
IEEE Transact. on Appl..Supercond. 11 No. 1, 3209-3212 (2001)

Linear Defects in Epitaxial Y-Ba-Cu-O Films: Their Role in Anisotropic Vortex Pinning and Microwave Surface Resistance
V. V.M. Pan, V. S. Flies, V. A. Komashko, O. P. Karasevska, V. L. Svetchnikov, M. Lorenz, A. N.Ivanyuta, G. A. Melkov, E. A. Pashitskii, H. W. Zandbergen
IEEE Transact. on Appl. Supercond. 11 No. 1, 3960-3963 (2001)

High-quality Reproducible PLD (Y, Gd)-Ba-Cu-O Thin Films up to 4-inch Diameter for Microwave Applications
M. Lorenz, H. Hochmuth, D. Natusch, M. Grundmann
Extended Abstracts of 8th International Superconductive Electronics Conference ISEC 01, June 19-22, 2001, Osaka, Japan, Editors T. Kobayashi and M. Tonouchi, pp.105-106

Large-Area Epitaxial Y-Ba-Cu-O Films: Impact of Growth-Induced Linear Defects upon Microwave Properties
V. M. Pan, V. S. Flies, V. A. Komashko, A. A. Kalenyuk, M. Lorenz, E. A. Pashitskii, A. N. Ivanyuta, G. A.Melkov, H. W. Zandbergen, V. L. Svetchnikov
Extended Abstracts of 8th International Superconductive Electronics Conference ISEC 01, June 19-22, 2001, Osaka, Japan, Editors T. Kobayashi and M. Tonouchi, pp. 131-132

Thermal and Linear Defect Induced Instability in YBCO Thin Films for Microwave Applications
V. M. Pan, C. G. Tretiatchenko, E. A. Pashitskii, H. W. Zandbergen, V. L. Svetchnikov, M. Lorenz
Extended Abstracts of 8th International Superconductive Electronics Conference ISEC 01, June 19-22, 2001, Osaka, Japan, Editors T. Kobayashi and M. Tonouchi, pp. 445-446

Measurement of surface resistance distribution of large-area YBCO thin films
M. Kusunoki, Y. Takano, K. Nakamura, M. Inadomaru, D. Kosaka, A. Nozaki, S. Abe, M. Yokoo, M. Lorenz, H. Hochmuth, M. Mukaida, S. Ohshima
Extended Abstracts of 8th International Superconductive Electronics Conference ISEC 01, June 19-22, 2001, Osaka, Japan, Editors T. Kobayashi and M. Tonouchi, pp. 503-504

Resonant microcavity edge-emitting laser with InAs/GaAs active region
J.Kvietková, S.Hardt, J.Kováč, B.Rheinländer, L.Kuna, V.Gottschalch, J.Jakabovič
Proc. 25th Intern.Conf. on the Physics of Semiconductors, 17.-22.09.00, Osaka, Japan (eds. N.Miura and T.Ando), Springer Proc. in Physics 87, 1727-1728 (2001)

Calorimetric investigation of intersublevel transitions in charged quantum dots
K. Goede, A. Weber, F. Guffarth, C.M.A. Kapteyn, F. Heinrichsdorff, R. Heitz, D. Bimberg and M. Grundmann
Phys.Rev. B 64, 245317 (2001)

Near and mid infrared spectroscopy of InGaAs/GaAs quantum dot structures
V.A. Shalygin, L.E. Vorobjev, A.V. Glukhovskoy, S.N. Danilov, V.Yu. Panevin, D.A. Firsov, B.V. Volovik, N.N. Ledentsov, D.A. Livshits, V.M. Ustinov, Yu.M. Shernyakov, A.F. Tsatsulnikov, A. Weber, M. Grundmann
Nanotechnology 12, 447-449 (2001)

Comment on “Room-temperature long-wavelength (λ = 13.3 μm) unipolar quantum dot intersubband laser“
A. Weber, M. Grundmann, N. N. Ledentsov
Electronics Letters 37 (2), pp. 96-97 (2001)

Mid-infrared properties of quantum dot lasers
M. Grundmann, A. Weber, K. Goede, F. Heinrichsdorff, D. Bimberg, V. M. Ustinov, A. E. Zhukov, N. N. Ledentsov, P. S. Kop'ev, Zh. I. Alferov
Photonics Technology in the 21st Century, Proceedings of SPIE, J. H. Marsh, P.Bhattacharya, O. Wada, eds., Vol. 4598, 44-57 (2001)

Optical phenomena connected with intraband carrier transitions in quantum dots and quantum wells
L.E. Vorobjev, S.N. Danilov, A.V. Glukhovskoy, V.L. Zerova, E.A. Zibik, V.Yu. Panevin, D.A. Firsov, V.A. Shalygin, A.D. Andreev, B.V. Volovik, A.E. Zhukov, N.N. Ledentsov, D.A. Livshits, V.M. Ustinov, Yu.M. Shernyakov, A.F. Tsatsulnikov, A. Weber, M. Grundmann, S.R. Schmidt, A. Seilmeier, E. Towe, D. Pal
Nanotechnology 12, 462-465 (2001)

Design and investigation of microwave bandpass filters for L- and R-frequency bands based on high-temperature superconducting films
I. V. Korotash, V. T. Tarasov, M. A. Skoryk, M. Lorenz
Proc. 4th Int. Symp. “Physics and Engineering of Millimeter and Submillimeter Waves” – MSMW 2001 Charkov, Ukraine, June 4-9, pp. 389-390 (2001)

Effect of Growth-Induced Linear Defects on High-Frequency Properties of Pulsed-Laser-Deposited $Yba_2Cu_3O_{7-\square}$ Films
V. M. Pan, V. S. Flies, O. P. Karasevska, V. I. Matsui, I. I. Peshko, V. L. Svetchnikov, M. Lorenz, A. N. Ivanyuta, G. A. Melkov, E. A. Pashitskii, H. W. Zandbergen
J. of Superconductivity: Incorporating Novel Magentism 14 No. 1, 105-114 (2001)

Band-Pass Filters for 1,8 GHz Frequency Range Using Double-Sided YBCO/Au Films on CeO_2 –Buffered Sapphire
V. F. Tarasov, I. V. Korotash, V. F. Taborov, C. G. Tretiatchenko, V. V. Vysotskii, V. M. Pan, A. N. Ivanyuta, G. A. Melkov, M. Lorenz
J. of Superconductivity: Incorporating Novel Magentism 14 No. 1, 115-125 (2001)

Band-gap energies, free carrier effects, and phonon modes in strained GaNAs/GaAs and GaNAs/InAs/GaAs superlattice heterostructures measured by spectroscopic ellipsometry
J. Sik, M. Schubert., G. Leibiger, V. Gottschalch., G. Wagner
J. Appl. Phys. 89, 294-305 (2001)

The influence of alternative group-V sources on heterointerface quality in the system GaInAs(P) on InP
M. Gerhardt, G. Kirpal, R. Schwabe, G. Benndorf, V. Gottschalch
Thin Solid Films 392 , 85–90 (2001)

Phonon Modes and Critical Points of GaPN
G. Leibiger, V. Gottschalch, R. Schwabe, G. Benndorf, M. Subert
phys.stat. sol. (b) 228 , 279–282 (2001)

Phonon Modes of $In_xGa_{1-x}As_{1-y}N_y$ Measured by Far Infrared Spectroscopic Ellipsometry
G. Leibiger, V. Gottschalch, M. Schubert
phys. Stat. sol. (b) 228, 259–262 (2001)

Phonon modes of $GaP_{1-y}N_y$($0.006 \leq 0.0285$) measured by midinfrared spectroscopic ellipsometry
G. Leibiger, V. Gottschalch, A. Kasic, M. Schubert
Appl. Phys. Lett. 79, 3407-3409 (2001)

Disorder-activated infrared modes and surface depletion layer in highly Si-doped hexagonal GaN
A. Kasic, M. Schubert, B. Kuhn, F. Scholz, S. Einfeldt, D. Hommel
J. Appl. Phys. 87, 3720 (2001)

Optical Constants, Critical Points, and Phonon Modes of GaAsN Single Layers
G. Leibiger, V. Gottschalch, A. Kasic, B. Rheinländer, J. Sik, M. Schubert
Mat. Res. Soc. Symp. 639, G6.35 (2001)
IR-VUV Dielectric Function of $Al_{1-x}In_xN$ determined by spectroscopic ellipsometry
A. Kasic, M. Schubert, B. Rheinländer, J. Off, F. Scholz, C. M. Herzinger
Mat. Res. Soc. Symp. 639, G6.13 (2001)

Strain and composition dependence of the E_1(TO) mode in hexagonal $Al_xIn_{1-x}N$ thin films
A. Kasic, M. Schubert, J. Off, F. Scholz
Appl. Phys. Lett. 78, 1526 (2001)

Phonons and free carriers in strained hexagonal GaN/AlGaN superlattices measured by Infrared ellipsometry and Raman spectroscopy
M. Schubert, A. Kasic, J. Sik, S. Einfeldt, D. Hommel, V. Härle, J. Off, F. Scholz
Mat. Sci. & Eng. B 82, 178 (2001)

Effective carrier mass and mobility versus carrier concentration in p- and n-type GaN determined by infrared ellipsometry and Hall resistivity measurements
A. Kasic, M. Schubert, B. Rheinländer, V. Riede, S. Einfeldt, D. Hommel, B. Kuhn, J. Off, F. Scholz
Mat. Sci. & Eng. B 82, 74 (2001)

Model dielectric function spectra of GaAsN for far-infrared and near-infrared to ultraviolet wavelengths
G.Leibiger, V.Gottschalch, B.Rheinländer, J.Sik, M.Schubert
J.Appl.Phys. 89, 4927-4938 (2001)

Nanotechnolgische Entwicklungen – Konvergenz mit den IuK Technologien
Jahrbuch Telekommunikation und Gesellschaft 2001, Band 9 „Internet@Future:
M. Grundmann, D. Bimberg
Technik, Anwendungen und Dienste der Zukunft“,
(Hüthig, Heidelberg, 2001), p. 68

Optical properties of $Al_xIn_{1-x}N$ thin films determined by spectroscopic ellipsometry
A. Kasic, M. Schubert, B. Rheinländer, J. Off, F. Scholz, C. M. Herzinger
IEEE 27th Int. Symp. on Compound Semiconductors, Piscataway, NJ, p. 513 (2001)

Infrared spectroscopic ellipsometry for nondestructive characterization of free-carrier and crystal-structure properties of group-III-nitride semiconductor device heterostructures
M. Schubert, A. Kasic, S. Figge, M. Diesselberg, S. Einfeldt, D. Hommel, U. Köhler, D. J. As, J. Off, B. Kuhn, F. Scholz, J. A. Woollam, C. M. Herzinger
SPIE Vol. 4449, 58 (2001)

Infrared ellipsometry – a novel tool for characterization of group-III nitride heterostructures for optoelectronic device applications
M. Schubert, A. Kasic, S. Einfeldt, D. Hommel, U. Köhler, D. J. As, J. Off, B. Kuhn, F. Scholz, J. A. Woollam
phys. Stat. sol. (a) 228, 437 (2001)

Optical constants, critical points, free carrier effects, and phonon modes of GaAsN single layers and GaAsN/InAs/GaAs superlattices
G. Leibiger, V. Gottschalch, A. Kasic, B. Rheinländer, J. Sik, M. Schubert,
IEEE 27th Int. Symp. on Compound Semiconductors, Piscataway, NJ, p. 7 (2001)

6.11.2 in press

Optical phonon modes and interband transitions in cubic AlGaN films
A. Kasic, M. Schubert, T. Frey, U. Köhler, D. J. As, C. M. Herzinger
Phys. Rev. B

Plasma-Enhanced Chemical Vapor Deposition of SiO_x/SiN_x Bragg reflectors
V. Gottschalch, R. Schmidt, B. Rheinländer, D. Pudis, S. Hardt, G. Wagner, R. Franzheld,
Thin Solid Films

Effective electron mass and phonon modes in n-type hexagonal InN
A. Kasic, M. Schubert, Y. Saito, Y. Nanishi, G. Wagner
Phys. Rev. B

Infrared spectroscopic ellipsometry - a new tool for characterization of semiconductor heterostructures
A. Kasic, M. Schubert, S. Einfeldt, D. Hommel
Vibrational Spectroscopy

High-quality reproducible PLD Y-Ba-Cu-O:Ag thin films up to 4-inch diameter for microwave applications
M. Lorenz, H. Hochmuth, D. Natusch, M. Grundmann
Physica C Superconductivity (2001) (Proc. European Conference on Applied Superconductivity 2001 Kopenhagen)

Investigation of the temperature features forming the passband of microwave HTSC bandpass filter
I. V. Korotash, M. Lorenz
Physica C Superconductivity (2001) (Proc. European Conference on Applied Superconductivity 2001 Kopenhagen)

6.11.3 Invited Talks

M. Grundmann
Semiconductor lasers based on quantum dots
Workshop on "Growth, electronic and optical properties of low-dimensional semiconductor quantum structures", February 2001, Schloss Ringberg, Germany

M. Grundmann
Selbstorganisierte Halbleiter-Nanostrukturen, Grundlagen und optoelektronische Anwendungen
155. PTB Seminar "Selbstorganisierte Halbleiter-Nanostrukturen, Grundlagen und Anwendungen", 1.2. 2001, Braunschweig, Germany

M. Grundmann
Quantum dots as gain medium in diode lasers
COST 268 International workshop on novel gain materials, 25.-28. 2. 2001, Würzburg, Germany

M. Grundmann
The contribution of nano-physics to optoelectronics
Workshop "Nanophysics and bioelectronics - a new Odyssey", MPI Dresden, Aug. 2001, Dresden, Germany

M. Grundmann
I. Basic quantum dot physics
II. Quantum dot laser and amplifier devices
NKT Advanced Photonics Summer School, August 2001, Kopenhagen, Denmark

M. Grundmann
I. Fabrication, structural and optical properties of self-organized semiconductor QDs
II. Device applications of self-organized semiconductor quantum dots
SAIP Symposium "Low-dimensional physics", 2.-3. 7. 2001, University of Natal, Durban, South Africa

M. Grundmann, A. Weber, K. Goede, F. Heinrichsdorff, D. Bimberg, V.M. Ustinov, A.E. Zhukov, N.N. Ledentsov, P.S. Kop'ev, Zh.I. Alferov
Mid-infrared properties of quantum dot lasers
Int. Symp. on Photonics and Applications (ISPA 2001), 26.-30. 11. 2001, Singapore

M. Grundmann
Nanostrukturen für die Optoelektronik
Kolloquium des Instituts für Physik, Technische Universität Ilmenau, Nov. 2001

M. Grundmann
Applications of quantum dot structures to micro- and optoelectronics
1st Nanotechnology School, 27.-28. 9. 2001, Aveiro, Portugal

M. Grundmann
Long wavelength quantum dot lasers
9th European Workshop on Metalorganic Vapor Phase Epitaxy (EW-MOVPE-9), June 10-13 2001, Wrexham, UK

M. Lorenz, H. Hochmuth, D. Natusch, M. Grundmann
High-quality Reproducible PLD (Y, Gd)-Ba-Cu-O Thin Films up to 4-inch Diameter for Microwave Applications
TM-2, 8th International Superconductive Electronics Conference ISEC 01, June 19-22, 2001, Osaka, Japan

M. Lorenz
High-quality reproducible PLD YBCO-Ag thin films for microwave application
Invited talk at High-Temperature Superconductive Electronics Symposium
25 June 2001, Faculty of Engineering, Yamagata University, Yonezawa, Japan

6.11.4 Conference contributions

(talk: T, poster: P)

Generalized infrared ellipsometry - a new tool for the characterization of semiconductor heterostructures
A. Kasic, M. Schubert
1st International Vibrational Spectroscopy, Turku, Finnland, August 2001 (P)

Generalized Infrared Ellipsometry - A novel tool for the characterization of group -III-nitride heterostructures for electronic and optoelectronic device applications
M. Schubert, A. Kasic, S. Einfeldt, D. Hommel, D.J. Ass, J. Off, B. Kuhn, F. Scholz
4th International Conference on Nitride Semiconductor Research, Denver, U.S.A., Juli 2001 (P)

Characterization of III-nitride optoelectronic device heterostructures using infrared ellipsometry
M. Schubert, A. Kasic, S. Einfeldt, D. Hommel, J. Off, F. Scholz
European MRS-Meeting, Strasbourg, Frankreich, Juni 2001 (P)

Ellipsometrische Untersuchungen von Gitterschwingungen und Bandlückenenergien kubischer $Al_{1-x}Ga_xN$-Filme
A. Kasic, M. Schubert, D. J. As
65. Frühjahrstagung der DPG, Hamburg, Deutschland, März 2001 (P)

Ellipsometrie und optische Konstanten von SiNx und SiOy für Bragg-Reflektoren
R.Schmidt, D.Pudis, B.Rheinländer, V.Riede, S.Hardt, V.Gottschalch, J.Kvietkova
Frühjahrstagung des AK Festkörperphysik bei der DPG, 26.-30.03.01, Hamburg (T)

Modular inductive j_c-scanning system for single- and double-sided HTSC thin films up to 4 inch diameter
H. Hochmuth, D. Natusch, M. Lorenz
Poster D3.2-21, European Conference on Applied Superconductivity, 26-30 August 2001, Kopenhagen, Denmark (T)

Investigation of the temperature features forming the passband of microwave HTSC bandpass filter
I. V. Korotash, M. Lorenz
Poster M2.3-15, European Conference on Applied Superconductivity, 26-30 August 2001, Kopenhagen, Denmark (T)

Microwave bandpass filters for R-band based on high-tempoerature superconducting films for extreme working conditions
I. V. Korotash, M. Lorenz, V. F. Tarasov, M. A. Skoryk
Poster M2.3-16, European Conference on Applied Superconductivity, 26-30 August 2001, Kopenhagen, Denmark (T)

M. Schubert, A. Kasic, C. M. Herzinger, J. A. Woollam
Spectroscopic Ellipsometry from 2 µm to 50 µm for nondestructive characterization of free-carrier and crystal-structure properties of III-V semiconductor device heterostructures
46th Annual SPIE Meeting, San Diego, U.S.A., July/August 2001 (T)

A. Kasic, M. Schubert
Verallgemeinerte Infrarot-Ellipsometrie – eine neue Charakterisierungsmethode für Halbleiter-Heterostrukturen
65. Frühjahrstagung der DPG, Hamburg, Deutschland, März 2001 (T)

A. Vincze, J. Kovac, R. Srnanek, M. Gasparovic, G. Leibiger, V. Gottschalch, B. Rheinländer
Light Emitting Diode Based on GaInAsN/GaAs Heterostructures
Conference APCOM 2001, 19.09.01, Demanovska Dolina, SK (T)

B.Rheinländer, D. Pudis, R.Schmidt, S.Hardt, V.Gottschalch, J. Kvietkova
Ellipsometrie und optische Konstanten von SiO_x und SiN_x für Bragg-Reflektoren
DPG-Frühjarstagung Hamburg 2001, 26. - 30. 3. 2001, DS 31.48 (T)

6.12 Graduations

6.12.1 PhD

Thomas Thärigen
Makroskopische Eigenschaften und Mikrostruktur von Kohlenstoff-Dünnfilmen aus Laser-Plasmareaktionen von Graphit mit Stickstoff-Radikalen, Siliciumnitrid oder Bornitrid

7 NFP — SCIENTIC ACTIVITIES

7.1 The high-energy ion nanoprobe LIPSION

J. Vogt, D. Lehmann, F. Menzel, T. Reinert, M. Schwertner, D. Spemann, L. Thomas, T. Butz

The high-energy ion nanoprobe LIPSION at the University of Leipzig has been operational since October,1998 (Fig.1). Its magnetic quadrupole lens system, arranged as a separated Russian quadruplet, was developed by the Microanalytical Research Centre (MARC), Melbourne and has a symmetrical demagnification factor of about 130. The single-ended 3 MV SINGLETRON^{TM} accelerator (High Voltage Engineering Europa B.V.) supplies H^+ and He^+ ion beams with a beam brightness of approx. 20 A $\cdot rad^{-2}\ m^{-2}\ eV^{-1}$. Due to this high brightness, the excellent optical properties of the focussing system of the nanoprobe and the suppression of mechanical vibrations by founding the bed-plates of accelerator and probe in greater depths separately from the surroundings, lateral resolutions below 100 nm for the low current mode (STIM) and 300 nm at a current of 10 pA (PIXE) were achieved routinely. Due to an improved shielding of the beamline against magnetic stray fields a beam diameter of 41 nm (new world record) could be obtained (Fig. 2).

Figure 1: LIPSION laboratory.

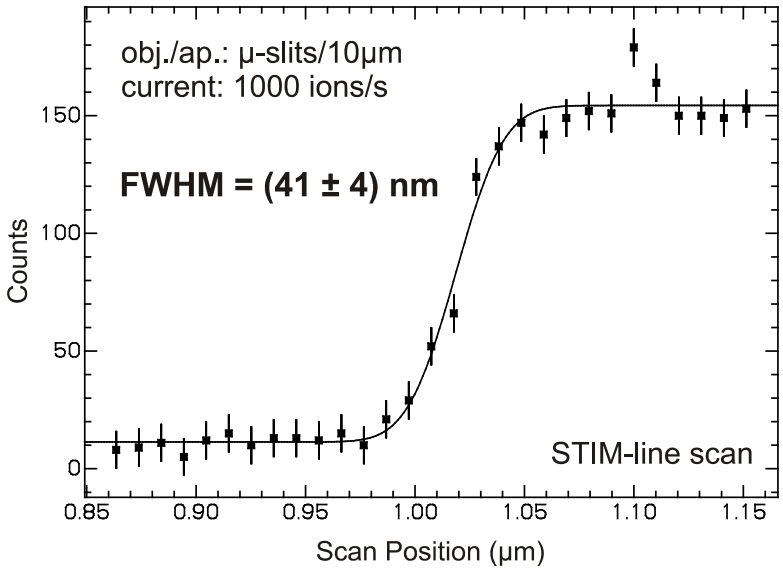

Figure 2: Beam profile in the low current mode derived from a line scan over an atomically flat semiconductor heterostructure

The UHV experimental chamber is equipped by electron, X-ray, and particle detectors to detect simultaneously the emitted secondary electrons (Ion Induced Electron Emission, IE), the characteristic X-rays (Particle Induced X-Ray Emission, PIXE), as well as the backscattered ions (Rutherford Backscattering, RBS) and -- in case of thin samples – the transmitted ions (Scanning Transmission Ion Microscopy, STIM). A newly installed optical microscope allows sample positioning and inspection during measurement. The magnetic scanning system moves the focussed beam across the sample within a scan field of adjustable extent. The data collection system MPSYS (MARC Melbourne) collects and stores the spectra of the several techniques at any beam position (Total Quantitative Analysis, TQA). In addition, optional windows can be set in the spectra for real-time elemental mapping. The images can be viewed and are printed as two-dimensional colour-coded intensity distributions.

<u>New installations in 2000/2001:</u>
closed cycle water cooling for the beam line components
replacement of the low pressure gas delivery system of the ion source by a high pressure system with much higher reliability
installation of a new beam line equipped with a goniometer chamber (Gonio 940 from HVEE)
development and installation of a beam energy stabilization system for the new beamline
replacement of the optical microscope already in use in the measuring chamber of the nanoprobe by a new one, which allows an inspection of the sample during ion beam analysis
installation of an additional magnetic shield

<u>Current work in nuclear nanoprobe performance is focussed on:</u>
installation of an external microbeam designed for the single ion bombardment of living cells
improvement of the lateral resolution of the nanoprobe by an shielding system actively compensating magnetic stray fields
replacement of the old data acquisition system by the new MicroDAS (MARC Melbourne)

7.2 Ion Beam Microanalysis (PIXE, RBS, STIM) of joint cartilage

T. Reinert, U. Reibetanz, A. Werner, W. Gründer, J. Vogt, T. Butz

Articular cartilage, i.e. the cartilage of joints, is a load-bearing elastic material that is responsible for the shock absorption and the frictionless movement in articulating joints. The ability to undergo reversible deformation depends on its structural organisation of the matrix molecules and the cartilage cells (chondrocytes). Collagen fibrils build up a tension stable network that is filled with pressure resistant hydrated macromolecules (proteoglycan). Chondrocytes are responsible for the anabolism and catabolism and for the internal remodelling of the cartilage. Age-related and pathological changes in the elemental distributions or in the balance of the cartilage components may contribute to structural changes in the collagen network leading to a loss of mechanical stiffness and subsequently to the initiation and progression of cartilage degradation.

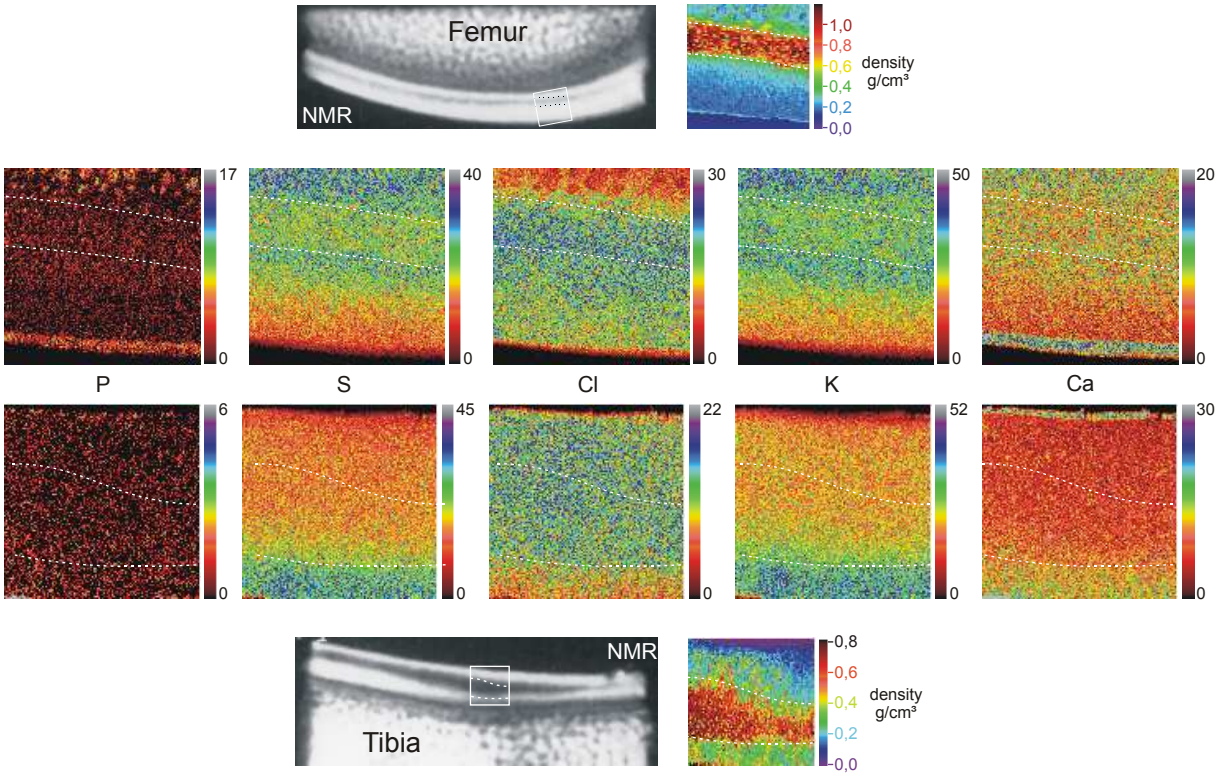

Figure 1: Elemental maps (~1 mm²) of phosphorus (P), sulphur (S), chlorine (Cl), potassium (K) and calcium (Ca) in correlation with NMR-images and density distributions of femoral and tibial joint cartilage (pig's knee). The areas between the dashed lines are the regions of higher collagen content that correlate with the hypointense regions (aligned collagen fibres) in the NMR-images.

High resolution magnetic resonance tomography (NMR-microscopy) is able to visualize anisotropic internal structures which are related to the collagen structure of the cartilage. Zones of aligned collagen fibres appear hypointense in the NMR-image. Thus, the high resolution MRT has a great diagnostic potential in the characterisation of early arthrotic changes in the cartilage structure. However, despite decades of cartilage research the cartilage structure and the interaction of matrix components are not yet fully disclosed. Notably, the distribution and the

arrangement of the matrix molecules (proteoglycans, collagen) are still under investigation and several structures of the collagen network are being discussed.

Ion microprobe techniques can answer of some open questions, especially questions concerning the elemental distributions and the collagen network. Using particle induced X-ray emission (PIXE), forward and backscattering spectroscopy (ERD, RBS) it is possible to investigate the elemental distribution and to derive the distribution of the matrix components within the cartilage. Scanning transmission ion microscopy (STIM) reveals the internal density distribution within the cartilage. In the high resolution mode fibres of collagen can be visualised.
Ion beam microanalysis was used to investigate the elemental and density distributions in cross-sections of pig's cartilage of the knee joint (Fig. 1). The results were compared with images of polarized light and NMR-microscopy to correlate the distributions with the histological zones.
In the NMR-hypointense zones (proliferation zone) there were an increase in chlorine concentration and spot-like accumulations of calcium. The NMR-hypointense zones were characterized by a three to fourfold higher density (freeze-dried samples). This density increase is based on the high content of the matrix elements H, C, N and O in this zone. Taking into account the density and elemental distributions and the structure of collagen (fibrillar) and proteoglycan (bottlebrush-like, high sulphur content) the NMR-hypointense zones have higher collagen and lower proteoglycan contents. On the contrary, the zones of hypertrophic cells (next to the zones of calcified cartilage/bone) are characterized by high contents of calcium, sulphur (proteoglycan) and potassium and less chlorine. In the outermost layer, just below the articulating surface (*lamina splendens*), we found a remarkable increase in the concentrations of phosphorous and calcium which could be a sign for calcifying processes.
The STIM-investigation of the orientation of the collagen network showed the radial orientation of the fibres as predicted by NMR measurements. However, in the zone of predicted tangential orientation no single collagen fibres could be found. The tangential orientation seems to be caused by tubular collagen structures (diameter < 1 µm) which form bunches perpendicular to the radial orientation (Fig. 2). Further investigations are needed to prove this assumption. Therefore, we focus on the development of STIM tomography in our laboratory to investigate the 3D structure of the collagen network in cartilage.

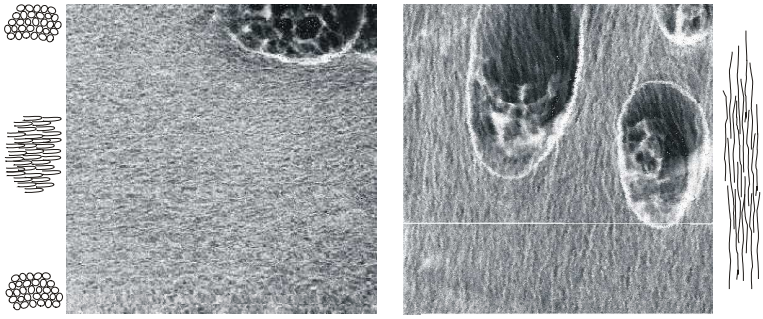

Figure 2: STIM-images (40 µm × 40 µm) of the collagen network in zones of suspected tangentially aligned (left) and radially aligned structures (right). The structures in the left image can be interpreted as bunches of collagen tubuli in different tangential alignment (horizontal plane) as the left sketch indicates. In the right image the radially aligned (vertical) collagen fibres are readily visible. The large globular objects are chondrocytes. The white horizontal line is due to data loss during data acquisition.

7.3 High Resolution STIM Tomography

T. Reinert, M. Schwertner, A. Sakellariou, J. Vogt, T. Butz

High resolution Scanning Transmission Ion Microscopy (STIM) is a powerful tool to visualize internal structures of small objects with a resolution down to 100 nm. The main advantage of ion microscopy is the capability of the high energy ions to penetrate the relatively thick samples (~ 10 µm) without significant beam spreading. Therefore, this method is ideally suited for the investigation of the 3D structure of the collagen network in articular cartilage.
A 3D-STIM-tomography experiment consists of recording a number of 2D-STIM images of the sample, called projections, under different incident angles from 0°...180° degrees (the 3rd dimension). For the experiments 360 projections of the samples were taken, each having a pixel resolution of 250×250 pixel. The data sets were reconstructed using the Backprojection of Filtered Projections (BFP) technique. In the first tomographic experiments, performed with 2 MeV protons, the resolutions did not reach 100 nm. The reason is a beam position instability during the STIM measurements due to magnetic stray fields in the laboratory. Therefore, we plan to install an active compensation of these fields.

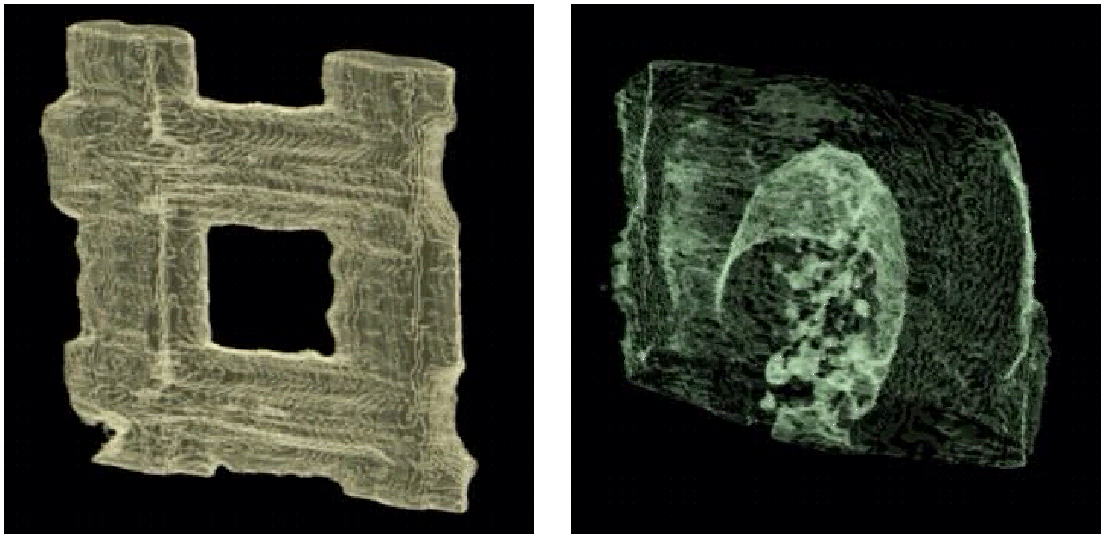

Figure 1: High resolution 3D representations of left: a 2000 mesh Cu grid and right: a cartilage sample (10 µm × 25 µm × 25 µm) containing a cell. The morphological properties were highlighted by rendering a fixed density value.

7.4 Skin as a barrier to ultra-fine particles

T. Reinert, F. Menzel, U. Anderegg, M. Sticherling, J. Vogt, T. Butz

Up to date, the potential risk of percutaneous uptake of ultra-fine particles has been neglected. Several attempts have been made to clarify the controversially discussed dermal uptake of micronized particles (TiO_2 or SiO_2). The feasibility of our approach was demonstrated in recent pilot studies on domestic pig skin exposed to a liposome formulation containing 5% micronized TiO_2 (20 nm) for 24 hours.

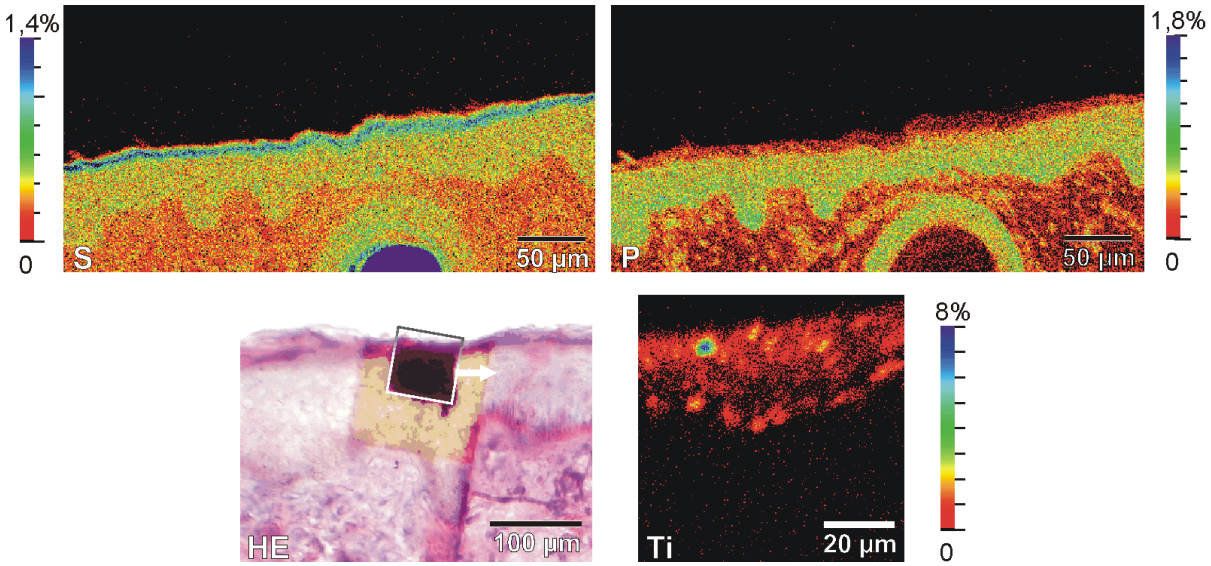

Figure 1: Examples of PIXE-maps showing the distribution of sulfur (S) and phosphorus (P) in a cross-section of pig skin. Bottom: haematoxylin-eosin (HE) stained histological image (left) with the proton scanned area marked by the square, from this region the titanium (Ti) distribution was obtained (right).

Fig. 1 shows as an example a PIXE-map for sulphur (top left) and phosphorus (top right) for a cross-section of 800 µm × 400 µm which allow a clear-cut delineation for the horny layer (thin bluish top layer in the S-map; the dark blue semicircle is a hair) and the onset of the dermis (onset of reddish-brown region below yellow-green region in the P-map). The lower left panel shows a haematoxylin-eosin (HE) stained histological image where two proton scanned areas are clearly visible as light brown and dark brown areas. The titanium-map for the indicated square, 76 µm × 76 µm, is shown in the lower right panel. Whereas the average concentration (red) corresponds to about 1–2%, there is a “hot spot” with about 7.5%. These observations corroborate previous tape stripping results and extend them to two dimensions and deeper strata. The unambiguous delineation between stratum corneum, stratum granulosum, and stratum spinosum requires further studies. Hence, it is to early to speak about penetration beyond the horny layer which may be as thick as 30 µm at this position. On the other hand, the lower part of the map contains less than 1 ppm Ti (which is the detection limit). Thus penetration into the dermis, which is not covered by the map, is very unlikely.

7.5 Single Ion Bombardment of Living Cells

J. Vogt, J. Tanner, J. Österreicher, T. Butz

The LIPSION nanoprobe facility is a prerequisite to study the effects of the single ion bombardment of individual living cells. Up to now, there is still little knowledge about this effect on the single cell basis. The understanding of what exactly happens on a molecular basis in the irradiated cell is crucial for progress in radiotherapy and radiation oncology as well as for radiation safety at low doses. For this research we have established a tissue culture laboratory adjacent to the accelerator laboratory. We are now in a position to keep living cell cultures in the incubator, to transfer them in the laminar flow-hood, to treat them with a variety of markers, and to perform irradiation experiments. Actually, we use HUVEC, a human endothelial cell line, originating from the human umbilical cord, supplied by Dr. G. Hildebrand, University Hospital Leipzig, Clinic and Policlinic for Radiation Oncology.
As a starting point we have taken a Scanning Transmission Ion Microscopy (STIM) image of a single HUVEC cell and compare this with an optical image (see Fig. 1) This proves that our hit accuracy is good enough to aim at intracellular targets, like the nucleus or the cytoplasm. The next steps will address questions of hit verification and individual ion counting. Finally, cell biological methods will be applied to study the cellular response after single ion bombardment.

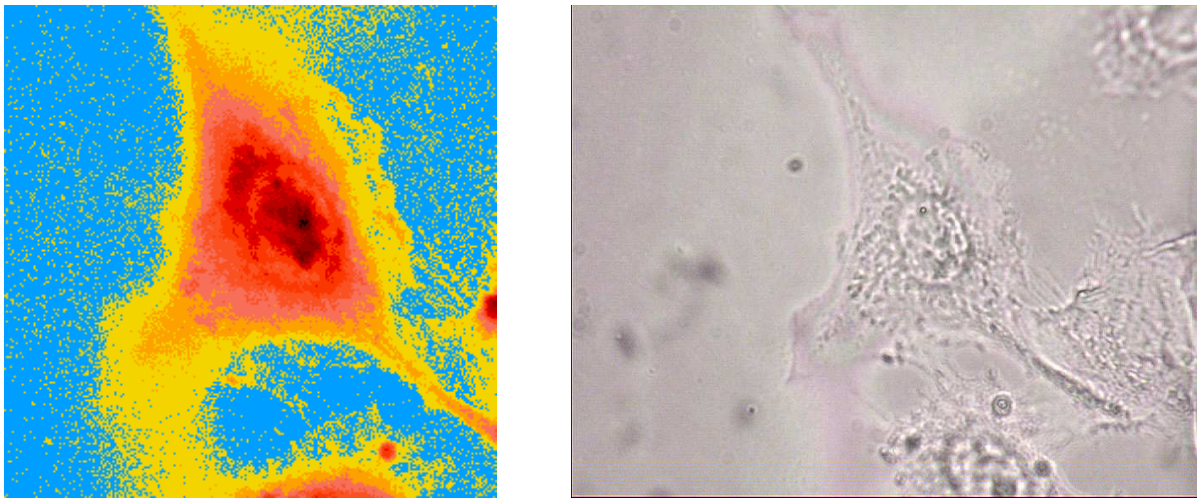

Figure 1: STIM image taken with 2 MeV protons with a scan area of 80µm x 80µm (left) and optical bright-field image of a fixated HUVEC cell (unstained) on a mini-Petri dish with a 200 nm thick Si_3N_4 bottom to allow for proton transmission (right).

7.6 Investigation of ancient human bone by means of ionoluminescence and *μ*PIXE

D. Spemann, St. Jankuhn, J. Vogt, T. Butz

We studied diagenetic alterations on ancient human bones by means of ionoluminescence and μPIXE. It was found that diagenetically altered regions show an orange-red luminescence activated by Mn^{2+} ions. In order to study the incorporation of Mn into the bone mineral in more detail, μPIXE measurements were performed in the periosteal region of a bone cross section from which maps of elemental distributions could be obtained.

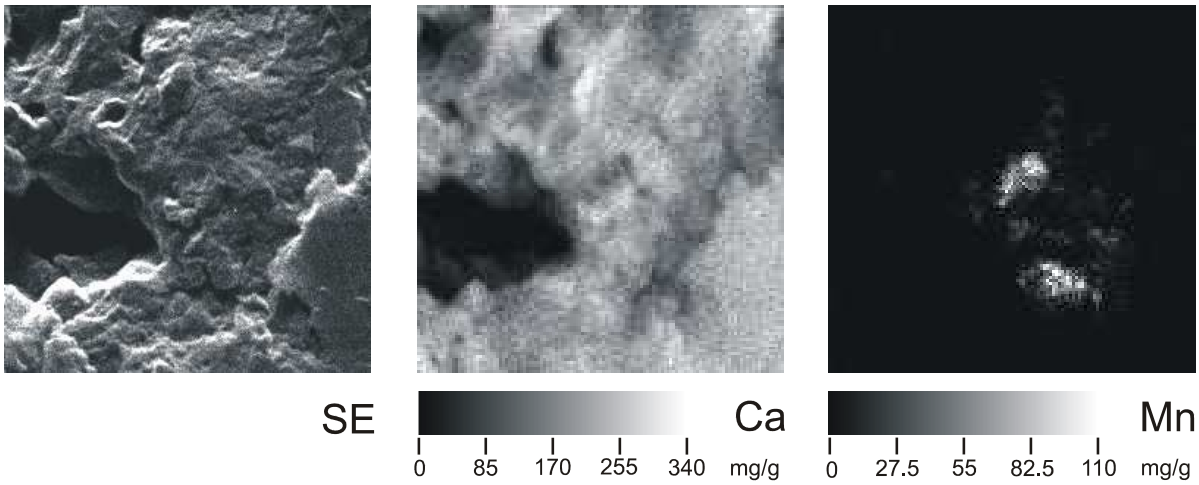

Figure 1: Secondary electron (SE) image and elemental maps of Ca and Mn (scan size 84×84 μm^2). The Mn-map shows the elemental distribution within an area of high Mn concentration. As can be seen from the SE image, this area is dominated by cracks and pores in the bone mineral

The Mn distribution is characterized by a rather uniform Mn concentration of 130 μg/g over the scanned area and additional small areas with concentrations up to 110 mg/g. These areas are mainly located at holes and pores in the bone mineral indicating that they act as suitable pathways for the incorporation of Mn (see fig.1). Furthermore a line scan was made which showed an enhanced concentration of Mn, Fe, and Zn in the area of the periosteal surface which shows that this region is strongly influenced by diagenetic alterations.

7.7 Novel test structures for submicron ion beam analysis

D. Spemann, T. Reinert, K. Otte, K. Zimmer, D. Dobrev, J. Vogt, T. Butz

So far, the beam spot sizes and scanning properties of nuclear microprobes have been determined using standard samples (e.g. EBEAM test sample, Chessy test sample and TEM Cu-grids) which are not suitable for this purpose for different reasons (material combination, design of the structures, accuracy of the edge profiles). Due to the lack of suitable test samples, the precise determination of submicron beam spot sizes was hardly possible. Therefore a novel test sample with nanometer structures for the use in submicron ion beam analysis has been developed by the University of Leipzig and the Institute of Surface Modification (IOM). The test sample provides horizontally and vertically arranged periodic structures, which range from 4 µm to 150 nm in size (see fig.1). The structures have been produced in SiO_2 and Ag for topographic and elemental contrast, respectively, using electron beam lithography and various etching techniques. Due to the excellent definition of the edge profiles (see fig.2), the ion beam spot size can be directly derived from a line scan across an edge even in the submicron regime. The structures on the test sample also allow the determination of scan sizes of a few microns.

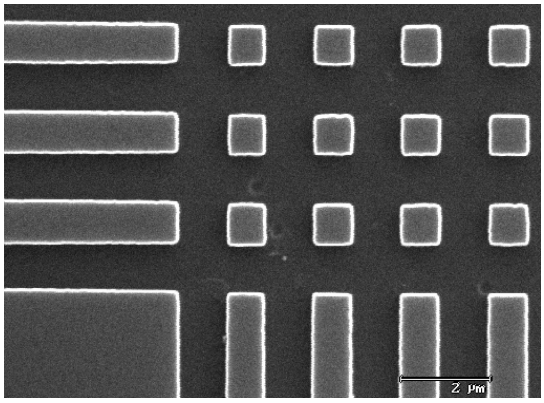

Figure 1: Top view SEM micrograph of the gratings with a period of 2 µm. The rectangular dots are formed in the region, where the horizontal and the vertical gratings overlap.

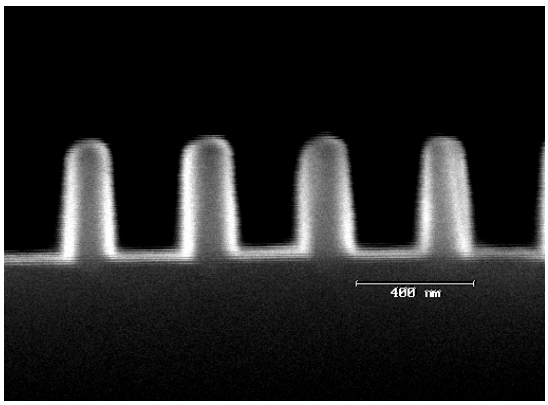

Figure 2: SEM micrograph of a cleaved grating with a period of 400 nm. Note the high aspect ratio as well as the almost vertical side walls (angle of better than 85°).

However, this test sample cannot be used in transmission mode and does not allow to obtain 2-dimensional images of the shape of a beam spot directly. For this purpose a semiconductor heterostructure consisting of an 1.62 µm GaInP epi-layer grown on (001) GaAs proved very useful, which provides atomically sharp edges for beam spot size measurements (see fig.3).

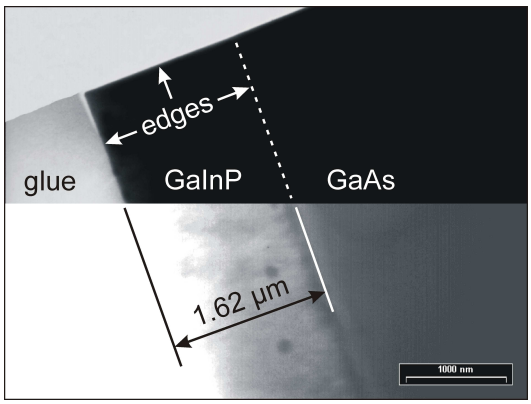

Figure 3: TEM image of the GaInP/GaAs (001) heterostructure showing the width of the GaInP epi-layer (top defines left edge; bottom (brightness enhanced) defines right edge).

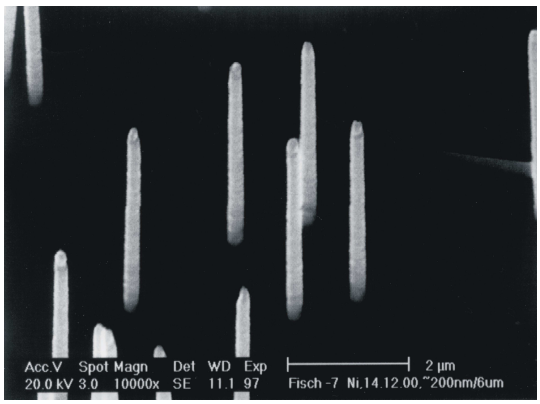

Figure 4: SEM image of the Ni-nano-whiskers used for the imaging of the beam spot shape. The whiskers have diameters ranging from 200 nm to 240 nm and a length of 6 µm.

Since the sample has been thinned down by standard TEM preparation techniques, it can be used for both PIXE and STIM. The sample has been investigated with a TEM and the ion nanoprobe LIPSION. The beam spot size in the low current mode was determined by a STIM measurement using 2 MeV protons and yielded (41±4) nm, which sets a new world record.

Furthermore, Nickel nano-whiskers produced at the GSI Darmstadt by electro-chemical preparation of etched ion track membranes have been used to obtain 2-dimensional images of the shapes of submicron beam spots (see fig.4). For these measurements a scan over a single Nickel nano-whisker having a diameter of 220 nm and a height of about 6 µm was performed and the secondary electrons emitted under ion bombardment were detected (see fig.5).

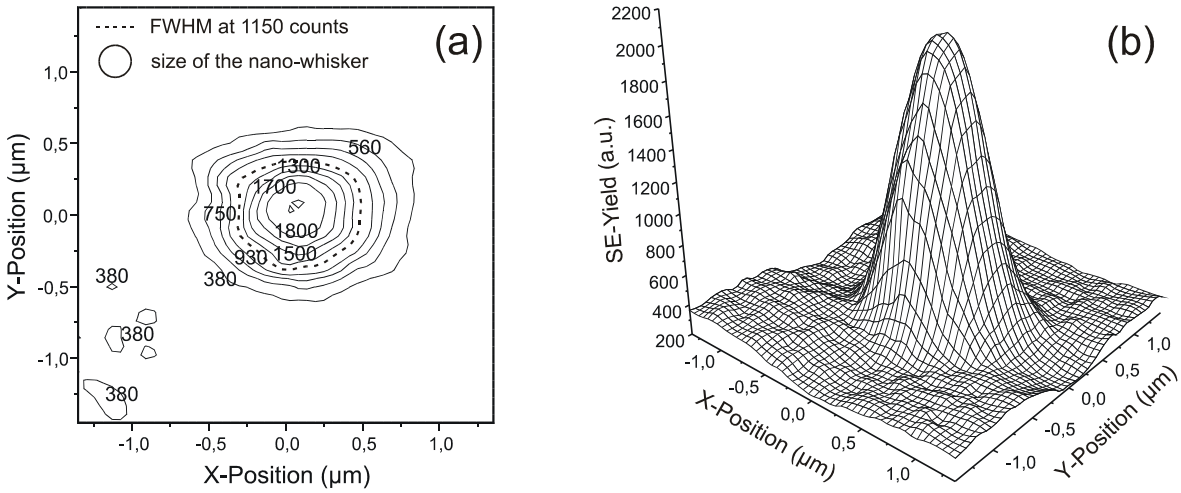

Figure 5: SE yield distribution obtained using an object and aperture diaphragm with a diameter of 50 µm and 100 µm, respectively. (a): Contour plot showing the shape of the beam spot. The dashed line represents the beam spot size. (b): 3D-wire frame of the SE yield. Apart from the peak in the SE yield caused by the nano-whisker, the SE yield from the Cu substrate shows minima along the scan positions with x=0 and y=0.

7.8 Si-doped luminescence gratings

J. Heitmann, J.C. McCallum, J. Meijer, A. Stephan, T. Butz, M. Zacharias

We have produced ordered Si-dot arrays with micron and submicron lateral dimensions by ion implantation using the heavy ion projector at the Ruhr-Universität Bochum. For this purpose we implanted 500 keV Si^+ ions into SiO_2 with doses ranging from 1×10^{16} Si^+/cm^2 and 3×10^{17} Si^+/cm^2 using 400 and 750 mesh grids as objects. After annealing at 1100°C under N_2-atmosphere the implanted arrays show strong photoluminescence at room temperature. Figure 1 shows a µPL-map from a sample with a structure size of 2 microns. A complete separation of smaller structures down to 700 nm could be proved by AFM. Figure 2 shows the dependency between the position of the PL signal and the implantation dose. The remarkable red-shift of the luminescence with increasing dose could be explained by the quantum confinement model, however, it was not possible to prove the existence of Si-nanocrystals by HRTEM or XRD. The mechanisms with are responsible for the observed luminescence are subject to further investigations.

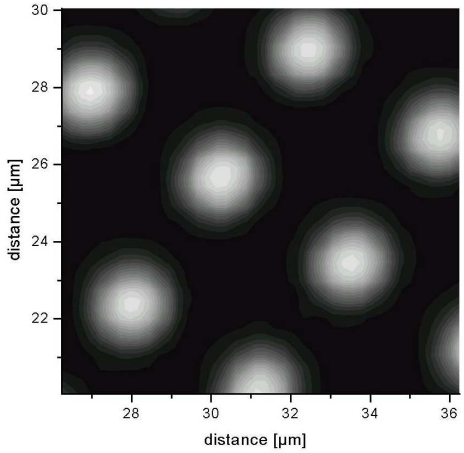

Figure 1: µPL-map from a sample with an implantation dose of 1×10^{17} Si^+/cm^2.

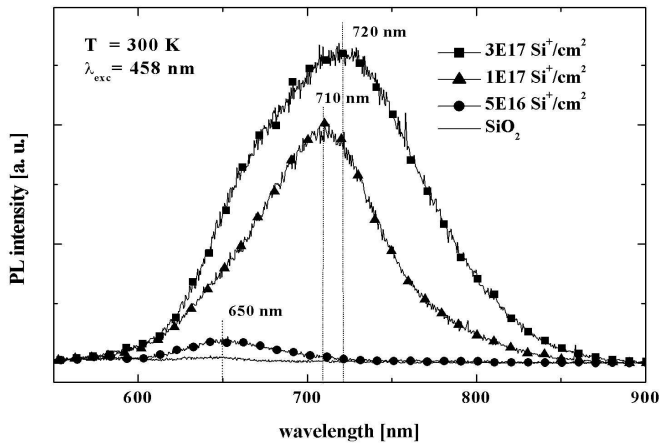

Figure 2: PL-spectra from samples with different implantation doses.

7.9 Ion beam analysis of $Zn_{2-2x}Cu_xIn_xS_2$ films

D. Spemann, J. Vogt, T. Butz, D. Oppermann, M. Lorenz, G. Wagner, K. Bente

Thin layers of ZnS-$CuInS_2$ mixed crystals (called ZCIS) may be promising absorber materials for thin film solar cell applications. The ZCIS films studied here have been grown on (001)GaP, SiO_2 and (012)CeO_2/Al_2O_3 substrates with different stoichiometries by Pulsed Laser Deposition (PLD). In order to optimize the film deposition process the thickness, stoichiometry and crystallinity of the films were determined by means of Rutherford Backscattering Spectrometry (RBS), Particle Induced X-ray Emission (PIXE) and RBS/Channeling using a 2 MeV He^+ ion beam. Furthermore the stoichiometry of the targets used for the PLD was determined with Backscattering Spectrometry (BS) and PIXE using a 2 MeV H^+ ion beam.
A large variation in film thickness was observed and the film stoichiometry did not agree with the PLD-target stoichiometry in general. Figure 1 shows the element transfer of Zn, Cu and In for the different substrates used. Linear functions with parameters shown in fig. 1 were used as approximations for the observed transfers. While the transfer efficiency of sulfur was near unity for all films studied here, the transfer efficiencies varied substantially for Zn, Cu and In. In general the Zn-concentration in the films was smaller than in the corresponding targets (see fig. 1(a)). The negative offset, especially for SiO_2-substrates indicates that there is an unknown sink. As shown in fig. 1(b) the transfer efficiency of Cu is 1.34, significantly larger than unity, and independent of the substrate material used. Consequently all films investigated had a higher Cu-concentration than the corresponding targets. Contrary to Cu, the transfer efficiency of In differs significantly for the different substrate materials (see fig. 1(c)). While the transfer efficiency for SiO_2-substrates is unity, it is only 0.78 for GaP-substrates. It should be noted that some of the data points deviate remarkably from the linear fit. These deviations were predominantly found on samples which were affected by a Cu-outdiffusion into the GaP substrate, which was detected with RBS and confirmed by Secondary Neutral Mass Spectroscopy (SNMS) and TEM.
RBS/Channeling measurements show that mono-crystalline films can be grown on (001)GaP and (012)CeO_2/Al_2O_3 substrates, however, they are characterized by a large defect density.

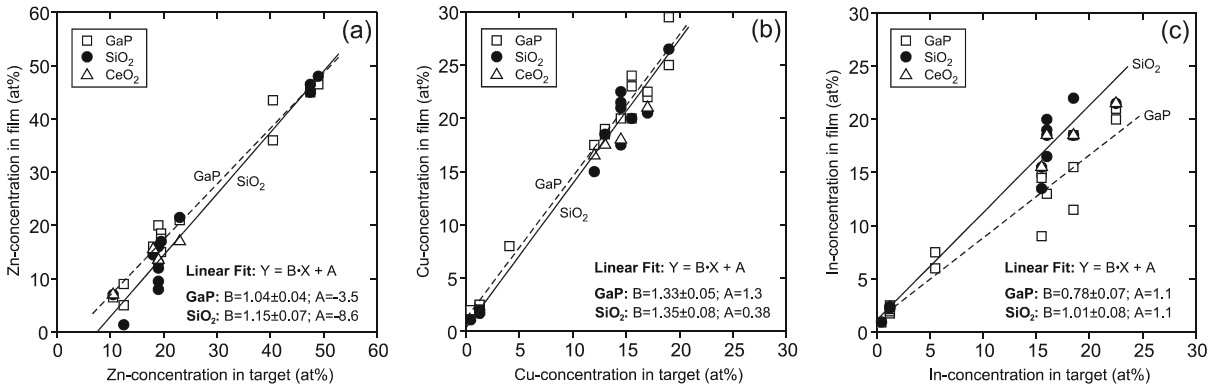

Figure 1: Element transfer from the PLD target to the deposited film for different substrate materials for (a): Zn, (b): Cu and (c): In.

7.10 Quantitative multi-element analysis of impurities in graphite

D. Spemann, R. Höhne, A. Setzer, P. Esquinazi, J. Vogt,T. Butz

Ferromagnetic properties of graphite have gained massive interest in the scientific community very recently. However, in order to distinguish between ferromagnetism caused by impurities and ferromagnetism that can be attributed to graphite itself, a very sensitive quantitative multi-element analysis of the impurities contained in the graphite samples is of great importance. The magnetic properties of the graphite samples were characterized by Prof. Esquinazi and co-workers (SUM). We determined the concentrations of the elements with $Z>12$ in the graphite samples by means of Particle Induced X-Ray Emission (PIXE). The minimum detection limit for elements like Ti,...,Zn was ~0.3 ppm. The information about the impurity content in the samples proved very useful for the interpretation of their observed magnetic properties.

7.11 TDPAC-Laboratory

W. Tröger, F. Heinrich, T. Butz

Nuclear probes are used to study the interaction of metals with biological macromolecules like, e.g., DNA and proteins. Many life processes are based on such interactions. The structure and dynamics of metal sites in biomolecules are important in determining the functional efficiency of these macromolecules. In order to study those metal sites close to physiological conditions a highly sensitive spectroscopic method is required, like Time Differential Perturbed Angular Correlation (TDPAC). Here, a radioactive atom is placed at the site of interest and by correlating the emitted γ-quanta in space and on a nano-second time scale local structural information is provided. These investigations allow a deeper insight into the detoxification processes, switches, adaptivity and rigidity of metal sites in electron transfer proteins, and also the development of new radiopharmaceuticals in cancer therapy.

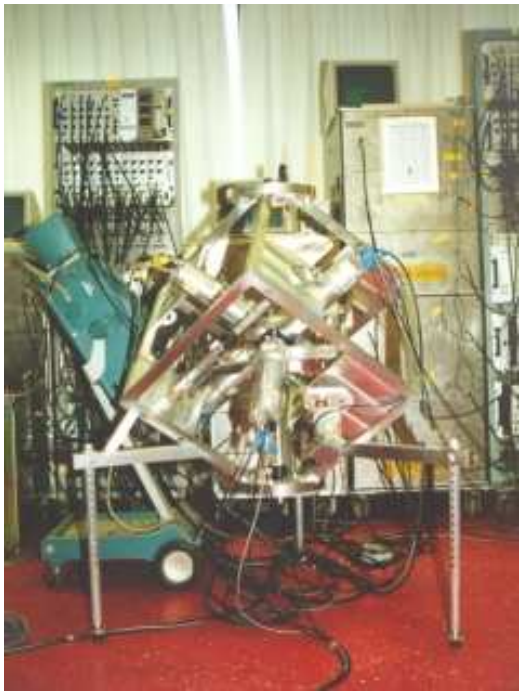

Furthermore, TDPAC is also used in material science to obtain a better understanding of the corrosion of battery electrodes or the behaviour of impurities in metals.

7.12 Investigation of the Corrosion of Nickel Electrodes via Time Differential Perturbed Angular Correlation

F. Heinrich, W. Tröger, T. Butz

The corrosion of nickel plated steel electrodes in non-rechargeable batteries during storage up to 2 years is investigated by Time Differential Perturbed Angular Correlation (TDPAC). The internal resistance of batteries is significantly influenced by this corrosion. The non-destructive in situ analysis of the chemical changes is carried out by TDPAC studies using the nuclear probes ^{111}In(EC)^{111}Cd and ^{181}Hf(β^-)^{181}Ta with a half-life of 2.83 days and 42.4 days, respectively. With TDPAC the hyperfine interaction of the nuclear probes in these electrodes is monitored. Taking into account known battery characteristics an effective storage time of 2 years can be achieved by storing battery models for 28 days at 70 °C.
The nuclear probes ^{111}In and ^{181}Hf are placed into the nickel electrodes into various depths from 7 nm to 150 nm by ion implantation (see figure 1), electrolytic deposition and surface diffusion. The progress of the corrosion process leads to a decrease of the amplitude of the Ni magnetic hyperfine interaction signal and an increase of quadrupolar and/or magnetic signals arising from the corroded material. The corrosion process reaches a depth of 10 nm to 20 nm after an effective storage time of 1.5 years (see figure 2). The kinetics of the corrosion process can be described as a “diffusion controlled” reaction.

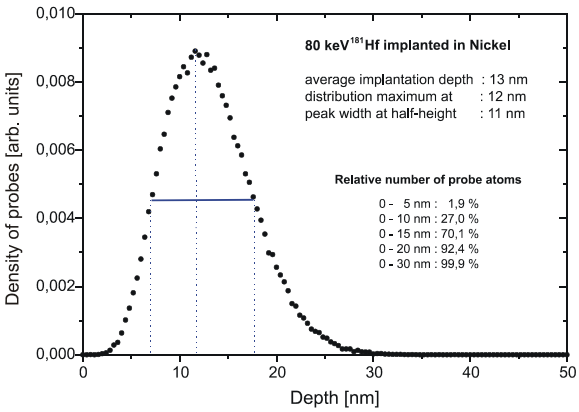

Figure 1: Depth distribution of the nuclear probes after 80 keV ^{181}Hf ion implantation (simulated with TRIM).

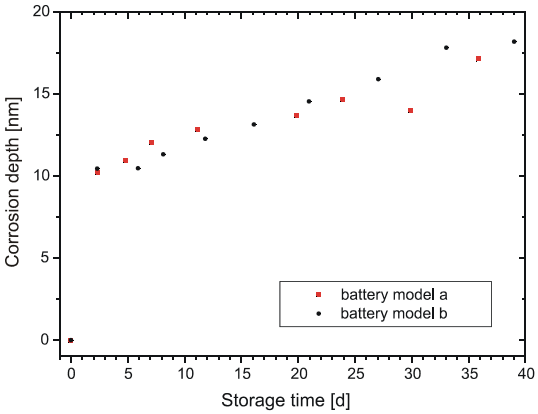

Figure 2: Progression of the corrosion depth assuming a homogeneous corrosion starting from the surface of the Nickel electrodes.

7.13 pH Dependent Hg(II) Coordination in Metallothioneins: A ^{199m}Hg TDPAC-Study

W. Tröger, P. Faller, M. Vašák, ISOLDE Collaboration

Mammalian metallothioneins (MT) are ubiquitous, cysteine-rich proteins of low molecular weight which bind d^{10} metal ions such as Zn(II), Cd(II), Cu(I) and Hg(II) in metal-thiolate clusters. They play an important role in the metabolism and in the modulation of the essential trace element zinc and copper and in the binding of toxic heavy metals. The latter suggests also the involvement in cellular detoxification mechanisms. Several 3D structures have been solved for mammalian Me(II)7-MT, containing Zn(II) and/or Cd(II) ions. These metal ions are tetrahedrally coordinated by both bridging and terminal thiolates in cluster structures. We studied the Hg(II) coordination in rabbit liver MT by time differential perturbed angular correlation (TDPAC) spectroscopy. With TDPAC the local environment of a local probe nucleus, here ^{199m}Hg, can be studied by the correlation of two subsequent gamma quanta in space and time emitted by the probe. The titration of apo-MT with Hg(II) (1-7 equiv.) revealed mainly two- and fourfold Hg(II) coordinations depending on Hg(II) concentration and pH. At pH 2.0 twofold coordinations dominate whereas at pH 8.6 also higher coordination numbers occur (see figure 1).

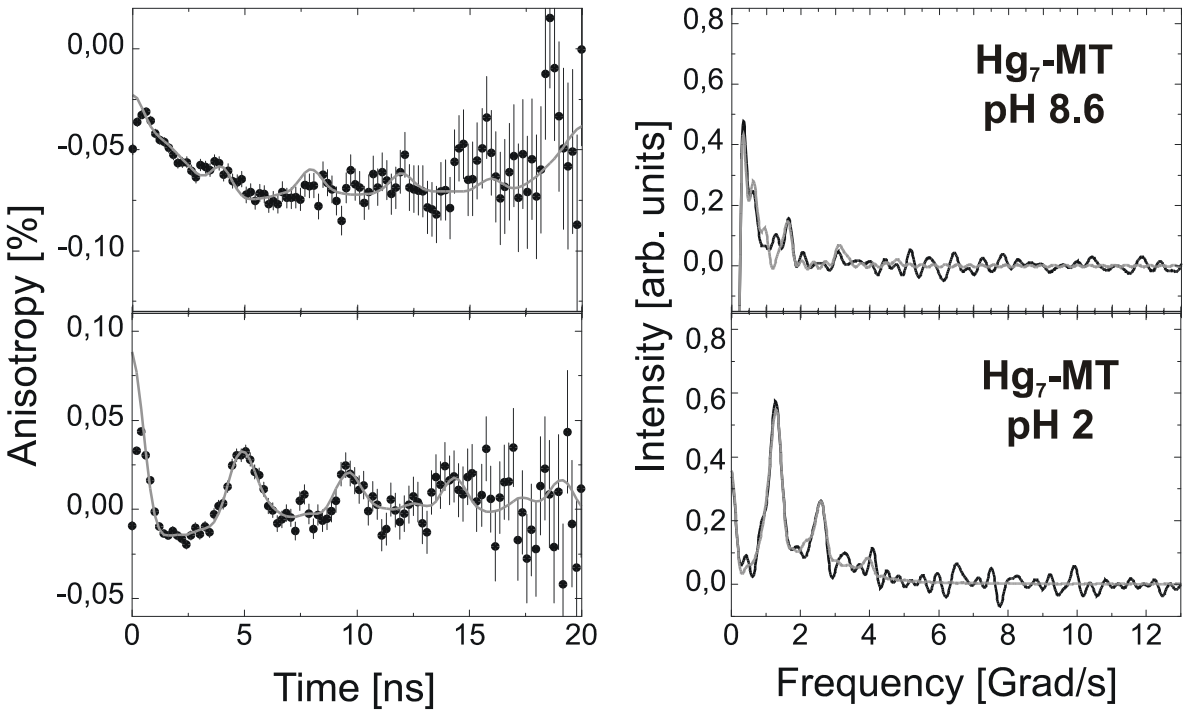

Figure 1: TDPAC time spectra (left) and their Fourier transforms (right) of Hg_7-MT at pH 8.6 (top) and pH 2 (bottom). The low frequency at pH 8.6 indicates a tetrahedral and the high frequency at pH 2 a digonal Hg coordination geometry.

7.14 Hg(II) Coordination Studies in Penicillamine Enantiomers by ^{199m}Hg-TDPAC

W. Tröger, ISOLDE Collaboration

Sulfhydryl ligands have a strong affinity to mercury. Therefore inorganic mercury, Hg(II), in fluids and tissue of living organisms is bound by the sulfhydryl groups of cysteine-containing peptides and proteins. However, despite the high thermodynamic stability of Hg(II)-thiol complexes, there is evidence that Hg(II)-thiol binding in cells is quite labile. Therefore, sulfhydryl-containing therapeutic agents like, e.g., 2,3-dimercaptoethanol or penicillamine, can be used to extract Hg(II) from the body.

Penicillamine (see fig.1) is a characteristic degradation product of penicillin type antibiotics. It is given orally or intravenously as a chelating agent in the treatment of mercury poisoning, Wilson's disease (too much copper in the body), or other heavy metal poisoning, especially lead. The typical dose for humans is 0.5 to 2 g daily.

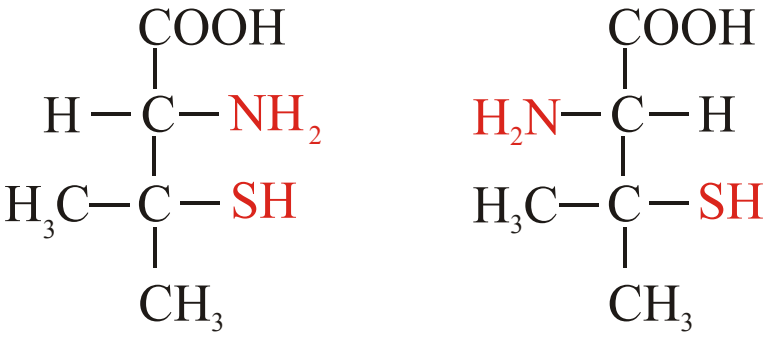

Figure 1: The enantiomeric forms of penicillamine (molecular weight 149.21 g/mol). The potential metal ligands are sulfur and nitrogen.

This investigation was triggered by the question whether Hg(II) also forms trigonal coordinations without being forced to, e.g., by a rigid protein structure as it is the case in the regulatory protein MerR of the mercury detoxification system. A detailed knowledge might also be helpful for the development of more efficient detoxification pharmaceuticals.

The nuclear quadrupole interaction of the mercury isotope ^{199m}Hg monitored by time differential perturbed angular correlation (TDPAC) was used to elucidate the coordination geometry of Hg(II) bound by penicillamine enantiomers (D-Form, L-Form, DL-Racemate) at different stoichiometries.

The TDPAC probe ^{199m}Hg was supplied by the mass separator ISOLDE/CERN which allowed to perform these studies at much lower Hg(II) and ligand concentrations as a previous ^{13}C-NMR study. In fig. 2 the recorded TDPAC spectra at a 1:1-stoichiometry are shown. The high frequency component in the spectra of the D-form (top) arises from an almost linear, twofold Hg(II) coordination geometry whereas the low frequency component is due to a trigonal Hg(II) coordination. This trigonal coordination was also found under conditions of excess ligands. The spectra

of the other penicillamine enantiomers show also components with even lower frequencies indicating fourfold Hg(II) coordinations.

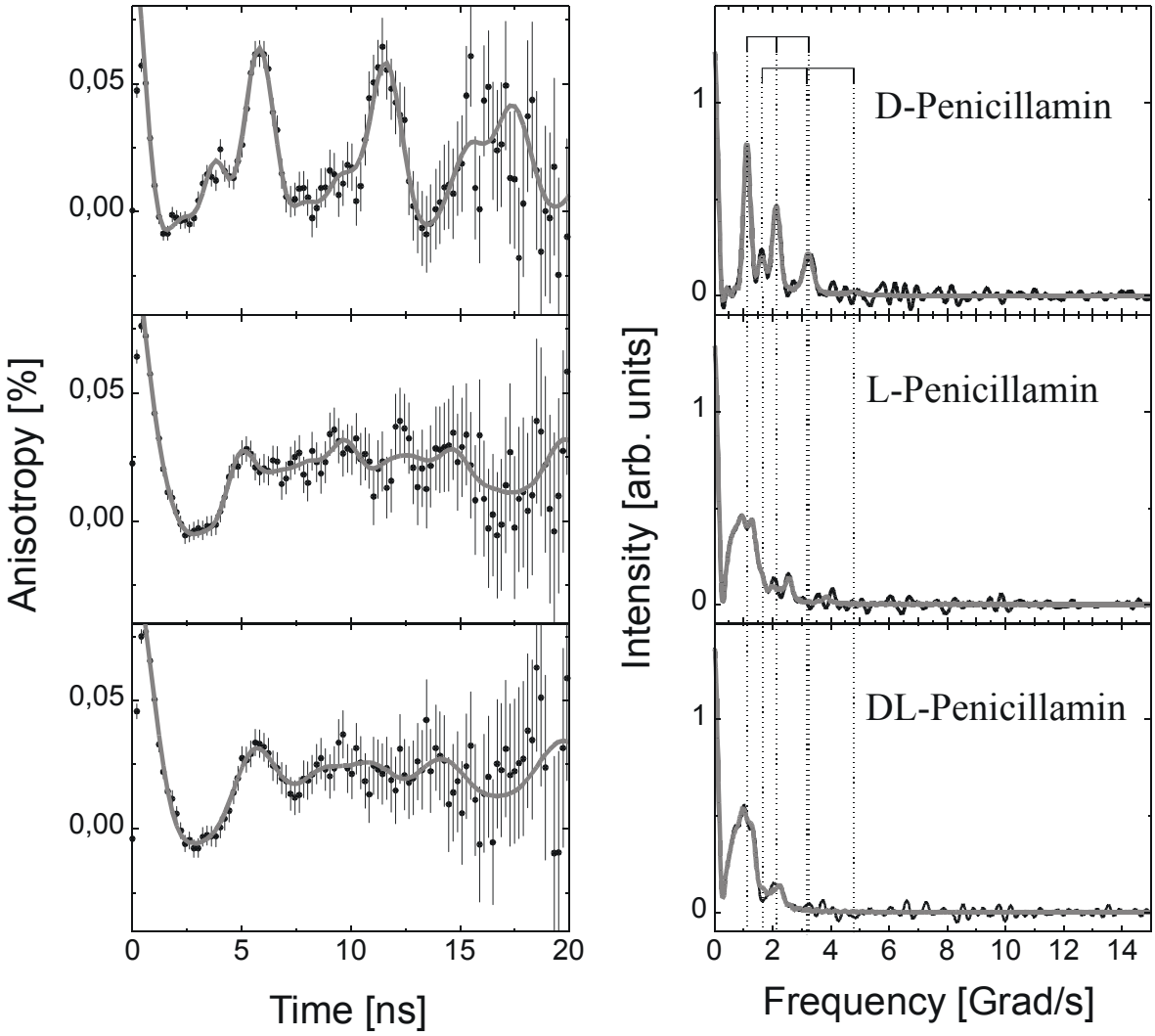

Figure 2: ^{199m}Hg-TDPAC time (right) spectra and their Fourier transforms (left) of the penicillamine enantiomers (frozen solutions and 77 K, Hg : Penicillamine = 1:1).

7.15 The Nuclear Quadrupole Interaction of ^{204m}Pb in Cadmium monitored by γ–γ Perturbed Angular Correlations

W. Tröger, H. Haas, J.G. Correia, J.P. Araujo, ISOLDE Collaboration

Electric field gradients (EFGs) in non-cubic metals are widely studied, and also the nuclear quadrupole interaction (NQI) of impurities in metallic host lattices has been investigated extensively. From the experimental systematics coupled with a tight-binding model a qualitative understanding of the EFGs at sp metal impurities in the simple metals Zn and Cd has been developed. Although there are already some studies of Pb as a probe in metals, mainly with the time differential perturbed angular distribution (TDPAD) method, reliable data on the NQI of Pb in zinc or cadmium are still missing.

For the first time the nuclear probe ^{204m}Pb was produced at the on-line isotope separator ISOLDE at CERN and used for time differential perturbed angular correlation experiments in order to determine the NQI of this isotope in cadmium. The EFG of ^{204m}Pb at room temperature in Cd metal was determined to be V_{zz} = 19(1) $\cdot 10^{21}$ V/m^2. The corresponding TDPAC spectrum is shown in figure 1. Ab initio-calculations of the EFG for the impurities Pt to Bi in cadmium were performed with the full-potential linearized augmented plane waves code WIEN97 with supercells of 36 atoms to interpret this result. For Au, Hg and Pb, where experimental results are now available, these agree with the calculations to within 10 %.

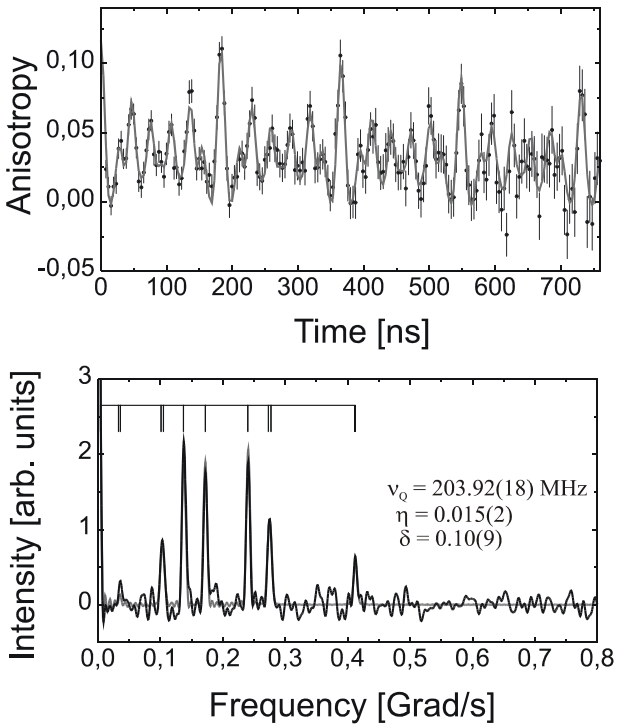

Figure 1: The TDPAC time spectrum (top) and its Fourier transform (bottom) of ^{204m}Pb in Cd metal. The grey lines show the least-squares-fitting for the NQI parameters given in the inset of the Fourier spectrum. The frequency bar in the Fourier spectrum indicates the nuclear precession frequencies.

In life sciences an application of the ^{204m}Pb probe would be the investigation of the coordination and the dynamics of the Pb binding site in new catalytic DNA molecules which can be used as metal sensitive biosensors or for the design of more efficient heavy metal detoxification drugs. A more detailed understanding of the interaction of heavy metal ions with biomolecules acting as sensors or drugs is essential to optimize their efficiency and selectivity - a quite beneficial role for the toxic triple of TDPAC probes ^{111m}Cd, ^{199m}Hg and ^{204m}Pb which are now available at the ISOLDE facility at CERN.

7.16 Blue copper proteins adsorbed an atomically flat surfaces

W. Tröger, B. Ctortecka, M. Lösche, T. Butz, ISOLDE Collaboration

We studied the physisorption of the small blue copper proteins stellacyanin (Sc) (molecular weight: ≈ 20 kD, protein diameter ≈ 40 Å) from protein solutions onto atomically flat surfaces of single crystals of 1T-TaS_2 and 2H-MoS_2.

In these proteins the naturally occurring Cu ion can be easily replaced by the TDPAC probes ^{111m}Cd and ^{199m}Hg (TDPAC = Time Differential Perturbed Angular Correlation). Scanning tunnelling microscopy (STM) was used to characterize the surfaces prior to adsorption. Tapping mode atomic force microscopy (AFM) on the adsorbed protein films is employed to characterize the topology of the adsorbed protein. TDPAC spectroscopy on Cd and Hg protein derivatives is performed to quantify their molecular integrity as a function of pH and the restrictions of motion imposed by adsorption, and to look for preferential orientation of the adsorbed proteins. Monomolecular protein layers on electrodes are an indispensible prerequisite for TDPAC studies of electron transfer processes in these proteins. According to different adsorption conditions (pH, protein concentration, substrate) various topologies of protein adsorbates are obtained, e.g. in monomolecular protein layer on 2H-MoS_2 substrates (see figure 1) or a flower like pattern on a gold surface (see figure 2). In the case of 2H-MoS_2, the layer thickness is 5.5 nm which is approximately the protein diameter.

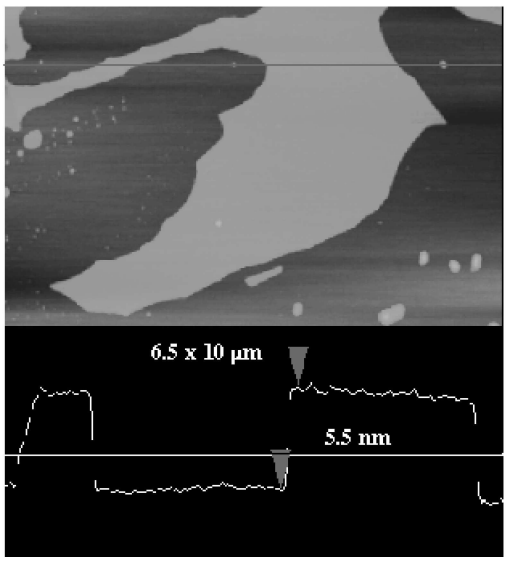

Figure 1: AFM image (tapping mode, U_t = 0.88 V, scan rate 0.86 Hz) of native stellacyanin on 2H-MoS_2 in air, area: 6.5 × 20 µm^2 (TRIS buffer, pH 9); line scan: layer thickness ≈ 5.5 nm (≈ protein diameter).

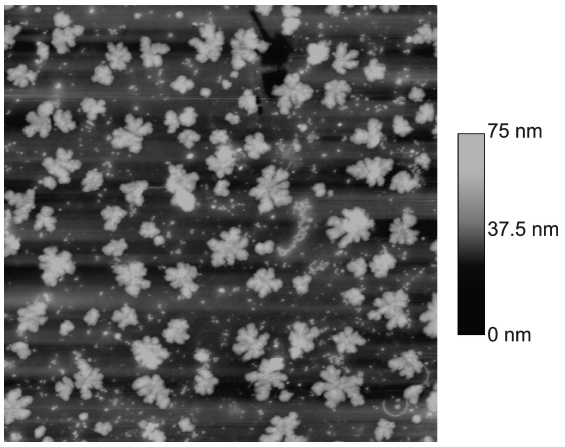

Figure 2: AFM image (tapping mode, U_t = 1 V, scan rate 1.07 Hz) of native stellacyanin on Au in air, area: 20 × 20 µm^2 (TRIS buffer, pH 6). Maximum height of the structures 75 nm (≈15 times the protein diameter).

7.17 Nuclear hyperfine techniques for studying the chemical states: The application of TDPAC to the development of new radiopharmaceuticals

W. Tröger, B. Ctortecka, R. Alberto

The selective destruction of malignant tumours is based on the concept that a carrier molecule possessing a preferred affinity for the target tumour should serve as a selective delivery system for a cytotoxic agent, e.g., a radioisotope, thereby achieving a localized cell killing while sparing normal body tissue. The β-emitter ^{111}Ag with its half-life of 7.5 days and almost no therapeutically useless γ-radiation would be ideally suited for such a systemic radiotherapy. In order to link the radioisotope to the carrier molecule an in-vivo stable complex has to be formed.
Promising ligands for such an in vivo stable complex might be thiocrownethers, macrocyclic ligands having thioether donors for selective heavy metal binding, e.g., the thiocrown ether (18S6) consists of a ring of 18 atoms, i.e. 12 carbon atoms and 6 sulphur atoms. Since thioether groups are soft Lewis bases they react selectively with soft Lewis acids like copper(I), silver(I) and mercury(II). Besides other thiocrowns and metal ions, we investigated the coordination of Ag in the thiocrowns (15S5), (18S6), (18S6-OH), (19S6-OH), and (20S6-OH) by monitoring the nuclear quadrupole interaction of ^{111}Ag by TDPAC. The nuclear quadrupole intercation is the interaction between the known nuclear quadrupole moment of a nuclear probe, here ^{111}Ag, and the electric field gradient tensor (EFG) arising from all extra-nuclear charges. The EFG is therefore a fingerprint of the coordination sphere of the nuclear probe. Since these studies have to be performed under physiological conditions with picomol amounts, classical methods like X-ray or NMR can not be employed for these studies.

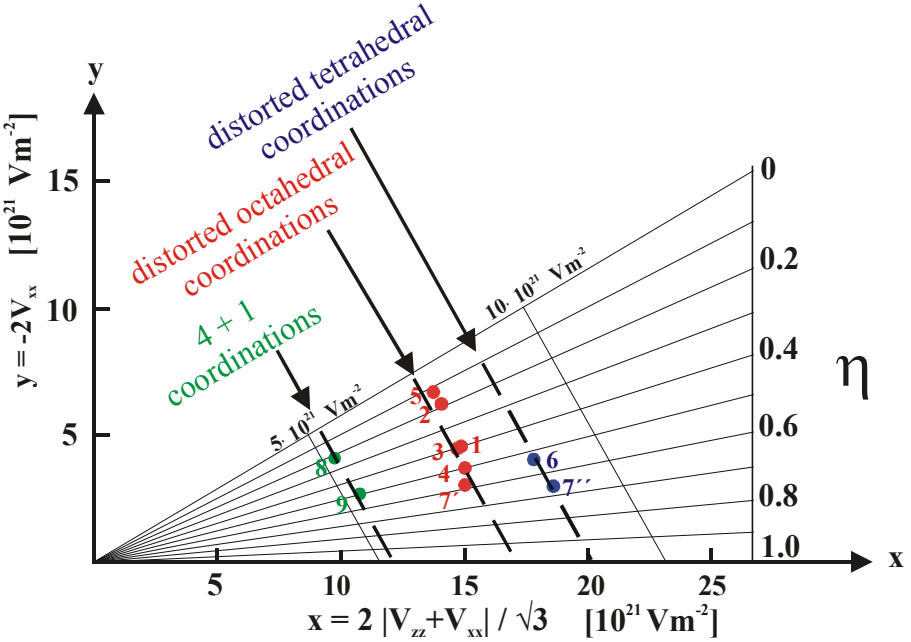

Figure 1: Czjzek diagram of the investigated Ag(I)thiocrownethers. For the sample numbers and the corresponding NQI parameter see table 1. The straight lines for constant Vzz (V_{zz}= 5 · 10^{21} Vm^{-2}, 10 · 10^{21} Vm^{-2}) and for constant η (η= 0, 0.1, ..., 1) are indicated.

Ag Thiocrownether	V_{zz} [10^{21}V/m^2]	η	Sample No.
[Ag(**18S6-OH**)] [CF_3SO_3] polycrystalline sample, 22 °C	7.60	0.399(2)	**1**
[Ag(**18S6-OH**)] [CF_3SO_3] DMSO, -51 °C	7.62	0.186(9)	**2**
[Ag(**18S6-OH**)] [CF_3SO_3], polycrystalline sample, 51 °C	7.55	0.399(3)	**3**
[Ag(**18S6**)]$^+$, n.c.a., THF, -70 °C, pH = 7.0	7.41	0.50(3)	**4**
[Ag(**18S6**)]$^+$, n.c.a., THF, -70 °C, pH = 0.5	7.60	0.12(3)	**5**
[Ag(**19S6-OH**)] [tosylat] polycrystalline sample, 22 °C	8.68	0.536(7)	**6**
[Ag(**20S6-OH**)] [CF_3SO_3], polycrystalline sample, 24 °C 1st site, pop.: 45(14)% 2nd site, pop.: 55(14)%	7.24 8.78	0.58(2) 0.66(1)	**7'** **7''**
[Ag(**15S5**)][BF_4], polycrystalline sample, 24 °C	5.45	0.323(5)	**8**
[Ag(**15S5**)][CF_3SO_3], ACCN, -196 °C	5.59	0.59(5)	**9**

Table 1: The electric field gradients and their asymmetry parameters η at ^{111}Ag of the investigated Ag(I) thiocrownether complexes.

In table 1 the ^{111}Ag-EFGs of thiocrownethers mentioned above are given and plotting these EFGs in a so-called Czjzek plot [12], which is essentially a linear plot of one EFG component (V_{xx}) versus a linear combination of V_{zz} and V_{xx} (see figure 1), reveals that the EFGs are found approximately on straight lines of constant V_{zz} which can be assigned to octahedral, tetrahedral, and "4+1" coordination geometries. Obviously, the optimal ring size for a quite stable coordination by all six thiols is the thiocrownether with 18 atoms whereas bigger crowns allow also tetrahedral coordinations and thiocrowns with a smaller ring size exhibit an additional bonding to a second thiocrown ether.
A higher in-vivo stability can be obtained by thio-cages, so-called cryptants, which provide a 3-dimensional enclosure of the metal. Here, the main obstacle to be over-come is the complete incorporation of the Ag(I) ion in the cage.

The fact that the EFGs coordinations belonging to a certain family of coordination form straight lines in the Czjek-diagram can be used for the identification of unknown coordinations and is a significant extension of the classic "fingerprint identification". In respect to an in-vivo stable complexation these studies allow also a rational design of radiopharmaceuticals aiming at a complex of highest possible in-vivo stability.

7.18 Funding

Interdisziplinäre Forschung mit dem Hochenergie-Nanoionenstrahl
Interdisciplinary Research with the High Energy Nano Ion Beam
T. Butz
Deutsche Forschungsgemeinschaft, Innovationskolleg INK24: „Phänomene an den Miniaturisierungsgrenzen“, Teilprojekt M, INK24 B1/2 TP M (until 12/00)

Monomolekulare Adsorbatschichten von Makromolekülen
Monomolecular layers of adsorbed macromolecules
Prof.Dr. T. Butz, Priv.-Doz.Dr. W. Tröger
Bundesministerium für Bildung und Forschung, 03-BU5LEI-1 (until 2/01)

Koordinationsstudien mit TDPAC an makrozyklischen Ag-Kronen und –Käfigen: Molekulare Integrität von ^{111}Ag-Radiopharmaka
Coordination studies with TDPAC on macrocyclic Ag-crowns and –cages: Molecular integrity of ^{111}Ag-radiopharmaca
Priv.-Doz.Dr. W. Tröger
Deutsche Forschungsgemeinschaft, Tr327/5-1,2 (until 6/01)

Untersuchung der Veränderung von Ni-Oberflächen als Batterieelektroden
Investigation of the modification of Ni-surfaces of battery electrodes
Priv.-Doz.Dr. W. Tröger
Hille & Müller GmbH & Co (until 6/00)

Radioactive Metal Probes as Diagnostic Tools in Biomolecules
Priv.-Doz.Dr. W. Tröger
Deutsche Forschungsgemeinschaft, Tr327/8-1

The Influence of Heavy Metals on Living Cells
Priv.-Doz.Dr. W. Tröger
Bundesministerium für Bildung und Forschung, Internationales Büro, Wissenschaftlich-technologische Zusammenarbeit mit Polen, POL-021-99

Kombinierte ortsaufgelöste Analyse der Elementzusammensetzung, Struktur und elektrischen Eigenschaften von (Fe, Zn)S-$CuInS_2$-Mischkristallen mittels Hochenergie-Ionenmikroskopie
Combined spatially resolved analysis of the composition, structure and electrical properties of (Fe, Zn)S-$CuInS_2$ mixed crystals using high energy ion microscopy
Prof. T. Butz
Deutsche Forschungsgemeinschaft, Fl211/5-1 (until 5/01)

Single Ion Bombardment of Living Cells
Prof. T. Butz
Marie Curie-Development Host Fellowship, HPMD-CT-2000-00028

Forschungsförderung 2000 (S. Lebed)
T. Butz
SMWK, AZ: 4-7531.50-04-0361-00/1 (until 11/00)

7.19 External Cooperations

Beijing Institute of Petrochemical Engineering, Beijing, Prof. G. Sun
CERN, Genf, ISOLDE Collaboration
Chalmers Technical Highschool, Göteborg
CSIRO, Exploration and Mining, Sydney, Dr. C. Ryan
Fa. Hille & Müller, Dr. W. Olberding
FRM, Garching, Prof. E. Wagner, Dr. U. Wagner
FU Berlin, Prof. U. Abram
Gray Laboratory, London, Prof. B. Michael
GSI Darmstadt, Dr. D. Dobrev, Dr. B. Fischer
HMI, Berlin, Dr. D. Alber
IIF Leipzig, PD Dr. H. Kupsch, K. Franke
Institute of Applied Physics, Sumy, Ukraine, Dr. S. Lebed
Institute of Nuclear Physics, Krakow
Institute of Nuclear Technology, Lisbon, Prof. J.C. Soares
IOM Leipzig, Dr. K. Otte, Dr. K. Zimmer
KVL, Kopenhagen, Prof. R. Bauer, Dr. E. Danielsen, Dr. L. Hemmingsen
LMU München, Prof. H. Knözinger
Massenseparator-Kollaboration Bonn-Göttingen
MLU Halle, Dr. J. Tanner
MPI für Biochemie, Martinsried, Prof. R. Huber, Dr. A. Messerschmidt
MPI für Mikrostrukturphysik, Halle/S., Dipl.-Phys. J. Heitmann
MPI für Polymerforschung, Mainz, Prof. W. Knoll
MPI für Strahlenchemie, Mühlheim/Ruhr, Prof. W. Lubitz
Petroleum Institute, Fushun, China, Prof. W. Liu
Prähistorische Staatssammlung München, Dr. R. Gebhard
PSI Villigen, Schweiz, Dr. R. Alberto
Shanghai Institute of Nuclear Research, Shanghai, Prof. J. Zhu
The University of Melbourne, Microanalytical Research Centre
TU Wien, Prof. K. Schwarz, Prof. P. Blaha
Universidade de Aveiro, Portugal, Prof. V.S. Amaral
Universität Frankfurt/M., Anthropologie, Prof. Protsch von Zieten, Dr. J. Hammerl
Universität Frankfurt/M., Kernphysik, Prof. K. Bethge
Universitätsklinik Frankfurt/M., Dr. R. Weiss, Prof. U. Runne
Universität Saarbrücken, Prof. M. Zeppezauer, Dr. R. Hoffmann
Universität Zürich, Prof. M. Vašák, Dr. P. Faller, Prof. P. Schubiger
Dr. E. Zschau, Self-employed expert in materials research

7.20 Accelerator Statistics

Year	operating hours	maintenance and conditioning
2000	938 h	480 h *)
2001	1228 h	160 h

*) including a longer shutdown caused by light-guide breakdown and budgetary shortcuts

7.21 Publications

7.21.1 Journals

Investigation of the Negative Thermal Expansion of ZrW_2O_8.
N. Ulbrich, W. Tröger, T. Butz, and P. Blaha.
Z. Naturforsch. 55a, 301 (2000).

The Leipzig high-energy ion nanoprobe: A report on first results.
T. Butz, R.-H. Flagmeyer, J. Heitmann, D.N. Jamieson, G.J.F. Legge, D. Lehmann, U. Reibetanz, T. Reinert, A. Saint, D. Spemann, R. Szymanski, W. Tröger, J. Vogt, J. Zhu.
Nucl. Instr. Meth. Phys. Res. B 161-163, 323 (2000).

Concentration profiles and structural changes of silver intercalated titanium disulfide.
J. Heitmann, J.C. McCallum, W. Tröger, T. Butz, R. Hesse.
Nucl. Instr. Meth. Phys. Res. B 161-163, 619 (2000).

Study of metal bioaccumulation by nuclear microprobe analysis of algae fossils and living algae cells.
P. Guo, J. Wang, X. Li, J. Zhu, T. Reinert, J. Heitmann, D. Spemann, J. Vogt, R.-H. Flagmeyer, T. Butz.
Nucl. Instr. Meth. Phys. Res. B 161-163, 801 (2000).

Identification of air pollution sources by single aerosol particle fingerprints - micro-PIXE spectra.
J. Wang, P. Guo, X. Li, J. Zhu, T. Reinert, J. Heitmann, D. Spemann, J. Vogt, R.-H. Flagmeyer, T. Butz.
Nucl. Instr. Meth. Phys. Res. B 161-163, 830 (2000).

Ionoluminescence investigations of ancient human bone with an external ion beam.
D. Spemann, St. Jankuhn, J. Vogt, T. Butz.
Nucl. Instr. Meth. Phys. Res. B 161-163, 867 (2000).

Determination of the elemental status of ancient human bones from Bockenheim / Rheinland-Pfalz by PIGE and PIXE.
St. Jankuhn, J. Vogt, T. Butz.
Nucl. Instr. Meth. Phys. Res. B 161-163, 894 (2000).

Local O_δ probing in the high-T_c superconductor $HgBa_2CuO_{4+\delta}$.
J.G. Correia and ISOLDE Collaboration, J.P. Araujo, S.M. Loureiro, P. Toulemonde, S. Le Floch, P. Bordet, J.J. Capponi, R. Gatt, W. Tröger, B. Ctortecka, T. Butz, H. Haas, J.G. Marques, and J.C. Soares.
Physical Review B 61(17), 11769 (2000).

Source Identification of Lead Pollution in the Atmosphere of Shanghai City by Analyzing Single Aerosol Particles (SAP).
J. Wang, P. Guo, X. Li, J. Zhu, T. Reinert, J. Heitmann, D. Spemann, J. Vogt, R.-H. Flagmeyer, T. Butz.
Environ. Sci. Technol. 34, 1900 (2000).

Solid State Analysis with the New Leipzig High-Energy Ion Nanoprobe.
J. Vogt, R.-H. Flagmeyer, J. Heitmann, D. Lehmann, T. Reinert, St. Jankuhn, D. Spemann, W. Tröger, T. Butz.
Mikrochim. Acta 133, 105 (2000).

Optical and TDPAC spectroscopy of Hg(II)-rubredoxin: model for a mononuclear tetrahedral $[Hg(CysS)_4]^{2-}$ center.
P. Faller, B. Ctortecka, W. Tröger, T. Butz, ISOLDE Collaboration, M. Vasák.
J. Biol. Inorg. Biochem. 5, 393 (2000).

Combination of Micro-PIXE with the Pattern Recognition Technique for the Source Identification of Individual Aerosol Particles.
P. Guo, J. Wang, X. Li, J. Zhu, T. Reinert, J. Heitmann, D. Spemann, J. Vogt, R.-H. Flagmeyer, T. Butz.
Applied Spectroscopy 54(6), 807 (2000).

Local probing of Hg neighboorhood in $HgBa_2CuO_{4+\delta}$.
J.G. Correia, J.P. Araújo, S.M. Loureiro, P. Toulemonde, S. Le Floch, P. Bordet, J.J. Capponi, R. Gatt, W. Tröger, B. Ctortecka, T. Butz, H. Haas, J.G. Marques, J.C. Soares and the ISOLDE collaboration.
Physica C 341-348, 1969 (2000).

Inorganic Biochemistry with Short-lived Radioisotopes as Nuclear Probes.
W. Tröger, T. Butz.
Hyp. Int. 511, 511 (2001).

Electric Field Gradient Tensor Distributions in 2-Dimensional Incommensurate Charge Density Wave Systems.
T. Butz.
Physica Scripta 63, 203 (2001).

Investigation of ancient human bone by means of ionoluminescence and μPIXE.
D. Spemann, St. Jankuhn, J. Vogt, T. Butz.
In: J.L.Duggan, I.L.Morgan (eds.) Proc. 16th Int. Conf. on Appl. of Accelerators in Res. and Ind. (CAARI), CP 576, 428, AIP Press, Melville, NY (2001).

Novel test sample for submicron ion-beam analysis.
D. Spemann, T. Reinert, J. Vogt, T. Butz, K. Otte, K. Zimmer.
Nucl. Instr. Meth. Phys. Res. B 181, 186 (2001).

Spatially resolved elemental distributions in articular cartilage.
T. Reinert, U. Reibetanz, J. Vogt, T. Butz, A. Werner, W. Gründer.
Nucl. Instr. Meth. Phys. Res. B 181, 516 (2001).

Visualisation of collagen fibrils in joint cartilage using STIM.
T. Reinert, U. Reibetanz, J. Vogt, T. Butz, A. Werner, W. Gründer.
Nucl. Instr. Meth. Phys. Res. B 181, 511 (2001).

Si-doped luminescence gratings.
J. Heitmann, J.C. McCallum, J. Meijer, A. Stephan, T. Butz, M. Zacharias.
Nucl. Instr. Meth. Phys. Res. B 181, 263 (2001).

A novel ultra-short scanning nuclear microprobe: Design and preliminary results.
S. Lebed, T. Butz, J. Vogt, T. Reinert, D. Spemann, J. Heitmann, Z. Stachura, J. Lekki, A. Potempa, J. Styczen, B. Sulkio-Cleff
Nucl. Instr. Meth. Phys. Res. B 181, 32 (2001).

Ion Microscopy and Tomography.
T. Butz D. Lehmann, T. Reinert, D. Spemann, J. Vogt.
Acta Physica Polonica 100, 603 (2001).

7.21.2 Annual Reports

Scientific Report 1997 - 1999.
T.Butz (Editor).
ISBN 3-934178-08-1, Nukleare Festkörperphysik, Universität Leipzig (2000).

7.21.3 Invited Talks

T. Butz.
The High-Energy Ion Nanoprobe LIPSION.
Annual Meeting of the Japan Society for the Promotion of Science, 15. 5. 2000, Leipzig, Germany.

W. Tröger.
Nukleare Sonden und Makromoleküle.
Workshop des Sonderforschungsbereichs SFB 294 „Moleküle in Wechselwirkung mit Grenzflächen“, 19.-20. 10. 2000, Großbothen, Germany.

J. Heitmann.
Optical Properties of nc-Si Microstructures in SiO_2.
7th Int. Conf. on Nuclear Microprobe Technology & Applications, 10.-15. 9. 2000, Bordeaux, France.

T. Butz.
Ionenmikroskopie und –tomographie
Physik-Kolloquium der Universität Göttingen, 29. 10. 2000, Göttingen, Germany.

T. Butz.
First results of the Leipzig nuclear nanoprobe LIPSION in biomedical research.
16th Int. Conf. on Appl. of Accelerators in Res. and Industry (CAARI), 1.-5. 11. 2000, Denton (T.X.), USA.

D. Spemann.
Investigation of ancient human bone by means of ionoluminescence and μPIXE.
16th Int. Conf. on Appl. of Accelerators in Res. and Industry (CAARI), 1.-5. 11. 2000, Denton (T.X.), USA.

W. Tröger.
Short-lived Radioisotopes in Life Sciences: TDPAC Studies of Metal Sites in Macromolecules.
Plenary Lecture at the “2000 International Congress of the Pacific Basin Society: Nuclear Hyperfine and Exotic Particle Techniques for Studying Chemical States”, 14.-19. 12. 2000, Hawaii, USA.

T. Butz.
Nukleare Festkörperforschung in Leipzig: Anwendungen in Medizin und Biologie.
Physik-Kolloquium der Universität Jena, 15. 1. 2001, Jena, Germany.

J. Vogt.
Festkörperanalytik mit der Hochenergie-Nanosonde.
Kolloquiumsvortrag im Institut für Werkstoff-Forschung (IFW) Dresden, 9. 5. 2001, Dresden, Germany.

W. Tröger.
Spezifische Metallbindung in Makromolekülen, beobachtet mit zeitdifferentieller $\tilde{\gamma}\gamma$-Winkelkorrelation.
Kolloquium des Sonderforschungsbereichs 498 „Protein-Kofaktor-Wechselwirkungen in biologischen Prozessen“, 11.5.2001, Berlin, Germany.

T. Butz.
Ion Microscopy and Tomography.
XXXVI. Zakopane School of Physics, Int. Symposium Condensed Matter Studies by Nuclear Methods, 14.-19. 5. 2001, Zakopane, Poland.

T. Butz.
Ion Microscopy and Tomography.
National University of Singapore, 7. 9. 2001, Singapore.

W. Tröger.
Probing the Structure and Dynamics in Macromolecules via the Nuclear Quadrupole Interaction of Radioisotopes.
Plenary Lecture at the “XVI Nuclear Symposium on Nuclear Quadrupole Interaction”, 9.-14. 9. 2001, Hiroshima, Japan.

T. Reinert.
The Architecture of Cartilage: Elemental Maps and Scanning Transmission Ion Microscopy / Tomography.
7th European Conf. on Accelerators in Applied Research and Technology (ECAART),
21.-25. 8. 2001, Guildford, U.K.

T. Butz.
Ion Microscopy and Tomography.
Japan Atomic Energy Research Institute, 18. 9. 2001, Takasaki, Japan.

7.21.4 Conference Contributions

(T:talk, P:poster)

Ionenstrahluntersuchungen am Gelenkknorpel. (P)
T. Reinert. U. Reibetanz, J. Vogt, W. Gründer, T. Butz.
Frühjahrstagung der DPG, 27.-31. 3. 2000, Regensburg, Germany.

Investigation of ancient human bone with ionoluminescence and PIXE. (P)
D. Spemann, St. Jankuhn, J. Vogt, T. Butz.
Frühjahrstagung der DPG, 27.-31. 3. 2000, Regensburg, Germany.

pH Dependent Hg(II) Coordination in Metallothioneins: A ^{199m}Hg TDPAC-Study. (P)
W. Tröger, B. Ctortecka, T. Butz, P. Faller, M. Vasák and the ISOLDE collaboration.
3rd European Biophysics Congress, 9.-13. 9. 2000, München, Germany.

A novel ultra-short scanning nuclear microprobe with external beam: Design and first results. (T)
S. Lebed, T. Butz, J. Vogt, T. Reinert, D. Spemann, J. Heitmann, Z. Stachura, J. Lekki, A. Potempa, J. Styczen, B. Sulkio-Cleff.
7th Int. Conf. on Nuclear Microprobe Technology & Applications, 10.-15. 9. 2000, Bordeaux, France.

Spatially resolved elemental distributions in articular cartilage. (P)
T. Reinert, U. Reibetanz, J. Vogt, T. Butz, W. Gründer, A. Werner.
7th Int. Conf. on Nuclear Microprobe Technology & Applications, 10.-15. 9. 2000, Bordeaux, France.

Visualisation of collageneous fibrils in joint cartilage using STIM. (P)
T. Reinert, J. Vogt, T. Butz, U. Reibetanz, A. Werner, W. Gründer.
7th Int. Conf. on Nuclear Microprobe Technology & Applications, 10.-15. 9. 2000, Bordeaux, France.

Novel Test Sample for Submicron Ion Beam Analysis. (P)
D. Spemann, T. Reinert, J. Vogt, T. Butz, K. Otte, K. Zimmer.
7th Int. Conf. on Nuclear Microprobe Technology & Applications, 10.-15. 9. 2000, Bordeaux, France.

Ionenstrahluntersuchung am Gelenkknorpel. (T)
T. Reinert, U. Reibetanz, J. Vogt, W. Gründer, A. Werner, T. Butz.
Arbeitstreffen des Verbundes „Forschung mit nuklearen Sonden und Ionenstrahlen“, 9.-11. 10. 2000, Göttingen, Germany.

^{199m}Hg TDPAC am ISOLDE/CERN: Hochtemperatursupraleiter und Metallothioneine. (T)
W. Tröger.
Arbeitstreffen des Verbundes „Forschung mit nuklearen Sonden und Ionenstrahlen“, 9.-11. 10. 2000, Göttingen, Germany.

Bombardment of Living Single Cells: Design of the Leipzig High Energy Ion-Nanoprobe LIPSION. (P)
J. Tanner, J. Vogt, T. Reinert, D. Spemann, T. Butz, J. Dunst.
Abteilung Experimentelle Krebsforschung Congress 2001, 5.-6. 4. 2001, Heidelberg, Germany.

Enzymatic Mercury Detoxification: The Mercuric Ion Reductase MerA. (P)
W. Tröger, B. Ctortecka, St. Engst, S. Miller and the ISOLDE collaboration.
Joint Meeting of the French and German Biophysicists, 24.-27. 5. 2001, St. Bonifatius Monastery, Hünfeld, Germany.

The Leipzig High-Energy Ion-Nanoprobe LIPSION: design of single ion bombardment of living cells. (T)
T. Butz, J. Tanner, D. Spemann, T. Reinert, J. Vogt.
5th Int. Workshop on Microbeam Probes of Cellular Radiation Response, 26.-27. 5. 2001, Stresa, Italy.

Zerstörungsfreie ionenstrahlanalytische 3D-Charakterisierung von $Zn_{2-2x}Cu_xIn_xS_2$-Dünnschichten. (P)
D. Spemann, J. Vogt, T. Butz, D. Oppermann, K. Bente.
11. Tagung Festkörperanalytik, 25.-28. 6. 2001, Chemnitz, Germany.

STIM Tomography at the Leipzig Nanoprobe LIPSION. (T)
T. Reinert, A. Sakellariou, M. Schwertner, J. Vogt, T. Butz.
15th Int. Conf. on Ion Beam Analysis, 15.-20. 7. 2001, Cairns, Australia.

Suitable Test Structures for Submicron Ion Beam Analysis. (P)
D. Spemann, T. Reinert, J. Vogt, D. Dobrev, T. Butz.
15th Int. Conf. on Ion Beam Analysis, 15.-20. 7. 2001, Cairns, Australia.

Ion Beam Analysis of $Zn_{2-2x}Cu_xIn_xS_2$ Films. (T)
D. Spemann, J. Vogt, T. Butz, D. Oppermann, M. Lorenz, G. Wagner, K. Bente.
15th Int. Conf. on Ion Beam Analysis, 15.-20. 7. 2001, Cairns, Australia.

Hg(II) Coordination Studies in Penicillamine Enantiomers by ^{199m}Hg-TDPAC. (T)
W. Tröger.
12th Int. Conf. on Hyperfine Interactions (HFI-XII), 12.-17. 8. 2001, Park City, USA.

Feasibility Study on Delay-Line Localization in a Mini-PET Scanner. (P)
T. Butz, S.C. Bedi, W. Tröger.
12th Int. Conf. on Hyperfine Interactions (HFI-XII), 12.-17. 8. 2001, Park City, USA.

Improving the Energy Resolution of BaF_2 Scintillators by Cooling. (P)
S.C. Bedi, W. Tröger, T. Butz.
12th Int. Conf. on Hyperfine Interactions (HFI-XII), 12.-17. 8. 2001, Park City, USA.

pH Dependent Hg(II) Coordination in Metallothioneins: A ^{199m}Hg TDPAC-Study. (P)
W. Tröger, B. Ctortecka, P. Faller, M. Vasák and the ISOLDE collaboration.
10th Int. Conf. on Bioinorganic Chemistry (ICBIC10), 26.-31. 8. 2001, Florenz, Italy.

The Leipzig High-Energy Ion-Nanoprobe LIPSION: design of single ion bombardment of living cells. (P)
J. Tanner, D. Spemann, T. Reinert, J. Vogt, T. Butz.
European Radiation Research 2001, 1.-5. 9. 2001, Dresden, Germany.

A Single Ion Single Living Cell Bombardment Facility at LIPSION. (P)
J. Tanner, J. Österreicher, D. Spemann, T. Reinert, J. Vogt, T. Butz.
31st Annual Meeting of the European Society for Radiation Biology (ESRB), 1.-5. 9. 2001, Dresden, Germany.

On the Calculation of Electric Field Gradients in Layered Compounds. (T)
T.Butz.
14th Int. Symposium on Nuclear Quadrupole Interactions, 9.-14. 9. 2001, Hiroshima, Japan.

The Nuclear Quadrupole Interaction of $^{187}W(\tilde{\beta})^{187}Re$ in W(VI)-EDTA Complexes. (P)
G.Sun, W.Liu, T.Butz.
14th Int. Symposium on Nuclear Quadrupole Interactions, 9.-14. 9. 2001, Hiroshima, Japan.

The Nuclear Quadrupole Interaction of ^{204m}Pb in Cadmium Monitored by $\tilde{\gamma}\gamma$-Perturbed Angular Correlations. (P)
W. Tröger, M. Dietrich, J.G. Correia, H. Haas and the ISOLDE collaboration.
14th Int. Symposium on Nuclear Quadrupole Interactions, 9.-14. 9. 2001, Hiroshima, Japan.

Coordination Studies of the Metal Center of Hemocyanin by ^{199m}Hg Nuclear Quadrupole Interaction. (P)
W. Tröger, B. Ctortecka, P. Faller, H. Decker and the ISOLDE collaboration.
14th Int. Symposium on Nuclear Quadrupole Interactions, 9.-14. 9. 2001, Hiroshima, Japan.

High Resolution Scanning Transmission Ion Microscopy / Tomography. (P)
T. Reinert, A. Sakellariou, M. Schwertner, J. Vogt, T. Butz.
Jahrestagung Dt. Gesell. für Biophysik e.V., 23.-25. 9. 2001, Münster, Germany.

A Single Ion Bombardment of Living cells at LIPSION – A Joint Effort of Medical Doctors and Physicists. (T)
J. Österreicher, J. Tanner, D. Spemann, T. Reinert, J. Vogt, D. Lehmann, T. Butz.
Marie Curie Fellows Workshop, 24.-26. 9. 2001, Berlin, Germany.

Ionenstrahltomographie an der Leipziger Nanoionensonde LIPSION. (T)
M. Schwertner, T. Reinert, A. Sakellariou, J. Vogt, T. Butz.
Arbeitstreffen des Verbundes „Forschung mit nuklearen Sonden und Ionenstrahlen“, 3.-5. 10. 2001, Freiberg (Sachsen), Germany.

^{111m}Cd, ^{199m}Hg, ^{204m}Pb: ein tolles toxisches Trio. (T)
W. Tröger.
Arbeitstreffen des Verbundes „Forschung mit nuklearen Sonden und Ionenstrahlen“, 3.-5. 10. 2001, Freiberg (Sachsen), Germany.

The Bystander Effect of Ionizing Irradiation: Its Mechanisms, Role in Theory and Clinical Pratice, and Future Research. (T)
J. Österreicher, J. Tanner, J. Vogt, D. Spemann, T. Butz.
NATO HFMP TG006 Final Meeting, 22.-24. 10. 2001, Hradec Králové, Czech Republic.

7.22 Graduations

7.22.1 Diploma Theses

F. Heinrich
Untersuchung der Korrosion von HILUMIN-Batterieelektroden mittels zeitdifferentieller $\tilde{\gamma}\gamma$-Winkelkorrelationsspektroskopie.
28. 9. 2001

L. Thomas
Ion Beam Induced Charge Collection (IBICC) am LIPSION: erste Ergebnisse.
31.12.2002

7.22.2 Ph.D. Theses

T. Reinert
Ionenstrahluntersuchungen am Gelenkknorpel.
26. 11. 2001

8 PDF — SCIENTIC ACTIVITIES

8.1 Considerable improvement of NMR equipment

D. Michel
For our NMR based research several spectrometers with super conducting wide bore (89mm) magnets are available covering a magnetic field range from 2.35 T to 17.62 T (that means 1H resonance frequency between 100 and 750 MHz). The new wide-bore NMR spectrometer “AVANCE 750”, one of the few existing worldwide, was built up in 2001 and provides best available technology. All NMR spectrometers are suitable for experiments on solid-state matter as well as for investigations at systems with restricted mobility (e.g. interface systems, biological membranes). We now have possibilities to measure with very strong (more than 1000 W) radio-frequency fields at any desired form in 2 or more channels simultaneously. Magic Angle Spinning (MAS) up to 32 kHz is possible to simplify powder patterns, but we can also orient and rotate stepwise single crystals using goniometer probeheads. Typical solid state NMR-measurements using broad band excitation may be performed in a wide temperature region from 4.2 K to about 800 K.
For more details please contact Dipl.-Phys. Gert Klotzsche and Dr. André Pampel.
klotzsch@physik.uni-leipzig.de, anpa@physik.uni-leipzig.de

Figure 1:The magnet of the AVANCE 750 with a height of approx. 4 m


Figure 2:The magnet of the AVANCE 750 comes into our building through a big window (height approx. 4 m)

8.2 Study of active surface sites in heterogeneous catalysts

Andreas Pöppl

A major research topic of our group is the study of active surface sites in heterogeneous catalysts by electron paramagnetic resonance (EPR) spectroscopy. To apply ESR methods to such systems the catalytically active sites have to be either paramagnetic species by themselves (eg. paramagnetic transition metal ions) or paramagnetic probe molecules have to be adsorbed on the studied diamagnetic surface sites (eg. acid centers).
The last approach has been used to characterize Lewis acid sites in various zeolite materials. Nitric oxide (NO) and Di-tert-butyl nitroxide (DTBN) probe molecules were employed in these studies. The geometrical and electronic structures of the resulting adsorption complexes with Lewis acid aluminum defect centers and alkali metal cations could be determined by a combined application of several EPR techniques at low temperatures. Besides continuous wave multifrequency EPR spectroscopy, pulsed electron nuclear double resonance (ENDOR) at X and W band as well as hyperfine sublevel correlation (HYSCORE) spectroscopy have been used to measure the weak superhyperfine (shf) interactions between the unpaired electron spin at the probe molecule and the nuclear spins at the metal ion adsorption sites. These shf interactions are the key information in the structural analysis of such paramagnetic surface sites. ESR methods give also access to the acid properties of the Lewis sites. Their electron pair acceptor strength could quantitatively be characterized from the spin density distribution in the adsorption complexes and the dynamics and stability of the formed complexes at elevated temperatures.

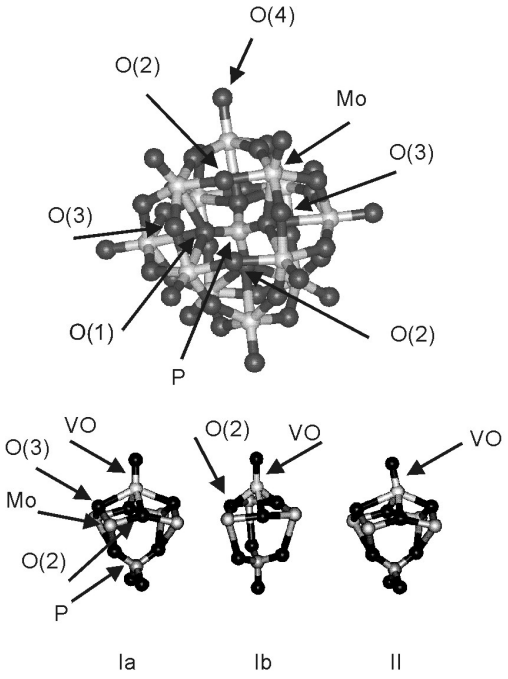

Fig. Structure of the $PVMo_{11}O_{40}^{-4}$ heteropolyanion (top) and schematic drawings of the proposed vanadyl complexes in dehydrated catalyst (bottom).

An attractive example for the application of modern ESR methods for the study of catalytically active transition metal ion species is the elucidation of the incorporation site of vanadyl ions in $H_4PVMo_{11}O_{40}$ heteropolyacid catalysts. In these materials the

heteropolyanions have the well-known structure of the Keggin molecule. Interactions of the unpaired electrons of the paramagnetic vanadyl ions (VO^{2+}) with all relevant nuclei (^{1}H, ^{31}P and ^{51}V) could be resolved. The complete analysis of the hyperfine coupling tensor for the phosphorous nucleus in the fourth coordination sphere of the V(IV) ion by HYSCORE and ENDOR spectroscopy at W- and X-band allowed for the first time a detailed structural analysis of the paramagnetic ions in in hydrated and dehydrated heteropolyacid catalysts. The vanadyl species are found to be coordinated to four or three bridging oxygen atoms from one $PVMo_{11}O_{40}^{-4}$ heteropolyanion in a trigonal-pyramidal or slightly distorted square-pyramidal coordination geometry, respectively.

Currently, this research subject is extended to the study of V(IV) ions in alkali metal ion modified heteropolyacid catalysts. Recent progress has been achieved by the development of an home-built Q band pulsed ENDOR spectrometer that allowed the measurement of weak ^{133}Cs shf couplings between the unpaired electron at the V(IV) ion and the cesium nuclei in the void space between the Keggin molecules.

8.3 Study of local ordering using electron paramagnetic resonance

Georg Völkel

EPR can be a powerful tool for the study of the peculiar local ordering occuring in ferroelectrics, dipolar glasses and modulated phases. Often, NMR and EPR complement each other because of their different time windows of investigation. Such an interesting case we meet with Dimethylammonium Aluminum Sulfate Hexahydrate (DMAAS) and Dimethylammonium Gallium Sulfate Hexahydrate (DMAGaS) where EPR investigations are the appropriate tool to enlighten the until now unknown nature of the low-temperature phaseof DMAGaS.
DMAGaS and DMAAS are isomorphous and ferroelastic at room temperature. Both they show an order-disorder type transition into a ferroelectric phase but only DMAGaS exhibits a further first-order transition into a low temperature non-ferroelectric phase. We performed electron paramagnetic resonance (EPR) measurements of chromium doped DMAAS and DMAGaS giving a new insight into the peculiar reorientation order of the polar DMA units on a microscopic level not known before. We found that the low-temperature phase of DMAGaS below T_{C2} = 115 K is a modulated phase with commensurate regions and discommensurations before it becomes antiferroelectric at T* = 60 K. This unusual phase sequence can be well explained by means of a Landau approach using a large number of sublattice polarizations and more generally by the microscopic extended DIFFOUR (discrete frustrated ϕ^4) model of a linear chain of electric dipoles (van Raij, van Bemmel, Janssen, 2000). DMAGaS and DMAAS seem to represent a similar interesting model system with a very complex phase sequence of commensurate and incommensurate phases as the famous betaine calcium chloride dihydrate (BCCD).

8.4 Soft and Semi-Solid Matter

André Pampel

Part of the research program of our group is also the investigation of so called “soft-matter” or “semi-solid matter”, especially of systems in liquid-crystalline phases as drug delivery systems and models for biological membranes. We are applying a multidisciplinary approach centered around NMR spectroscopy to reveal structural and dynamical aspects of such systems.
NMR spectroscopy has definite advantages over diffraction techniques in the structure elucidation of liquid-crystalline structures, which exhibit very low short-range order. These advantages, however, are frequently offset by resonance broadening mechanisms, which are caused by the anisotropic NMR parameters. Therefore, for this research we are using methods, which have been developed for the High-resolution NMR spectroscopy of solids. Main parts of our activities include the development and the optimization of methods of High-resolution MAS techniques for the investigation of liquid-crystalline phases.
We are currently investigating cubic liquid-crystalline phases (cubic phases), which can be used as drug delivery systems. A schematic sketch of a cubic phase is given in figure 1. This so-called bicontinuous phase is composed by a minima surface forming lipid bilayer that is interlaced by water channels. Such a porous system can be used as a host system for several drugs of different polarity. Cubic phases can be accounted as generally applicable host for drugs; nevertheless, they cannot be fashioned uniquely. In fact, it requires systematic research to find a suitable chemical composition and protocols to prepare the desired cubic phase structure for the drug to be used. We are performing NMR experiments for the determination of biophysical parameters on sub-nanometer scale, which are necessary for detailed understanding of the behavior of the system. This research has direct impact into the drug development and medical research, which is being done at the MDC in Berlin.
Ongoing research projects include investigations of models of biological membranes. The main focus is on the determination of structure and dynamical behavior of molecules within membranes, e.g. peptides and proteins.

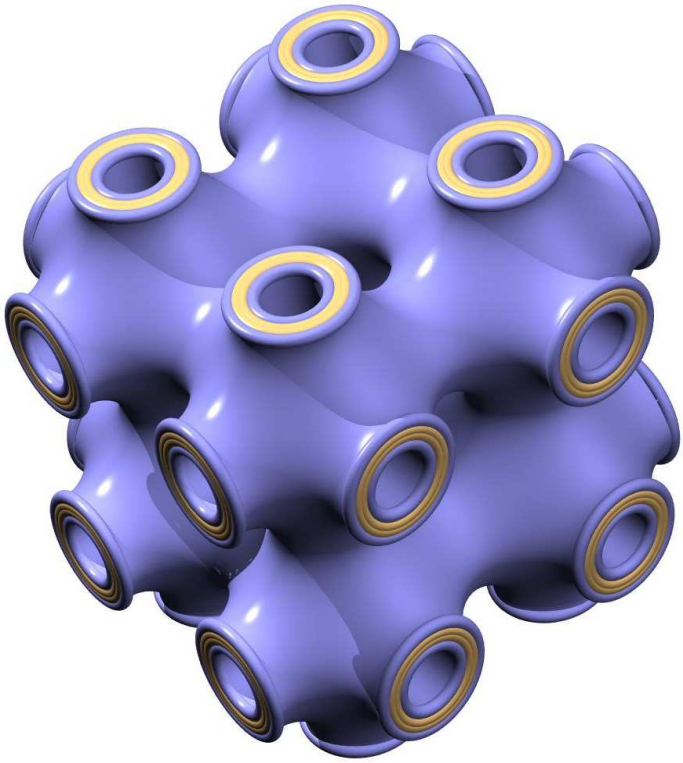

Figure 2: A schematic sketch of a cubic liquid-crystalline phase is given in figure 1. This so-called bicontinuous phase is composed by a minima surface forming lipid bilayer that is interlaced by water channels.

8.5 Nanocrystalline Ferroelectrics

R. Böttcher

The examination of nanocrystalline ferroelectrics with perovskite structure and the determination of their physical and chemical properties are one of the challenges of the solid state physics and modern material science due to their potential application (thin film capacitors, micro-mechanical devices, chemical and pyroelectric sensors, non-linear optics non-volatile random access memories). The aim of a further research topic of our group focuses on the investigation of the structure of nanocrystallites with perovskite structure ($BaTiO_3$ and $PbTiO_3$) as well as the structure-property relations by means of the high field EPR spectroscopy in W band. Starting from microcrystalline samples and going to nanocrystalline powders doped with paramagnetic ions ($S > ½$) it is the purpose to get more information about the change of the local structure of nanocrystallites by measuring the spectral parameters and their distribution functions, to determine the structure and the thickness of the surface layer in dependence on the preparation route and to probe the ferroelectric properties by measuring their temperature dependence.

Novel information on the structure and the structure-property relation of the nanocrystalline state are expected by modelling the spectral parameters in the frame of the Newman superposition model and the Landau theory.

The results of the high-field EPR investigation on nanocrystalline $BaTiO_3$ doped with Mn^{2+} ions were published in Phys. Rev. B62, 2085-2095 (2000). For the first time EPR spectroscopy in combination with XRD measurement and numerical calculations based on the Landau theory were used to study the size effects of ferroelectric $BaTiO_3$ nanoparticles.

8.6 Structure and Dynamics of Molecules Sorbed in Zeolites

J. Roland, D. Michel

^1H NMR spectra of molecules sorbed in porous materials may be strongly influenced by the presence of local magnetic fields in particular if the measurements are run in strong magnetic fields. The reason is the susceptibility broadening, i.e. the inhomogeneity of the local magnetic field mainly introduced by the polarization of the adsorbent grains, which can be essentially reduced by the application of magic angle spinning (MAS) techniques. The resolution achieved depends also on the distribution of the grain sizes. In order to understand the limitations for the spectral resolution in high resolution NMR measurements in the case of such heterogeneous systems and to estimate the advantage of using very high resonance frequencies, the residual line widths in the ^1H MAS NMR spectra were discussed in detail [1]:

It was shown that this line width is determined by interference of the influences of MAS and of the translational motion of the adsorbed species over mean distances which are comparable with the dimensions of the grains of the solid adsorbents, like zeolitic molecular sieves. At higher MAS frequencies the line shape becomes of Lorentzian type and the residual line width is proportional to B^2.

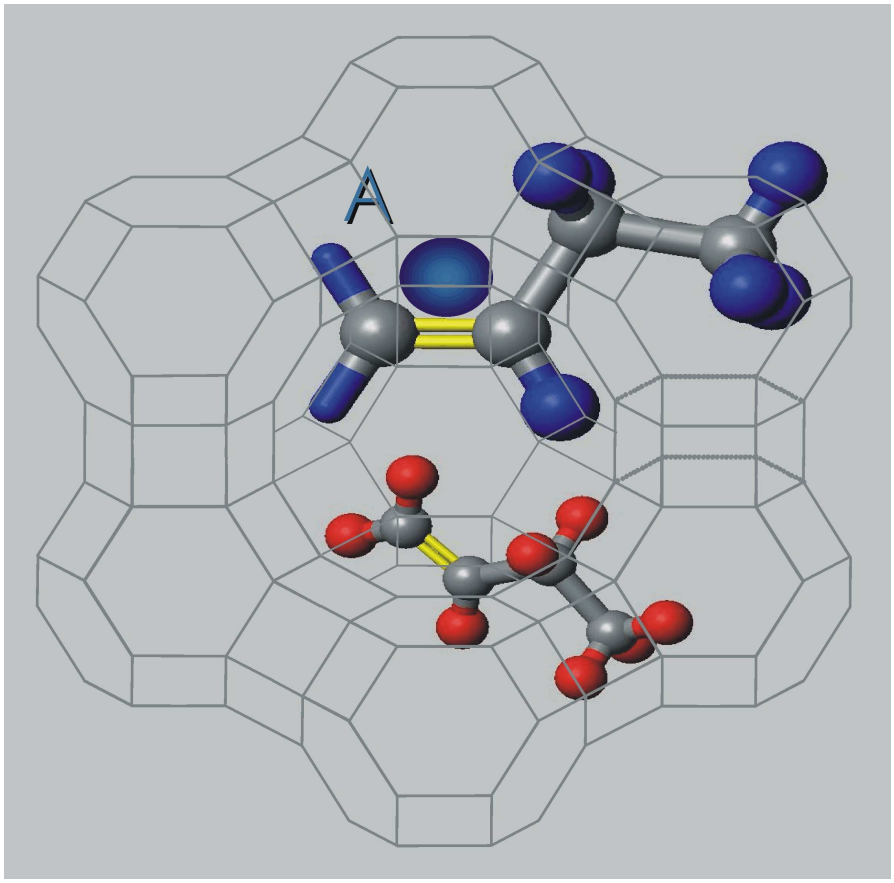

Figure 1: For 1-butene sorbed in NaX zeolite the spectra are characterized by a fast exchange between essentially two different kinds of molecules: one, which is adsorbed at the adsorption sites and the residual ones one which moves in from cage to cage through the zeolite structure.

The results are compared with measurements of ^{1}H NMR spectra for butene molecules sorbed in NaX type zeolites. In the situation presented the line broadening in the spectra, up to highest fields used (17.6T), is smaller than the increase in resolution with respect to the increasing frequency difference due to the chemical shift. Thus, a considerable gain in the resolution of chemical shifts is established by using high magnetic fields [2] while the line splitting due to spin-spin coupling can only be detected if the measurements are run at lower magnetic fields: Hence, we were able to choose an optimum magnetic field of 14.6 T for resolving both, chemical shift and spin-spin coupling patterns in the study of the adsorption behavior of simple hydrocarbons in zeolites. By the way high resolution (HR) MAS NMR spectroscopy was used to investigate the dynamics of olefinic hydrocarbons in NaX zeolites and their conformational changes in the adsorbed state. For the first time conformational changes of adsorbed molecules could be investigated (as shown in Fig. 1) by means of heteronuclear high resolution NMR spectroscopy in combination with proton NMR NOESY spectroscopy.

A further part of our work is the synthesis and characterization of zeolites and mesoporous molecular sieves (for example: ZSM-5, MCM-41, $ALPO_4$, etc.)

8.7 Study of the dynamic of incommensurately modulated crystals by means of nuclear magnetic resonance spectroscopy

D. Michel, A. Taye (in close cooperation with Professor Petersson, University of the Saarland, Saarbrücken)

The dynamics of the incommensurate (IC) modulation is investigated for several one-dimensionally incommensurately modulated crystals near the transition to the normal high temperature phase at the temperature T_i by means of quadrupolar perturbed nuclear magnetic resonance (NMR) spectra and nuclear spin-lattice relaxation. In the IC phase, at least one local physical quantity is modulated in such a way that the characteristic wave vector q_i is not a rational multiple of the reciprocal lattice vectors of the N phase, i.e. the modulation does not fit to the underlying basic structure and the translational symmetry of the lattice is broken. As a consequence, the initial phase of the modulation wave is arbitrary, and the IC structure is continuously degenerate with respect to a phase shift [1, 2]. Hence, not only the amplitude of the modulation wave is required to characterize each configuration but also the phase at an arbitrary lattice site. Therefore, a complex order parameter (OP) $Q = \rho \exp(i\phi)$ must be employed in order to describe the phase transition from an N phase to an IC modulated one. Its two components represent the global amplitude ρ and the initial phase ϕ of the primary modulation. The dimension of the OP is identical with that of a two-component spin (S_x, S_y), and the effective Hamiltonian is thus that of the 3d-XY model. Consequently, one-dimensionally incommensurately modulated structures are assumed to belong to the universality class of this model. It will be demonstrated that highly precise quadrupolar perturbed NMR measurements have contributed unambiguously and sensitively to a verification of this assumption for the systems investigated by us. All results can be described consistently in terms of a static modulation in the IC phase without any indication for „floating“ or large scale fluctuations of the modulation wave. The critical exponents derived from the NMR line shape and the relaxation times T_1 very nicely fit to the universality class of the 3d-XY model. For Rb_2ZnBr_4 and Rb_2ZnCl_4 crystals the characteristic frequency of the critical dynamics of the order parameter (OP) slows down below the Larmor frequency used in the ^{87}Rb NMR relaxation time measurements. In this particular case one can derive the characteristic frequency of the critical dynamics of the OP above T_i and of the phason below T_i from the Larmor frequency dependence of T_1. Recently similar investigations are carried out on dichlorobiphenylsulfone [BCPS] showing a very broad IC region below about 150 K presumably down to 0 K.

8.8 Local ordering of tetramethylammonium (TMA) groups in quasi one-dimensional crystal of the type $(CH_3)_4NMX_3$

D. Michel, S. Mulla-Osman, G. Völkel

Crystals of the isostructural family $(CH_3)_4NMX_3$, with the bivalent metals M = Mn, Ni, Cd, Cu, or V and the halogen atoms X = Cl, Br or I, have attracted much attention because of their one-dimensional type structure. They are built up from infinite chains of MX_6 octahedra. The space between the chains is occupied by the $[(CH_3)_4N]^+$ (tetramethylammonium, TMA) cations. In particular, crystals of $(CH_3)_4NMnCl_3$ (TMMC) has been intensively investigated because of its quasi-ideal one-dimensional magnetic properties. $(CH_3)_4NCdCl_3$ (TMCC) is a diamagnetic analogue for TMMC for which also a quasi-one-dimensional behaviour was found. TMMC and TMCC undergo a number of structural phase transitions which are suggested to be governed essentially by the dynamics of the TMA groups. Quadrupolar perturbed ^{14}N NMR and ^{35}Cl NMR investigations are performed on TMCC in the temperature range from 297 to 80 K. At the phase transition into the monoclinic phase II at 118 K the quadrupole coupling tensor (QCT) shows abrupt changes in accordance with its first order type. In complete agreement with a recent ^{35}Cl NMR study, the ^{14}N spectra in phase II clearly show a ferroelastic twin domain structure. The saturated rotational angle between the epitaxially grown domains of $\Theta_{exp.} = 4°$ is in a very good agreement with the theoretical value of $\Theta_s = 3.5°$ calculated from the ferroelastic strain tensor.

The ordering behaviour below the phase transition at 118 K is related with the rotation of the largest component V_{ZZ} of the QCT in a plane perpendicular to the axis c and with changes of its principal axes values. A shift of the N atoms within the plane in relation with the phase transition was also found in recent low temperature X-ray diffraction measurements. This work has shown that NMR spectroscopy is able to derive subtle structural details which are also essential for the interpretation of structural data derived from XRD measurements.

8.9 External Collaborations

Institut für Oberflächenmodifizierung - IOM Leipzig
Dr. E. Hartmann
Universität Kaiserslautern, Fachbereich Chemie, Technische Chemie
Dr. M. Hartmann
Technische Universität München, Anorganisch-chemisches Institut
Prof. K. Köhler
The Weizmann Institute of Science, Dept. of Physical Chemistry, Rehovot, Israel
Prof. D. Goldfarb
Vilnius University, Radiophysics Department
Dr. J. Banys
Wroclaw University, Institute of Experimental Physics
Prof. Z. Czapla
University of Opole, Institute of Mathematics
Prof. V. A. Stephanovich
Max-Delbrück-Center for Molecular Medicine
Dr. R. Reszka
Universität des Saarlandes, Saarbrücken
Prof. J. Petersson et al.
St. Petersburg State University
Prof. E. V. Charnaya, Prof. B. N. Novikov, Prof. V. I. Chizhik
Ioffe Institute St. Petersburg
Prof. J. A. Kumzerov
Kirensky Institute of Physics of the Sibirian Branch of the Russian Academy of Sciences, Krasnoyarsk
Prof. I. P. Aleksandrova, Dr. J. Ivanov
A. Mickiewicz University of Poznan
Prof. S. Jurga
Universität Leipzig, Fakultät für Biowissenschaften, Pharmazie und Psychologie
Prof. A. Beck-Sickinger
Martin-Luther-Universität Halle-Wittenberg, Department of Physics
Dr. H. T. Langhammer, Prof. Dr. H. Schneider, Prof. Dr. H. Beige
Martin-Luther-Universität Halle-Wittenberg, School of Pharmacy,
Institute for Pharmaceutics
Prof. R. H. H. Neubert

8.10 Funding

Strukturaufklärung der Tieftemperaturphase des Dimethylammoniumgalliumsulfat (DMAGaS) und der Untersuchung des Ordnungs-Unordnungs-Verhalten der Dimethylammoniumgruppen mit Hilfe der EPR-Spektroskopie
Investigation of the low-temperature phase in demethylammoium gallium sulfate (DMAGaS) and the order disorder behaviour of the dimethylammonium groups (DMA) by means of EPR
R. Böttcher, D. Michel Bo 1080/7

Strukturaufklärung nanokristalliner Ferroelektika mit Perwoskitstruktur durch Hochfeld-EPR-Spektroskopie
Investigation of nanocrystalline ferroelectrics with pervoskite structure by means of high-field-EPR spectroscopy
(im Rahmen des Schwerpunktprogrammes 1051)
R. Böttcher Bo 1080/6-2

Hochfeld-ESR Spektroskopie von monomerem und dimerem Stickstoffoxid-Komplexen in Zeolithen
High field EPR spectroscopy of monomer and dimer nitric oxide complexes in zeolites
(im Rahmen des Schwerpunktprogrammes 1051)
A. Pöppl, M. Hartmann Po 426/2-2

ESR, ENDOR, und ESEEM Spectroskopie zum Studiium der Struktur und Dynamik paramagnetischer Moleküle in microporösen Festkörpern
ESR, ENDOR, and, ESEEM spectroscopy of the structure and dynamics of para-magnetic molecules adsorbed on acid sites in microporous solids
Pöppl, SFB 294, Teilprojekt F7

Untersuchung der Dynamik inkommensurabel modulierter Kristalle mit Methoden der kernmagnetischen Resonanz
Study of the dynamic of incommensurately modulated crystals by means of nucleamagnetic resonance spectroscopy
D. Michel Mi 390/9-3 (together with Professor J. Petersson, Saarbrücken)

Signalbearbeitung für Medizinische Magnetresonanz-Tomographie und –Spektroskopie
Advanced Signal Processing for Medical Magnetic Resonance Imaging and Spectroscopy
D. Michel (mit A. Pampel)
(im Rahmen des EU-Programms TMR: Contract No. ERBFMRXCT970160)

Etablierung und Anwendungen der Doppelrotations- und Multiquanten-Meßtechnik für Hochfeld-NMR-Untersuchungen an Quadrupolkernen in Festkörpern
Double Rotation and Multiple Quantum NMR Spectroscopy in High Magnetic Fields for the Study of Quadrupole Nuclei in Solids
D. Freude (mit D. Michel), Deutsche Forschungsgemeinschaft, Fr 902/9-2

Höchstauflösungs-Kernresonanzspektrometer mit einer Protonenspinresonanzfrequenz von 750 MHz

High-Resolution NMR Spectrometer with a Proton Resonance Frequency of 750 MHz
D. Michel, Deutsche Forschungsgemeinschaft, Mi 390/5-3

Dynamik, Ordnungsverhalten und Reaktivität von Molekülen in mikro- und mesoporösen Materialien
Dynamics, order behaviour and reactivity of molecules in microporous and mesoporous materials
D. Michel, SFB 294, Teilprojekt G8

8.11 Publications

8.11.1 Journals

S. Mulla-Osman, D. Michel, G. Völkel, I. Peral, G. Madariaga
35Cl NMR studies of the domain structure of tetramethylammonium cadmium chloride (TMCC) at lower temperatures
J. Phys.: Condens. Matter 13 (2001)5, 1119-1131

J. Banys, C. Klimm, G. Völkel, A. Kajokas, A. Brilingas, J. Grigas
Dielectric properties in the vicinity of the ferroelectric phase transition in a mixed crystal of deuterated BP0.01BPI0.99
J. Phys.: Condens. Matter 13 (2001) 1773-1780

B. Epel, A. Pöppl, P. Manikandan, S. Vega, D. Goldfarb
The Effect of Spin Relaxation on ENDOR Spectra Recorded at High Magnetic Fields and Low Temperatures
J. Magn. Res. 148 (2001) 388-397

A. Pöppl, P. Manikandan, K. Köhler, P. Maas, P. Strauch, R. Böttcher, D. Goldfarb
Elucidation of Structure and Location of V (IV) Ions in Heteropolyacid Catalysts H4PVMo11O40 as Studied by Hyperfine Sublevel Correlation Spectroscopy and Pulsed Electron Nuclear Double Resonance at W- and X-Band Frequencies
J. Am. Chem. Soc. 123 (2001) 4577 – 4584

T. Rudolf, A. Pöppl, W. Hofbauer, D. Michel
X, Q and W band electron paramagnetic resonance study of the sorption of NO in Na-A and Na-ZSM-5 zeolites
Phys. Chem. Chem. Phys. 3 (2001) 2167-2173

E. V. Charnaya, P. G. Plotnikov, D. Michel, C. Tien, B. F. Borisov, I. G. Sorina, E. I. Martynova
Acoustic studies of melting and freezing for mercury embedded into Vycor glass
Physica B 299 (2001) 56 - 63

W. Böhlmann, D. Michel
27Al-NMR studies on Al-MCM-41 molecular sieves synthesized with different Si/Al ratios and different aluminum sources, Stud. Surf. Sci. and Cat. 135 (2001) 202

M. Gutjahr, W. Böhlmann, R. Böttcher, A. Pöppl
Adsorption of Di – tert – butyl Nitroxide at Monovalent Cations in Zeolite Y As Studied by Electron Spin Resonance Spectroscopy, Stud. Surf. Sci. and Cat. 135 (2001) 347

D. Freude, T. Loeser, D. Michel, U. Pingel, D. Prochnow
17O NMR Studies of Low Silicate Zeolites
Solid State Nuclear Magnetic Resonance 20 (2001) 46 - 60

M. Gutjahr, A. Pöppl, W. Böhlmann, R. Böttcher
Electron pair acceptor properties of alkali cations in zeolite Y: an electron spin resonance study of adsorbed di-tert-butyl nitroxide
Colloids and Surfaces A: Physicochemical and Engineering Aspects 189 (2001) 93-101

S. Vasenkov, W. Böhlmann, P. Galvosas, O. Geier, H. Liu, J. Kärger
PFG NMR Study of Diffusion in MFI-Type Zeolites: Evidence of the Existence of Intracrystalline Transport Barriers
J. Phys. Chem. B 105 (2001) 5922 – 5927

F. Decker, U. Häcker, K.-P. Holzer, M. Irsch, D. Michel, P. Mischo, J. Petersson;
Study of Excitations in Structurally Incommensurately Modulated Solids by Means Nuclear Magnetic Resonance, in: B Kramer (ed.), Adv. in Solid State Physics, 41 (2001) 565 – 576

W. Böhlmann, D. Michel
1H MAS NMR Studies of Molecules Adsorbed on Activated Zeolites
J. of Catalysis 202 (2001) 421-426

F. Decker, J. Petersson, M. Irsch, D. Michel
Critical statics and dynamics of the prototype one-dimensional incommensurately modulated crystal Rb_2ZnBr_4 studied by NMR
Phys. Rev. B 64 (2001) 2141XX-1-11

J. Totz, D. Michel, Yu. N. Ivanov, A. A. Sukhovsky, I.P. Aleksandrova, J. Petersson
Mechanism of proton conductivity in quasi-one-dimensional hydrogen-bonded crystals
Magn. Reson. Chem. 39 (2001) S50-S58

G. Völkel, R. Böttcher, Z. Czapla, D. Michel
EPR Studies of the Low Temperature Phase of Chromium Doped Dimethylammonium Gallium Sulfate Hexahydrate (DMAGaS)
Phys. stat. sol. (b) 223 (2001) R6 – R7

H. Rumpf, H, Modrow, J. Hormes ,H.-J. Gläsel, E. Hartmann, E. Erdem, R. Böttcher, K.-H- Hallmeier
Preparation of nanocrystalline BaTiO3 characterized by in situ X-ray absorption spectroscopy
J. Phys. Chem. B 105 (2001) 3415-3421

8.11.2 Conference Contributions

(T:talk, P:poster)

Size effect in Mn-doped BaTiO3 nanopowders observed by XRD and EPR (P)
R. Böttcher, C. Klimm, H. J. Gläsel, E. Hartmann, H.-C- Semmelhack, G. Völkel
Physikertagung 2001, März 2001, Hamburg.

Size effects in BaTiO3 and PbTiO3 nanopowders studies by X-ray diffraction and high-field electron paramagnetic resonance (P)
R. Böttcher, E.Erdem, H. J. Gläsel, E. Hartmann, H.-C- Semmelhack, G. Völkel
Wissenschaftstreffen 2001, September 2001, Berlin.

Characterisation of nanocrystalline ferroelectrics with perovskite-type by high-field EPR (T)
R. Böttcher
Wissenschaftstreffen 2001, September 2001, Berlin.

Elucidation of Structure and Location of V(IV) Ions in Heteropolyacid Catalysts as studied by ESEEM and ENDOR Spectroscopy (T)
A. Pöppl
14th ISMAR International Conference, 2001, Rhodes.

Elucidation of the Structure of Paramagnetic Adsorption Complexes in Microporous Materials (T)
A. Pöppl
Symposium des SFB 294 „Structure, Relaxation and Transport Processes on Interfaces with Various Topology and Properties“, 2001, Leipzig.

High-Resolution Pulsed-ENDOR and ESEEM Spectroscopy at Interfaces (T)
A. Pöppl
Jahrestagung Chemie 2001 der GDCH, 2001, Würzburg.

EPR Studies of the Order-Disorder Behaviour of Chromium Doped Dimethylammonium Gallium And Aluminum Sulfate Hexahydrate (DMAGAS and DMAAS) (T)
G. Völkel, R. Böttcher, Z. Czapla, D. Michel
(IMF-10, Madrid 03. –07. 09. 2001

The Order-Disorder Behaviour of Chromium Doped Dimethylammonium Gallium and Aluminum Sulfate Hexahydrate (DMAGAS and DMAAS) - an EPR Study (T)
G. Völkel, R. Böttcher, Z. Czapla, D. Michel
(XXVI th International School on Ferroelectrics Physics, Wroclaw 17. –22. 09. 2001)

EPR Studies of the Low-Temperature Phase of Chromium Doped Dimethylammonium Gallium Sulfate Hexahydrate (DMAGaS) (T)
G.Völkel, R. Böttcher, Z. Czapla, D. Michel.
Physikertagung 2001, März 2001, Hamburg.

EPR Studies Of The Modulated Low-Temperature Phase Of Chromium Doped Dimethylammonium Gallium Sulfate Hexahydrate (DMAGAS) (P)
G.Völkel, R. Böttcher, Z. Czapla*, D. Michel
(IMF-10, Madrid 03. –07. 09. 2001)

Size Effect In Mn^{2+}-Doped $Batio_3$ Nanopowders Studied By Electron Paramagnetic Resonance And X-Ray Diffraction (P)
R. Böttcher, H.-J. Gläsel*, E. Hartmann*, C. Klimm, D. Michel,
H.-C. Semmelhack, G. Völkel,
(IMF-10, Madrid 03. –07. 09. 2001)

High-Resolution MAS-NMR-Investigations of a Drug Carrier System with Cubic Liquid-Crystalline Phase Structure (T)
14th ISMAR International Conference, 2001, Rhodes.
A. Pampel

High-Resolution MAS-NMR-Investigations of a Drug Carrier System with Cubic Liquid-Crystalline Phase Structure (T)
A. Pampel
Symposium des SFB 294 „Structure, Relaxation and Transport Processes on Interfaces with Various Topology and Properties“, 2001, Leipzig.

Time domain analysis of 2D NMR spectra (T)
D. Michel , A. Pampel
Annual Meeting of the Joint EU-TMR Research Project „Signal Processing in Magnetic Resonance Imaging and Magnetic Resonance Spectroscopy“ in Thessaloniki (Griechenland) March 7-11, 2001

Elementary Excitations in Incommensurately Modulated Crystals (T)
D. Michel, J. Petersson
DPG-Jahrestagung in Hamburg 26. bis 30. März 2001, Arbeitskreis Festkörperphysik, Eingeladener Hauptvortrag

^{1}H NMR NOESY spectroscopy of molecules adsorbed in porous media (T)
D. Michel, J. Roland
RAMIS-Conference, Poznan-Bedlewo, May 6 –10, 2001, Invited lecture

NMR and ESR for the study of porous media (T)
D. Michel, A. Pöppl, J. Roland, T. Rudolf
Ampere NMR School of the Jagellonian University Krakow in Zakopane, June 3-7, 2001, Invited lecture

NMR- and NQR-Study of Domain Structure in TMCC Crystals (T)
S. Mulla-Osman, D. Michel, G. Völkel and Z. Czapla Berichtskolloquium des DFG-SPP „Strukturgradienten in Kristallen“, Walberberg / Brühl, 25.06. bis 26.06.2001

NMR spectroscopy of molecules adsorbed on solid interfaces at high magnetic fields (T), D. Michel, J. Roland
Magnetic Resonance in Colloid and Interface Science, Specialized Colloque AMPERE, St. Petersburg, June 26-30, 2001, Invited lecture:

Proton conductivity in hydrogen-bonded crystals: 2D NMR and dielectric measurements (T), D. Michel, J. Totz, A. A.. Sukhovsky, Y. N. Ivanov, I. P. Aleksandrova , J. Petersson
Specialized Colloque Ampere, Stuttgart, July 22 – 26, 2001, Invited lecture

The Mechanism of Proton Conductivity in Quasi-one dimensional Hydrogen-bonded Crystals (T)
D. Michel, J. Totz, A. A.. Sukhovsky, Y. N. Ivanov, I. P. Aleksandrova , J. Petersson:
International Meeting on Ferroelectricity IMF-10, Madrid, September 2–7, 2001, Invited lecture

NMR Study of Molecular Dynamics in Porous Solids (T)
D. Michel, J. Roland
SFB 294: Molecules in Interaction with Interfaces: Symposium, September 12 – 14, 2001; University of Leipzig

NMR- and NQR-Study of Domain Structure in TMCC Crystals (T)
D. Michel, S. Mulla-Osman, G. Völkel, Z. Czapla
XXVI. International School on Ferrolectrics Physics of the University of Wroclaw, Wojtowice near Klodzko September 17-21, 2001

Adsorption Behavior of Di-tert-butyl Nitroxide on Zeolite HY: An ESR and NMR Study. (P)
W. Böhlmann, M. Gutjahr, A. Pöppl, and D. Michel
11. Deutsche Zeolithtagung, Erlangen, 7.3.- 9.3.2001

^{27}Al-NMR studies on Al-MCM-41 molecular sieves synthesized with different Si/Al ratios and different aluminum sources.(P)
Winfried Böhlmann and Dieter Michel
13th International Zeolite Conference, Montpellier, France, 8.7.- 13.7.2001
Adsorption of Di-tert.-butyl-Nitroxide at Monovalent Cations in Zeolite Y As Studied by Electron Spin Spectroscopy. (P)
M. Gutjahr, W. Böhlmann, R. Böttcher, and A. Pöppl
13th International Zeolite Conference, Montpellier, France, 8.7.- 13.7.2001

Petrographic and spectroscopic investigations of lignite hydrogenation residues (P)
W. Böhlmann and N. Volkmann
11th International Conference on Coal Science, San Francisco, CA, USA, 30.09.-05.10.2001

Solid Residues of Lignite Hydrogenation: News from Petrography and NMR Spectroscopy (P)
W. Böhlmann and N. Volkmann
18th Annual International PITTSBURGH COAL CONFERENCE, Newcastle, New South Wales, Australia, 03.12.-07.12.2001

8.11.3 Kolloquia

D. Michel
Universität Zürich (Prof. Dr. K. Alex Müller, Prof. Dr. Tony Keller), 10 January 2001: Elementary Excitations in Incommensurately Modulated Crystals. A NMR Study

D. Michel
Universität Ulm (Prof. Dr. R. Kimmich, Prof. Dr. P. Reineker), 15 January 2001
Dynamik und Struktur von Molekülen in nanoporösen Festkörpern: Beispiele aus Anwendungen der NMR- und EPR-Spektroskopie

D. Michel
Martin-Luther-Universität Halle, Festkolloquium zum 80. Geburtstag von Professor Dr. Günter Schmidt, 20. Dezember 2001
Critical phenomena at phase transitions

8.12 Graduations

8.12.1 Ph. D.

T. Rudolf
Adsorption and Desorption Behavior of Nitric Monoxide in Zeolites Na-A, Na-ZSM-5, and H-ZSM-5 – A Multi-Frequency Electron Paramagnetic Resonance Study
July 2001

8.12.2 M. Sc.

E. Erdem
Preparation and Characterisation of Ferroelectric/Ferrromagnetic Nanopowders and Polymeric Nanocomposites
July 2001

Kyuseok Cho
NMR Investigation of Drug Release System in Cubic Liquid-Crystalline Phase
December 2001

8.13 Awards

D. Michel
Honorary Professor of the State University of St. Petersburg

9 SUM — SCIENTIC ACTIVITIES

The group for Superconductivity and Magnetism is engaged in the study of basic properties of various superconducting, magnetic and ferroelectric materials. At present research activity focuses on

- the investigation of superconducting and ferromagnetic correlations in carbon-based compounds,
- the study of flux-line pinning and dynamics in high temperature superconductors and
- the study of spin-dependent transport phenomena in magnetic oxides as well as superconducting/ferromagnetic and ferromagnetic/ferroelectric heterostructures.

The group is well equipped with a variety of magnetocryostat systems. In the low temperature laboratory measurements can be performed from temperatures as low as 50 mK up to temperatures of 800 K in magnetic fields of 8-11 T. We employ a range of measurement techniques such as resistivity, Hall effect, thermal conductivity, ac-susceptibility, SQUID magnetometry, μ-Hall sensor-array and the vibrating reed method. Thin oxide films, namely: the colossal magnetoresistance compound $La_{0.7}Ca_{0.3}MnO_3$, magnetite (Fe_3O_4), $BaTiO_3$ and $YBa_2Cu_3O_7$ are fabricated on single crystal substrates with our pulsed laser deposition facility. X-ray diffractometry is used to characterize the crystallographic structure, especially phase purity, texture, crystallite size and micro-strains, and to study phase transitions and reaction kinetics. Thermogravimetry and dynamical differential calorimetry is employed to study synthesis and phase transitions in solids in the temperature range between room temperature and 1400°C.

9.1 Magnetic and Transport Properties of Carbon-based Compounds

R. Höhne, H. Kempa, K. Han, A. Setzer and P. Esquinazi

The discovery of superconducting- and ferromagnetic-like signals in graphite has triggered a series of characterization measurements in Highly Oriented Pyrolitic Graphite (HOPG) samples as well as in other carbon-based compounds like, e.g., polymerized Fullerene C_{60} and composites (graphite-sulphur mixtures). The group studies basic properties as the temperature- and magnetic-field- dependence of the electrical and thermal properties of pure graphite.

9.1.1 Magnetotransport in HOPG

One of the striking dependences found recently is shown in Fig.1. It shows the temperature dependence at constant magnetic fields of the longitudinal (upper left panel) and transverse (c-axis resistivity, lower left panel) as well as the scaling obtained in a determined temperature range for both resistivities (right upper and lower panels, respectively). These results show a metal-isolator transition driven by a magnetic field applied normal to the graphene layers. This transition is similar to that observed in 2D electronic systems and is quantitatively characterized by the scaling

given in the two right panels of Fig.1 and is at the moment not well understood. Recent theoretical work [D. V. Khveshchenko, Phys. Rev. Lett. **77**, 4938 (2001)] indicates that this transition should be driven only by the field component normal to the graphene layers, opening an energy gap in the spectrum of Dirac fermions. Future work should test this prediction.

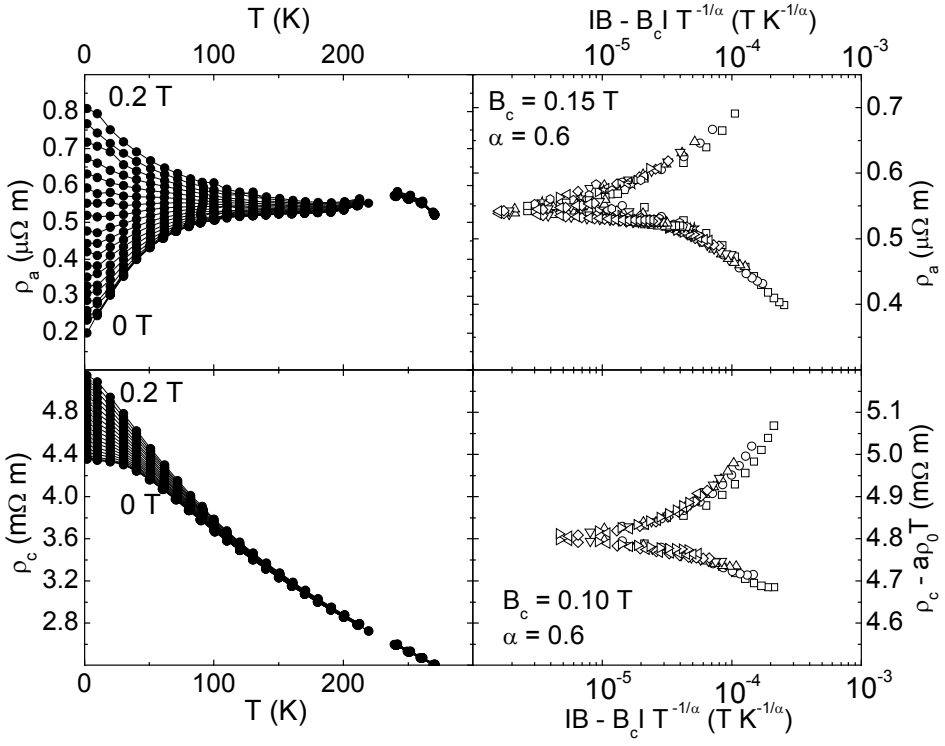

Fig.1: Left panels show the longitudinal (upper) and transverse (lower) resitivities as a function of temperature for different constant magnetic fields. The longitudinal resistivity shows a clear metal-insulator transition with field, whereas the transverse one shows smaller change with field. The right panels show the 2D scaling for both resistivities.

9.1.2 Ferromagnetism in graphite and fullerenes

Can Carbon-C_{60} be magnetic? The research on the magnetic properties of carbon-based compounds has been extended to polymerized fullerene. This polymerisation is reached at high pressures (6 GPa) and temperatures (1000K). The magnetization results for samples with rhombohedral structure show a ferromagnetic behavior with a Curie Temperature of 500 K. This finding is unusual since the constituent molecules have no magnetic moments. Further studies will be motivated by two factors. One is the question about what might cause magnetic behavior in a structure made solely by carbon. This question may be related to the ferromagnetic behavior found in HOPG in which we speculate that defects contribute to the measured signal. The other open question is the contribution of magnetic impurities. Although there are several experimental hints that speak against a simple contribution due to ferromagnetic impurities, no systematic studies have been realized yet and they will be part of our future research. The interest on magnetic carbon is enhanced by the possibility to use it in applications that require no metallic atoms. For more details see Nature **413**, 716 (2001).

9.2 Thermal Properties of High-Temperature Superconductors

R.Ocaña and P. Esquinazi

In the last years we have installed an equipment for measurement of thermal properties of crystals with high resolution in temperature and angle between magnetic field and a symmetry axis of a crystal. Our arrangement enables the measurements of the thermal Hall angle as well as the transverse thermal conductivity. One of our recent results is related to the angle dependence of the longitudinal and transverse thermal conductivity for fields applied parallel to the CuO_2 planes of Y123 single crystals. Our results show a twofold variation in the field-angle dependence of the transverse thermal conductivity and a fourfold in the longitudinal one. These results are discussed in terms of Andreev Scattering of quasiparticles by vortices as well as of the Doppler shift in the quasiparticle spectrum. The measurement of the angle dependence requires a very sensitive and stable arrangement where temperature gradients of the order of a few K/m have to be measured.

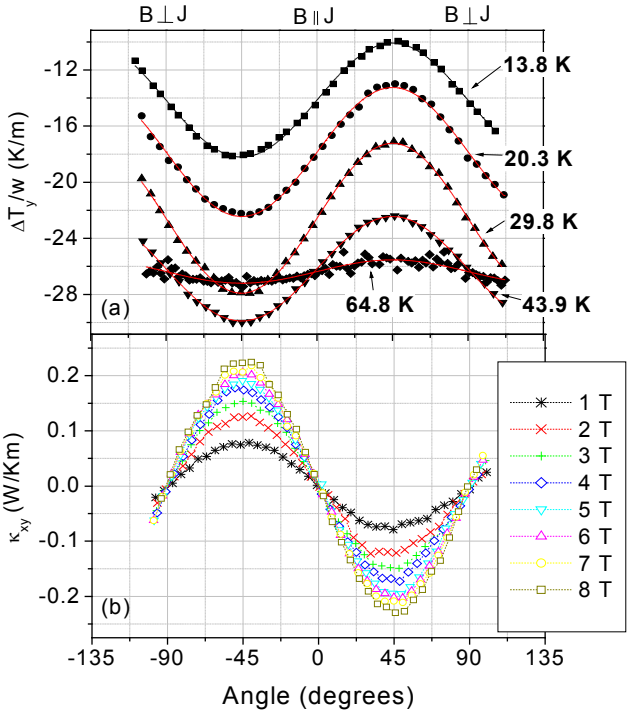

As an example we show in the upper figure the angle dependence of the transverse T-gradient at different temperatures and at a fixed field of 8T (a) for a Y123 crystal. In the panel (b) we show the angle dependence of the transverse conductivity for different fields at constant temperature. Similar measurements for the longitudinal thermal conductivity were performed as well as with the field perpendicular to the CuO2 planes. These measurements are bulk measurements sensitive to the symmetry of the order parameter and therefore of significant importance to understand the origin of superconductivity in high-Tc superconductors. For more details see Phys. Rev. Lett. **87**, 167006 (2001).

Our research will continue measuring these thermal properties at different angles and field directions in other superconductors and carbon-based compounds. Recent results obtained in HOPG reveal interesting angle dependence of the transverse conductivity.

9.3 Magnetic and Magnetotransport Properties of Oxides

One of the research topics of the group of Superconductivity and Magnetism is the investigation of the magnetic and magnetotransport properties of oxides, especially ferro- and ferrimagnetic films and superstructures. This work is directed towards the study of the fundamental properties of these strongly correlated materials, e.g. the mechanism for colossal magnetoresistance in ferromagnetic oxides of the type $La_{1-x}Ca_xMnO_3$, and towards the exploration of extrinsic magnetotransport phenomena in heterostructures such as ferromagnetic tunneling junctions, ferroelectric-ferromagnetic and ferromagnetic-superconducting hybrids as well as artificially created grain boundaries that might be relevant for applications. In the following some recent results are described in more detail.

9.3.1 Growth of Magnetite Films on Spinel Substrates

R. Höhne, M. Ziese, N. H. Hong, H. C. Semmelhack, H. Reckentin and P. Esquinazi

Magnetite (Fe_3O_4) is a half-metallic ferrimagnet with a high Curie temperature of 858 K; these characteristics make magnetite attractive for applications in bi- and multilayer systems such as tunneling junctions. In previous investigations, see [1] and references therein, Fe_3O_4 films were grown mainly on MgO substrates because of the small lattice mismatch. The lattice parameter of MgO, however, is about half of that of Fe_3O_4 and as a consequence in films grown on MgO high densities of antiphase boundaries are found [1]. The spinel substrate $MgAl_2O_4$ has the same crystallographic structure as Fe_3O_4 and is more stable against corrosion than MgO. A disadvantage is the larger lattice mismatch of 3.9%.

The aim of the present work was (1) to find the optimum growth conditions for the preparation of Fe_3O_4 on $MgAl_2O_4$ (100), (2) to check the reproducibility of film quality and (3) to study the influence of different growth conditions and film thicknesses on the structural, magnetic and magneto-transport properties of the samples.

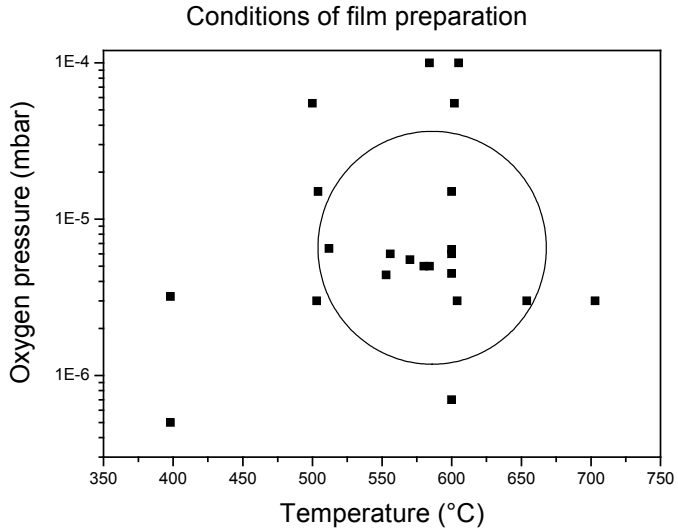

Fig. 1 : The figure demonstrates the conditions of magnetite film preparation using pulsed laser deposition. The symbols inside the circle represent the optimum conditions.

Fe_3O_4 films were prepared by pulsed laser deposition. Excellent films, judging from magnetic properties as well as structural characterization by X-ray diffraction, were grown in a window of substrate temperatures between 500 and 600°C and oxygen background pressures between $3x10^{-6}$ and $1x10^{-5}$ mbar. In these samples the Verwey transition temperature is between 115 and 123 K as determined from jumps in the magnetization and resistivity; the saturation magnetization is about 400 G ($4x10^5$ A/m). Films prepared under the same conditions were clearly reproducible. X-ray diffraction showed that the films were grown epitaxially with the thinner films (up to about 30 nm thickness) being fully strained, whereas thicker ones (> 100 nm) are fully relaxed.

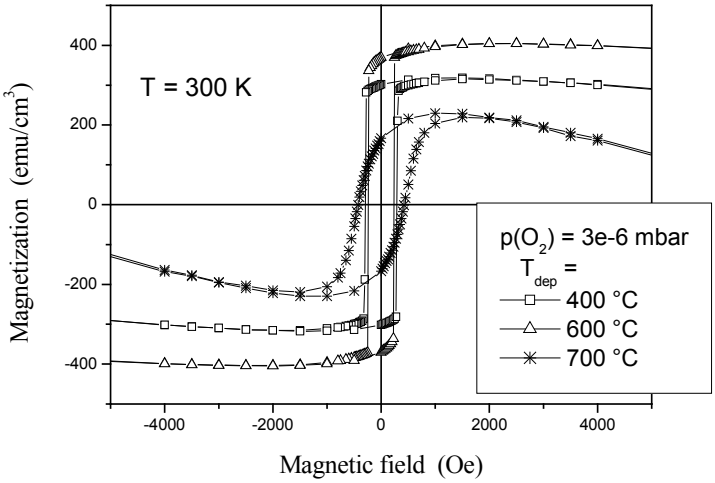

Fig.2 : Magnetization hysteresis loops for three magnetite samples deposited at three different temperatures. The sample prepared at 600 °C has excellent values of saturation magnetization.

Magnetoresistance (MR) measurements showed low MR values compared to films grown on MgO [2], this being an indirect indication of a low density of extended defects such as antiphase boundaries. The anisotropic MR, defined as the difference of MR values measured in longitudinal and transverse configurations,
changes systematically with film thickness; in thicker films it changes sign as a function of temperature at about 150 K.

[1] D. T. Margulies, F. T. Parker, M. L. Rudee, F. E. Spada, J. N. Chapman, P. R. Aitchison and A. E. Berkowitz, Phys. Rev. Lett. **79**, 5162 (1997).
[2] G. Q. Gong, A. Gupta, G. Xiao, W. Qian and V. P. Dravid, Phys. Rev. B **56**, 5096 (1997).

9.3.2 Magnetoresistance at Grain Boundaries Artificially Introduced in Magnetite Films

M. Ziese, R. Höhne, N. H. Hong, K. Zimmer* and P. Esquinazi

* Institute for Surface Modification, 04318 Leipzig, Germany.

The phenomenon of grain-boundary magnetoresistance in half-metallic oxides has attracted an intense research activity in recent years. The Curie temperature of ferromagnetic oxides, however, is too low in order to realize magnetoresistive devices operating at room temperature. There is only one notable exception: the half-metallic ferrimagnet magnetite (Fe_3O_4) with a Curie temperature of 858 K. It is shown here that grain boundaries introduced at step edges in magnetite films yield a considerable magnetoresistance.

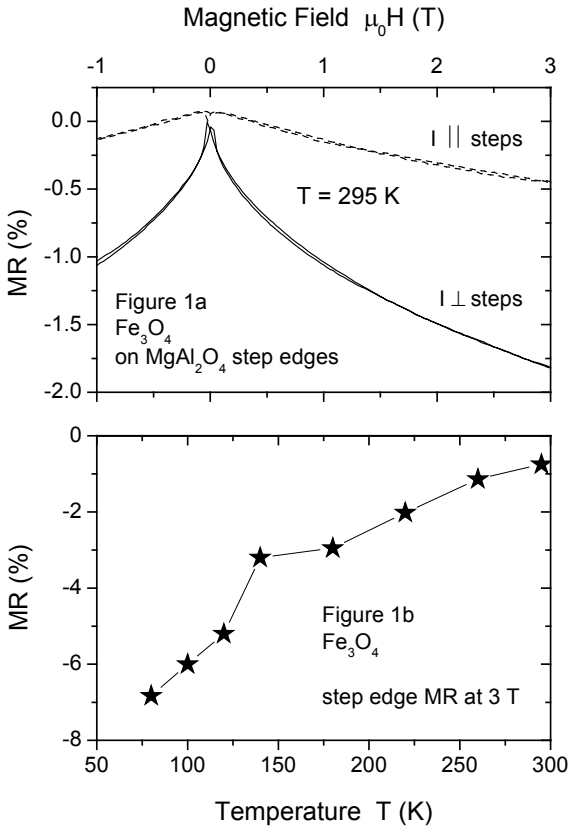

Figure 1 (a) Magnetoresistance (MR) of a step-edge array at 295 K for current parallel and perpendicular to the steps, respectively. (b) Step-edge magnetoresistance at 3 T as a function of temperature.

Step edges were patterned on epi-polished $MgAl_2O_4$ substrates using a conventional photolithography technique followed by chemically assisted ion-beam etching. Magnetite films were grown on these patterned substrates by pulsed laser deposition at a substrate temperature of 550°C in a background oxygen pressure of $5x10^{-6}$ mbar. Step height and film thickness were 80 nm. The films have a Verwey temperature of 115 K as evidenced by jumps in the magnetization and resistivity. The magnetoresistance was measured with the current flowing across and along the steps in magnetic fields applied parallel to the step edges. Magnetoresistance data in

both configurations at room temperature are shown in Fig. 1a; a clear magnetoresistance enhancement is seen when the current is perpendicular to the steps. Fig. 1b shows the grain boundary magnetoresistance at 3 T as a function of temperature; these data were corrected for anisotropic magnetoresistance which is significant below 100 K. The step-edge magnetoresistance decays gradually with temperature from -7% at 80 K to -1% at 295 K. These data indicate the possibility of fabricating grain-boundary structures from magnetite working at room temperature.

9.3.3 Spin Hopping in Ultrathin $La_{0.7}Ca_{0.3}MnO_3$ Films

M. Ziese, K. Han and P. Esquinazi

Granular ferromagnets show a magnetoresistance due to spin-polarized tunnelling between individual grains. Within a simple model Inoue and Maekawa [1] calculated the magnetoresistance ratio and obtained $[R_0\text{-}R(H)]/R(H) = P^2$. Here $R(H)$ denotes the resistance in an applied field H and $R_0 = R(H = 0)$; since the spin-polarization P is limited, $P \leq 1$, the magnetoresistance cannot exceed unity.

$La_{0.7}Ca_{0.3}MnO_3$ films with various thicknesses were prepared by pulsed laser deposition onto $LaAlO_3$ substrates. Films with a nominal thickness larger than 4 nm were continuous and showed a metal-insulator transition above 200 K, see Fig. 1.

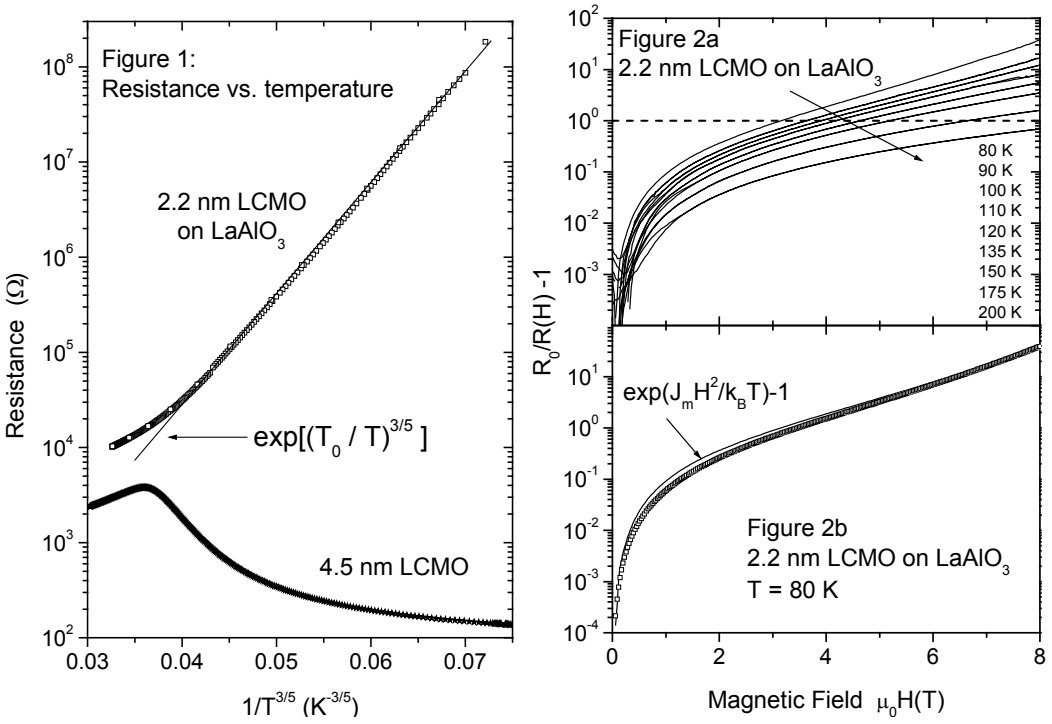

Films with a smaller nominal thickness were discontinuous as evidenced by atomic force microscopy. These films are superparamagnetic and show hopping conduction, see data for a 2.2 nm film in Fig. 1. The resistance follows a $\exp[(T_0/T)^{3/5}]$ law for temperatures T < 200 K; this might be related to a thermally assisted tunnelling process in a two-dimensional granular structure formed by surface diffusion.

The magnetoresistance $[R_0\text{-}R(H)]/R(H)$ of the 2.2 nm film is shown in Fig. 2a as a function of magnetic field; it clearly exceeds the theoretical limit as given by the theory of Inoue and Maekawa [1]. As shown in Fig. 2b the data can be convincingly

fitted by an exponential dependence, $\exp[J_m H^2/k_B T] - 1$, where $J_m H^2$ is an activation energy. This indicates that the intergrain coupling energy plays a major role in the tunneling process and that a new model has to be developed for the magnetotransport properties of highly spin-polarized granular ferromagnets.

[1] I. Inoue and S. Maekawa, Phys. Rev. B **53**, R11927 (1996).

9.3.4 Study of Exchange Biasing Between Ferrimagnetic Thin Patterned Films

R. Höhne, M. Ziese, H.-C. Semmelhack, K. Zimmer* and P. Esquinazi

* Institute for Surface Modification, 04318 Leipzig, Germany.

The current interest in the phenomenon of exchange anisotropy is mainly due to its application in giant magnetoresistance spin valves [1]. The term exchange anisotropy usually refers to the uni-directional magnetic anisotropy observed in a ferromagnet(F)–antiferromagnet(AF) system. A ferromagnetic coupling is also observed between interface spins in systems consisting of hard and soft ferro- or ferrimagnets. Actually, few experimental data on F–F coupling in thin films are available [2].

In the present work Fe_3O_4 /$Co_{0.16}Fe_{2.84}O_4$ bilayers were prepared by pulsed laser deposition on MgO substrates. The exchange biasing between the two ferrimagnetic layers of different coercive fields was investigated by magnetization measurements. The aim of the work was to study the influence of a decrease of the size of the film area on the exchange biasing field. For this the magnetic behaviour of the full film and patterned films consisting of stripes (with widths of 10 µm and 3 µm, respectively) and of dots (10x10 μm^2 and 3x3 μm^2, respectively) were compared with each other. Patterning of the samples was performed by ion-beam etching. The exchange biasing field H_{eb} was measured by the displacement of the minor hysteresis loop of the Fe_3O_4 layer in a field range where the magnetization of the magnetically harder $Co_{0.16}Fe_{2.84}O_4$ layer is unchanged. A clear exchange biasing field H_{eb} was detected both in samples with full film area as well as in patterned films. In samples with a more heterogeneous magnetic structure of the soft adjacent layer – i.e. in films consisting of dots, in stripes in perpendicular field and in zero field cooled films – H_{eb} is clearly reduced and the slope of the magnetization reversal of the magnetite layer is changed. H_{eb} decreases strongly with small magnetization changes of the harder Co-Fe ferrite layer; this change was brought about by relaxation at constant applied field or by a gradual increase of the absolute value of the reverse bias field. Obviously the magnetization reversal begins in sample parts near the interface. In summary, we conclude that H_{eb} depends not only on the film thickness and the properties of the interface, but additionally on the magnetic structure of both layers.

[1] P. J. van der Zaag, P. J. H. Bloemen, J. M. Gaines, R. M. Wolf, P. A. A. van der Heijden, R. J. M. van de Veerdonk and W. J. M. de Jonge, J.\ Magn.\ Magn.\ Mater. **211**, 301 (2000).
[2] C. H. Kleint, M. K. Krause, R. Höhne, T. Walter, H.-C. Semmelhack, M. Lorenz and P. Esquinazi, J. Appl. Phys. **84**, 5097 (1998).

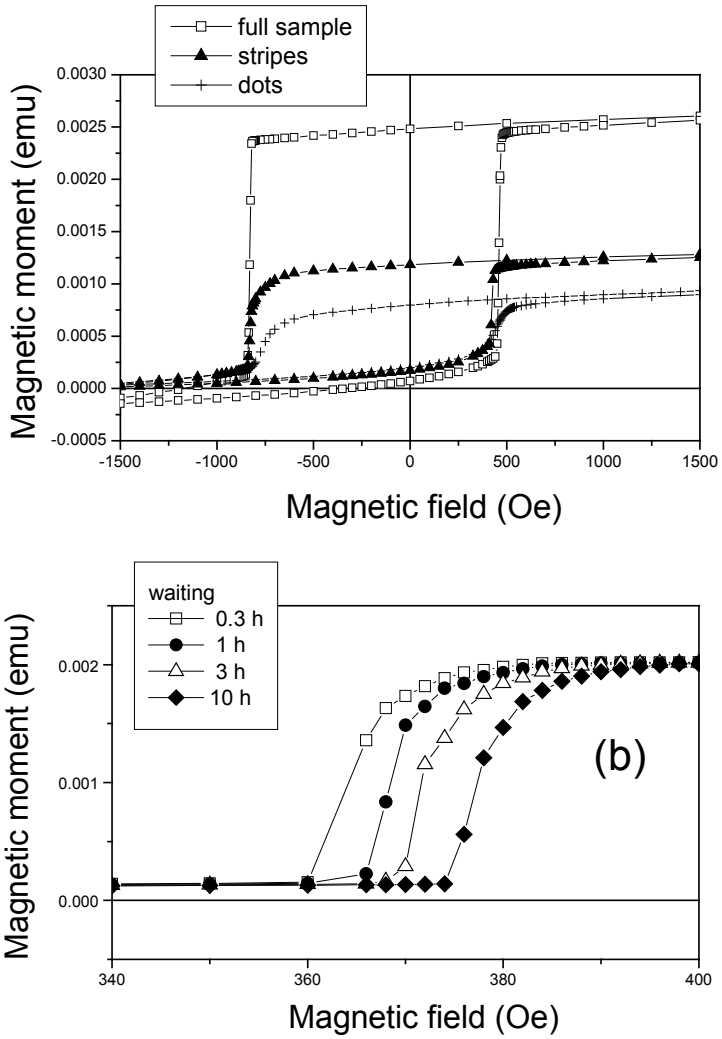

Fig. 1: (a) Minor hysteresis loops of a Fe_3O_4 /$Co_{0.16}Fe_{2.84}O_4$ bilayer with a thickness of 280 nm before (full sample) and after structuring (stripes or dots) measured at T = 5 K. The minor loops are offset from zero on the field axis by an “exchange field” H_{eb}. H_{eb} is clearly reduced in samples consisting of dots. (b) The right side of minor loops after different waiting times at a reverse bias field of – 875 Oe. H_{eb} decreases with the waiting time. This behaviour is caused by the beginning of the magnetization reversal of the magnetic harder layer.

9.3.5 Micromagnetic studies of magnetite films using *μ*-Hall sensor arrays

M. Ziese, R. Höhne, P. Esquinazi and P. Busch*

*Abteilung PAF

In this work μ-Hall sensors were developed into a high resolution tool for the local magnetic characterization of magnetic thin films.
The local field distribution on magnetite films fabricated on MgO and $MgAl_2O_4$ substrates was measured with a μ-Hall sensor array. The stray-field hysteresis loops observed mainly consist of a hysteretic contribution and superimposed field spikes near the coercive field. From an analysis of these Hall data, magnetization and magnetic force microscopy measurements as well as micromagnetic simulations it is concluded that the local field arises from (1) magnetic domain tilt, (b) out-of-plane domains due to a broad easy axis distribution and (c) stray fields emanating from domain walls.

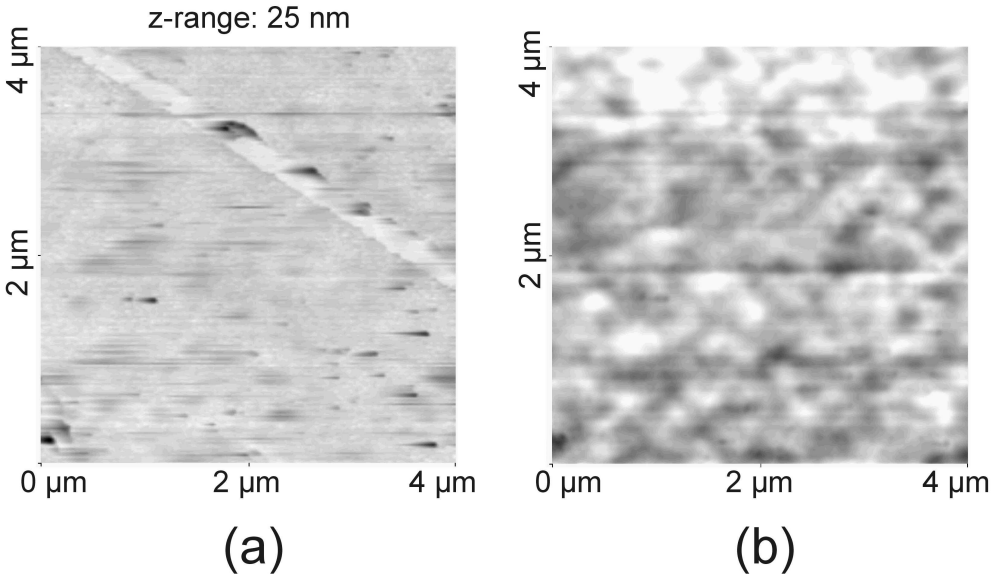

Figure 1: (a) Atomic force microscopy image of a magnetite film on $MgAl_2O_4$. (b) Magnetic force microscopy image of the same region as shown in (a). Magnetic domains are typically 0.5 μm in diameter. Images were recorded at room temperature.

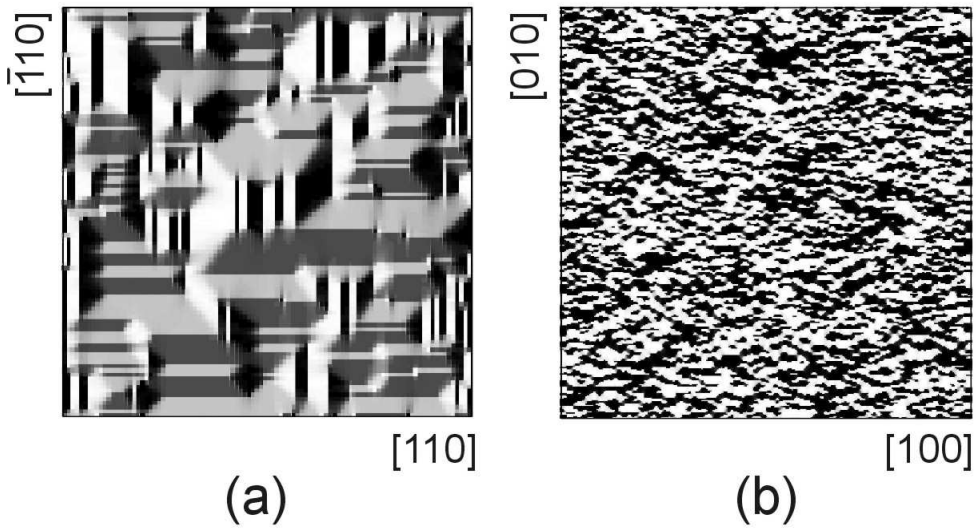

Figure 2: Magnetic domains as obtained from micromagnetic simulations using parameters appropriate for (a) the cubic phase of magnetite at room temperature and (b) the monoclinic phase at 10 K.

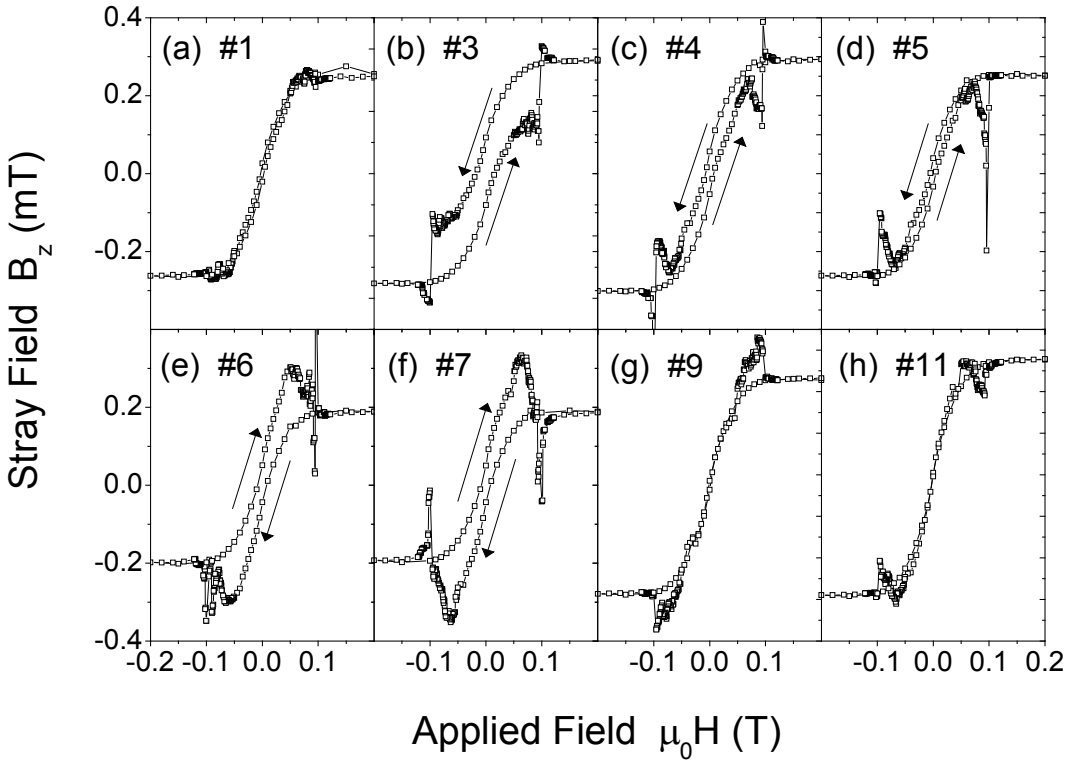

Figure 3: Stray field measured by μ-Hall sensors at eight locations on the sample. The stray field is composed of magnetic signals due to (a) magnetic domain movement near the coercive fields (b) magnetic domains oriented perpendicular to the plane due to local strains and (c) magnetic domain tilt due to a small misalignment between applied field and magnetite film. Spatial resolution is 10x10 μm^2 and worse than magneto-optical techniques; field resolution, however, is better than 0.01 mT and therefore superior to magneto-optics.

9.3.6 Critical Scaling and Percolation in Manganite Films

M. Ziese

The origin of colossal magnetoresistance in ferromagnetic manganites of the type $La_{0.7}A_{0.3}MnO_3$ has not yet been clarified. Here A stands for a divalent ion. Recent models indicate that intrinsic inhomogeneities and percolation might play a major role in determining the transport properties near the Curie temperature. In this work the critical behaviour of $La_{0.7}Ba_{0.3}MnO_3$, $La_{0.7}Sr_{0.3}MnO_3$, $La_{0.7}Ca_{0.3}MnO_3$ and $(LaMn)_{1-\delta}O_3$ films was studied. Apart from the $La_{0.7}Ca_{0.3}MnO_3$ film the other manganite films show a continuous phase transition with mean field critical exponents. The analysis of the critical amplitudes indicates the formation of spin polarons. The zero field resistivity of the $La_{0.7}Ca_{0.3}MnO_3$ film is consistent with a model of percolative phase separation. Since the charge carrier concentration is identical for these films, the magnetic and transport properties are only determined by structural effects; especially the Curie temperature is a smooth function of the so-called tolerance factor that quantifies the distortion of the perovskite structure. The results obtained here indicate that the manganites at optimum doping fall into two classes: materials with high Curie temperature > 270 K appear to be magnetically homogeneous, whereas in compounds with lower Curie temperature magnetic inhomogeneities determine the magnetotransport properties.

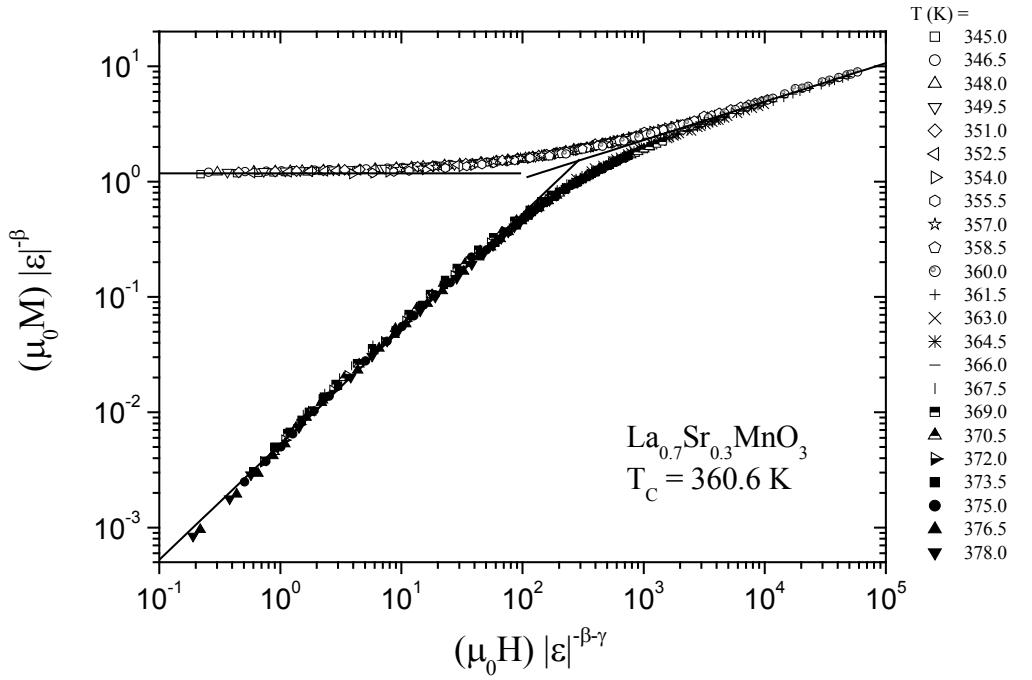

Figure 1: Critical scaling of 23 magnetization isotherms onto the two branches of the scaling function; critical exponents are β = 0.5 and γ = 1.0. Data were recorded with a SQUID magnetometer on a $La_{0.7}Ca_{0.3}MnO_3$ film.

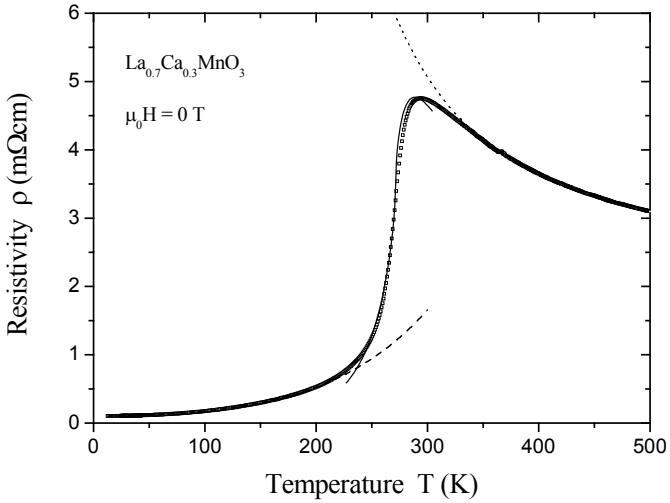

Figure 2: Zero field resistivity of a $La_{0.7}Ca_{0.3}MnO_3$ film and modelling within a percolation model.

9.3.7 Formation of Stripe Domains in thin Insulating $La_{0.7}Ca_{0.3}MnO_3$ Films

M. Ziese

$La_{0.7}Ca_{0.3}MnO_3$ (LCMO) films epitaxially grown on substrates with a significant lattice mismatch show a metal-insulator transition as function of film thickness. Very thin, fully strained films are usually insulating; the application of a magnetic field induces a metallic state. The nature of this metallic state is studied here in more detail using magnetotransport and current-voltage measurements.

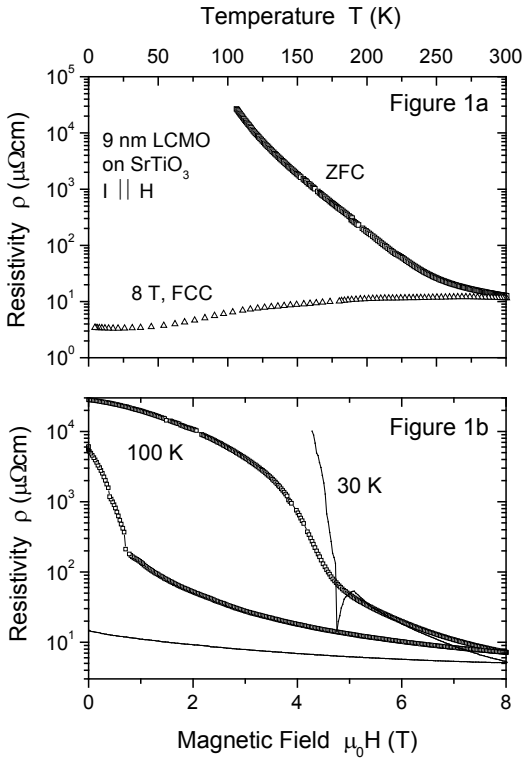

Figure 1: Resistivity of a 9 nm thick film while cooling in (a) zero field (ZFC) and (b) in a field of 8 T.

LCMO films were grown on $SrTiO_3$ using pulsed laser ablation. Below a thickness of about 30 nm the films are under full tensile strain and the magnetotransport properties deviate significantly from bulk properties. Figure 1a shows the resistivity of a 9 nm thick film while cooling in zero field (ZFC) and in a field of 8 T; the current is applied parallel to the field. In zero field the film is clearly insulating, although magnetization measurements show ferromagnetic ordering below about 250 K. After application of 8 T the film becomes metallic; this is clearly shown in Fig. 1b. The transition from insulating to metallic behaviour in a magnetic field is strongly hysteretic and thus indicative of a first order transition.

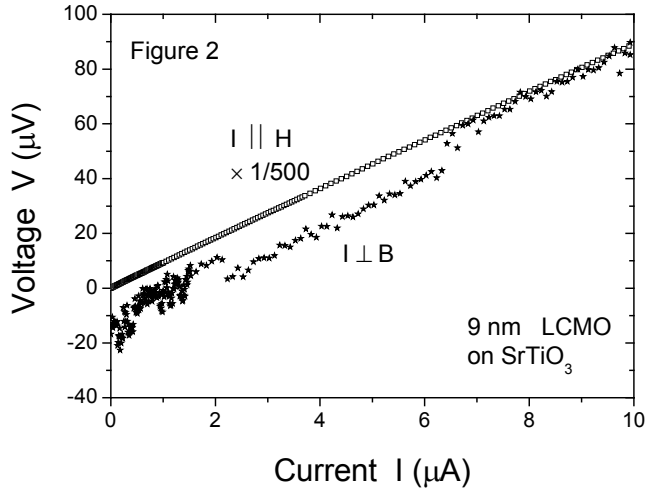

Figure 2: Current-voltage characteristics recorded in the metallic state at 10K and 8T.

Figure 2 shows current-voltage characteristics recorded in the metallic state at 10 K and 8 T. If the current is parallel to the field, a linear dependence is seen. In the configuration with current and field being perpendicular, however, three striking features emerge: (1) the voltage at small currents is negative, (2) the apparent resistance is a factor of 500 smaller than in the parallel configuration and (3) the noise is much larger. These features can be understood if the sample is assumed to consist of alternating metallic and insulating stripes mainly parallel to the field. In this case along the field Ohm's law is found, whereas for perpendicular currents a small spurious voltage due to the current meandering along the metallic stripes is observed. Further detailed magnetotransport measurements will be carried out to study the relation between strain, stripe formation and the metal-insulator transition.

9.4 Funding

Local and nonlocal studies of vortex dynamics in superconductors
Prof. Dr. Pablo Esquinazi, Prof. Dr. E. Zeldov (Weizmann Inst., Rehovot)
German-Israeli-Foundation, 1999-2002

Wechselspiel zwischen Supraleitung und Magnetismus in Graphit und in ungeordneten Metallen
Interplay between superconductivity and magnetism in graphite and disordered metals
Deutsche Forschungsgemeinschaft (07.2000-07.2002)

Magnetotransport in oxidischen Dünnfilm-Systemen
Magnetotransport in oxide thin film systems
Project of the Forschergruppe “Oxidische Grenzflächen” with the University of Halle and Max-Planck Institute for microstructure research in Halle
Deutsche Forschungsgemeinschaft (07.2000-07.2003)

9.5 External cooperations

Prof. Dr. Yakov Kopelevich, Campinas, Brazil.
Prof. Dr. Eli Zeldov, Weismann Institute of Sciences, Israel.
Dr. Tatiana Makarova, Ioffe Institute, St. Petersburg, Russia.
Prof. Bertil Sundqvist, Umea University, Sweden.
Prof. Dr. Miguel Angel Ramos, Universidad Autónoma de Madrid, Spain.
Priv. Doz. Dr. Reinhard König, University of Bayreuth, Bayreuth.
Prof. Dr. Vladimir Pan, Institute of Metal Physics, Kiev, Ukraine.
Dr. Klaus Steenbeck, IPHT Jena.
Dr. K. Zimmer and J. Dienelt, Institute for Surface Modification, Leipzig.

9.6 Publications

9.6.1 Books

“Spin Electronics”
edited by M. Ziese and M. J. Thornton
Springer-Verlag, Heidelberg, 2001

9.6.2 Journals

R. Ocaña, A. Taldenkov, P. Esquinazi and Y. Kopelevich
“Nonomonotonic Temperature Dependence of the Thermal Hall Angle of a Y123 Single Crystal”
J. Low Temp. Phys. **123**, 181-196 (2001).

R. Ocaña and P. Esquinazi
“Angle Dependence of the Transverse Thermal Conductivity in Y123 Single Crystals: Doppler Shift and Andreev Scattering Contributions”
Phys. Rev. Lett. **87**, 167006 (2001).

T. L. Makarova, B. Sundqvist, R. H\"ohne, P. Esquinazi, Y. Kopelevich, P. Scharff, V. Davydov, L. S. Kashevarova, and A. V. Rakhmanina
“Magnetic Carbon”
Nature **413**, 716 (2001).

M. Ziese
“Critical Scaling and Percolation in Manganite Films”
J. Phys.: Condens. Matter **13**, 2919-2934 (2001)

M. Ziese
“Phenomenological Scaling Relations between Anomalous Hall Effect, Anisotropic Magnetoresistance, Resistivity and Magnetization of $La_{0.7}Ca_{0.3}MnO_3$ Films”
phys. stat. sol. (b) **228**, R1-R3 (2001).

M. Ziese
“Spin transport in semiconductors”
in “Spin Electronics“, p. 396-415
edited by M. Ziese and M. J. Thornton
Springer, Heidelberg, 2001.

M. Ziese
“Spin Electronics“
in “Visions of the Future: Physics and Electronics”
edited by J. M. T. Thompson
Cambridge University Press, Cambridge, 2001.

9.6.3 Invited Talks

P. Esquinazi
“Die Entdeckung eines Bekannten: Supraleitung- und ferromagnetischähnliches Verhalten von Graphit", Frühjahrstagung des Arbeitskreises Kohlenstoff,
05.04.2001, Kassel.

P. Esquinazi
“Does the flux line lattice in HTSC really melt ?",
ISF International Workshop on Vortex Dynamics and Advances in high temperature superconductivity, Tel-Aviv, May 20-25 (2001).

9.6.4 Conference contributions

(T:talk, P:poster)

M. Ziese
International Workshop on „Oxide Interfaces“, Wittenberg 2001
“Magnetotransport properties of oxide systems: Ultrathin manganite films and artificial grain boundaries in Fe_3O_4“ (T)

M. Ziese
Frühjahrstagung des Arbeitskreises Festkörperphysik, Hamburg 2001
„Magnetische Eigenschaften von $La_{0.7}A_{0.3}MnO_3$ Schichten: Von kritischem Verhalten zu magnetokristalliner Anisotropie“ (P)

M. Ziese
Joint European Magnetic Symposium (JEMS) 2001, Grenoble
“Magnetoresistance at Grain Boundaries Artificially Introduced into Magnetite Films” (T)

R. Höhne
Joint European Magnetic Symposium (JEMS) 2001, Grenoble
“Study of Exchange Biasing Between Ferrimagnetic Thin Patterned Films” (P)

R. Ocaña
Frühjahrstagung des Arbeitskreises Festkörperphysik, Hamburg 2001
„Angle dependence of the Thermal Hall Angle in Y123 Crystals“ (T)

H. Kempa
Frühjahrstagung des Arbeitskreises Festkörperphysik, Hamburg 2001
„Ähnlichkeiten im Verhalten des „in-plane“-Widerstandes von HOPG mit Supraleiter-Isolator-Übergängen in 2D Elektronensystemen“ (P)

H. Kempa
Frühjahrstagung des Arbeitskreises Festkörperphysik, Hamburg 2001
„Temperature dependence of the mean carrier Lifetime in Graphite determined by Hall conductivity“ (P)

F. Mrowka
Frühjahrstagung des Arbeitskreises Festkörperphysik, Hamburg 2001
„Charge Imbalance Effects in Nonlocal Measurements on Y123 thin Films“ (P)

R.König
Frühjahrstagung des Arbeitskreises Festkörperphysik, Hamburg 2001
„Temperature and Intensity Dependence of the acoustic properties in the normal and superconducting state of amorphous ZrCu” (P)

9.7 Graduations

9.7.1 B.Sc.

Ngu Anyoh Nadege
Characterization of thin Magnetite Films by X-Ray Diffraction and SQUID Magnetometer
Submission date :23.08.2001

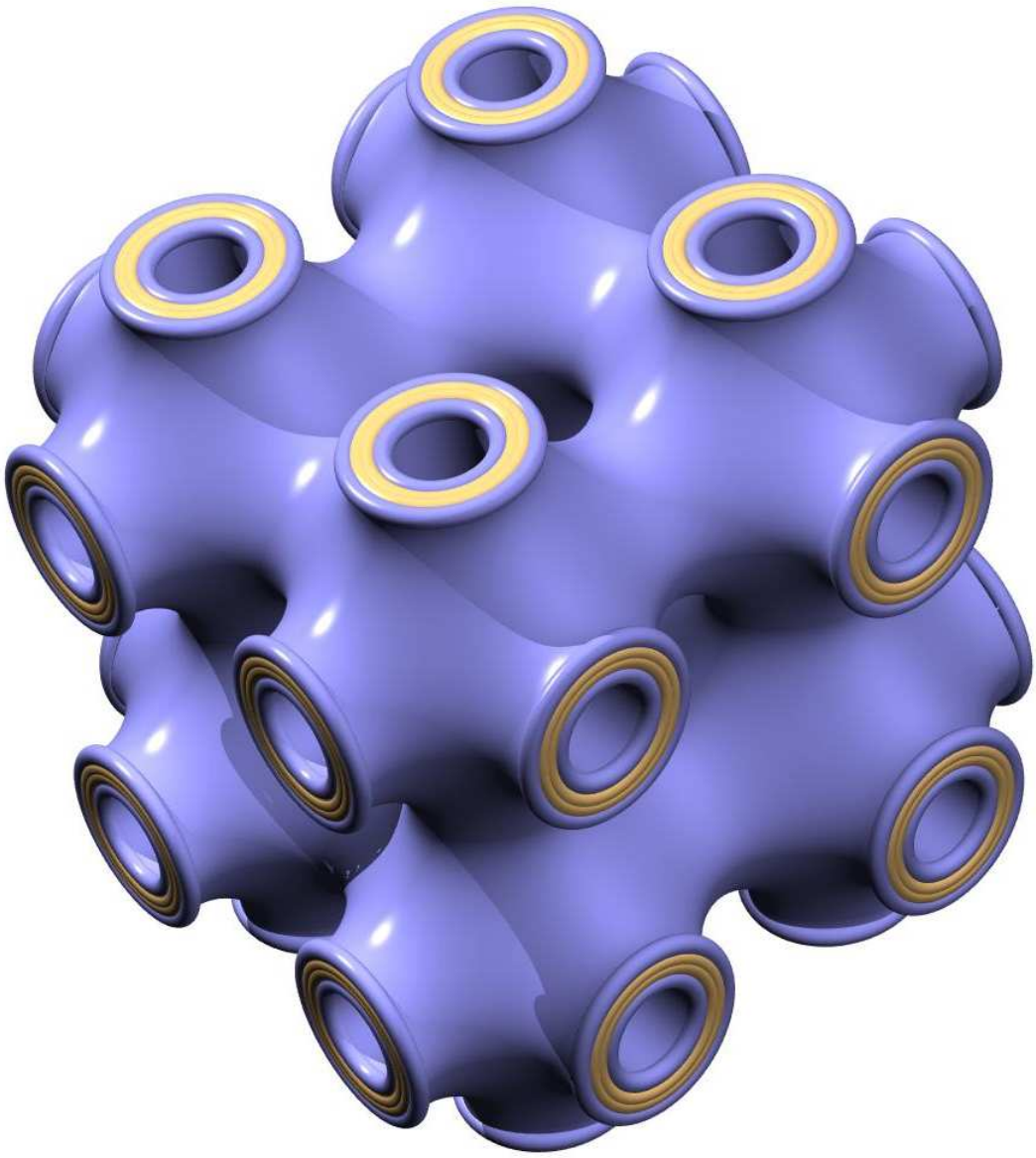

ISBN 3-934178-17-0